

**Deciphering the Catalytic Mechanism of the Zn Enzyme
Glutaminyl Cyclase and the Deduction of Transition-State
Analog Inhibitors**

Dissertation

for the award of the degree

"Doctor rerum naturalium" (Dr. rer. nat)

of the Georg-August-Universität Göttingen

within the doctoral program of the Faculty of Biology

of the Georg-August University School of Science (GAUSS)

submitted by

Alexander Piontek

from Weißenfels

Göttingen, 2014

Thesis Committee

Prof. Dr. Kai Tittmann Department of Bioanalytics,
Albrecht von Haller Institute for Plant Sciences
Georg-August-Universität Göttingen

Prof. Dr. Franc Meyer Institute for Inorganic Chemistry
Georg-August-Universität Göttingen

Members of the Examination board

Reviewer Department of Bioanalytics,
Prof. Dr. Kai Tittmann Albrecht-von-Haller Institute for Plant Sciences
Georg-August-Universität Göttingen

Second Reviewer Institute for Inorganic Chemistry
Prof. Dr. Franc Meyer Georg-August-Universität Göttingen

Further members of the Examination Board

Prof. Dr. Marina Bennati Electron Paramagnetic Resonance Spectroscopy Group
Max Planck Institute for Biophysical Chemistry, Göttingen

Prof. Dr. Jörg Stülke Department General Microbiology
Georg-August-Universität Göttingen

Dr. Manfred Konrad Max Planck Institute for Biophysical Chemistry
Enzyme Biochemistry
Georg-August-Universität Göttingen

Prof. Dr. Ralf Ficner Department of Molecular Structural Biology
Institute for Microbiology and Genetics

Date of oral examination: April 25th 2014

Herewith I declare that I prepared this thesis "Deciphering the Catalytic Mechanism of the Zn-Enzyme Glutamyl Cyclase and the Deduction of Transition-State Analog Inhibitors" independently and with no other sources and aids than those quoted.

Göttingen, 2013-03-01

Alexander Piontek

LIST OF FIGURES	9
ABBREVIATIONS	11
ACKNOWLEDGEMENTS	14
1 INTRODUCTION	16
1.1 Alzheimer’s Disease (AD) – a global challenge for a society in demographic transition - Current situation and future trends	16
1.2 The progress of Alzheimer’s Disease –a brief clinical review in terms of pathohistological abnormalities and symptoms	17
1.3 Leading hypothesis of AD-causing molecular mechanisms	17
1.3.1 A brief historical outline of AD-related investigative milestones	17
1.3.2 On the molecular origin of A β plaques and NFTs	18
1.3.2.1 Neurofibrillary tangles – hyperphosphorylated Tau proteins form neurotoxic fibers	18
1.3.2.2 Enzymatic cleavage of amyloid precursor protein (APP) provides fundamental aggregation seeds for neurotoxic plaque deposition	18
1.3.3 Neuron toxicity of A β peptides is mediated by posttranslational N-terminal and C-terminal modification steps	19
1.3.3 Deciphering pathoneurophysiological mechanisms unveils strategies for the treatment of AD	21
1.3.3.1 Acetylcholinesterase inhibitor	22
1.3.3.2 Inhibition of β - and γ -secretases can reduce A β peptide formation	22
1.3.3.3 Enhancing α -secretase activity can reduce A β formation in the human brain	23
1.3.3.4 Immunotherapy for AD leads to deaggregation of A β plaques	23
1.3.3.5 Inhibition of N-terminal pyroGlu-modification of truncated A β peptides reduces the accumulation of neurotoxic A β -species	24
1.4 Characterization of the QC as target protein in the treatment of AD	26
1.4.1 QC of animals and plants/bacteria – enzymes with convergent functionality but different archetypes – distribution, reaction, molecular 3D structure and evolutionary aspects	26
1.4.2 Discovering the physiological function of animal QC, posttranslational processing of peptide precursors by conversion of N-terminal glutamine into pyroglutamic acid	28
1.4.3 The postulated catalytic cycle of animal QCs	30
1.4.4 Structural characterization of <i>human</i> and <i>Drosophila melanogaster</i> QC	31
1.4.5 Distinct isoforms of mammalian and insect QCs are differently distributed in tissues and cell compartments	31
1.5 Aim of the work, strategy and motivation	33
1.5.1 Aim of the work	33
1.5.2 Strategy and motivation	34

2 MATERIALS AND METHODS	38
2.0 Materials	38
2.1 Expression of the mitochondrial isoform of glutaminyl cyclase from <i>Drosophila melanogaster</i> in <i>Escherichia coli</i>	41
2.2 Cell disruption	41
2.3 Purification	41
2.3.1 Purification of His ₆ -tagged QC	42
2.3.2 Purification of untagged QC	43
2.4 Determination of protein concentration	44
2.5 Preparation of Cobalt (II) substituted QC	45
2.5.1 Cobalt (II) insertion	45
2.6 Enzyme activity assays	46
2.6.1 UV/Vis absorption spectroscopic assay	46
2.6.2 Fluorescence spectroscopic assay	47
2.7 X-ray crystallography	49
2.7.1 Protein crystallization	49
2.7.2 Crystal harvesting and cryo-protection	49
2.7.3 Data collection	50
2.7.4 Data processing, structure refinement and modelling	50
2.8 Protein stability study based on circular dichroism spectroscopy	51
2.8.1 Data analysis	52
2.9 Substrate specificity of the His₆-tagged isoenzyme of the <i>Drosophila melanogaster</i> QC	52
2.9.1 Data analysis	54
2.10 pH Dependence of the isoenzyme of the <i>Drosophila melanogaster</i> QC and their variants	55
2.10.1 Data analysis	55
2.11 Fast Kinetics applying the stopped-flow UV/Vis absorbance method	56
2.11.1 Data analysis	56
2.12 Electron paramagnetic resonance spectroscopy (EPR)	57
2.12.1 Fundamental aspects of EPR spectroscopy and special details regarding the utilized techniques	57
2.12.2 Anisotropy	59
2.12.3 System parameters	59
2.12.3.1 Temperature and Power	59
2.12.3.2 Continuous wave X-band EPR	60
2.12.4 EPR-experiments with Co(II)-substituted enzymes	60
2.12.5 Experimental procedures and methods	61
2.12.5.1 Sample preparation	61
2.12.5.2 Samples which require a long reaction time	63
2.12.5.3 Manual freeze-quench EPR	63

Table of Contents

2.12.5.4 Rapid freeze-quench EPR	63
2.12.5.5 Sample concentration	63
2.12.6 Data analysis	64
3 RESULTS	65
3.1 Thermal stability study of His₆-tagged Zn(II)-isoDromeQC wild type and the variants employing CD-spectroscopy	65
3.1.1 Substitution of active center residues as a tool for structure-function analysis	65
3.1.2 Amino acid substitution may influence the structural stability	65
3.2 Kinetic investigation of His₆-tagged Zn(II)-isoDromeQC wild type and variants using photospectroscopic methods indicate a distinct substrate specificity pattern	68
3.3 Catalytic efficiency measurements as a function of the pH	72
3.4 Stopped-flow UV/Vis absorption analysis of Co(II)-isoDromeQC wild type and variants	75
3.4.1 Stopped-flow UV/Vis absorption analysis of the resting state	75
3.4.2 Stopped-flow analysis of Co(II)-isoDromeQC wild type and the variants incubated with the substrate QQ	77
3.4.3 Stopped-flow analysis of Co(II)-isoDromeQC wild type incubated with the substrate QFRH	80
3.4.4 Stopped-flow analysis of Co(II)-isoDromeQC wild type incubated with substrates possessing an N-terminal glutamate	80
3.4.5 Stopped-flow analysis of Co(II)-isoDromeQC wild type incubated with competitive inhibitors	82
3.5 Protein crystallization – X-Ray structure of Zn(II)- and Co(II)-isoDromeQC wild type and the variants Zn(II)-isoDromeQC_E190Q and Zn(II)-isoDromeQC_D228N	83
3.5.1 Overall crystal structure of Zn(II)-isoDromeQC and variants	84
3.5.2 The crystal structure of the active center in the resting state of the Zn(II)-isoDromeQC wild type and the variants Zn(II)-isoDromeQC_E190Q and Zn(II)-isoDromeQC_D228N	85
3.5.3 The crystal structure of Co(II)-isoDromeQC wild type soaked with the substrate QFRH	86
3.5.4 Co-crystallization of Co(II)-isoDromeQC wild type with the substrate EFRH	89
3.5.5 X-ray structure of the enzyme product complex	90
3.5.6 Crystal structure of Co(II)-isoDromeQC wild type co-crystallized with the tripeptide AFA reveals an enzyme inhibitor complex	91
3.6 Electron paramagnetic resonance spectroscopy (EPR)	93
3.6.1 EPR-analysis of Co(II)-isoDromeQC wild type and variants in the resting state	94
3.6.2 Freeze quench EPR analysis of Co(II)-isoDromeQC wild type and variants after defined incubation times with the substrate QQ	96
3.6.3 EPR spectroscopic analysis of the coordination sphere of the catalytically active Co(II) ion in Co(II)-isoDromeQC wild type and variants after incubation with N-terminal glutamine and N-terminal glutamate substrates	98
3.6.4 EPR spectroscopic analysis of the coordination sphere of the catalytically active Co(II) ion in Co(II)-isoDromeQC wild type and variants after incubation with competitive inhibitors	102
3.6.4.1 EPR analysis of Co(II)-isoDromeQC wild type and variants incubated with the tripeptide AFA	102
3.6.4.2 EPR analysis of Co(II)-isoDromeQC wild type and variants incubated with the reaction product pEFA	104

4 DISCUSSION	107
4.1 Characterization of the active center and the binding mode of N-terminal glutamine substrate binding	107
4.1.1 The lock-and-key principle – Basic correlations between active center and the substrate	107
4.1.1.1 The electronic surface charge around and in the binding pocket is crucial for substrate selectivity	107
4.1.1.2 The length of the substrate sequence is decisive for substrate affinity and catalytic efficiency	108
4.1.1.3 Hydrophobic effects between aromatic amino acids in the second N-terminal position of the substrate and the active center may improve kinetic constants	109
4.1.1.4 Active-center residues correlate with thermal stability	109
4.1.2 The function of the native Zn(II) ion in the catalysis of animal QCs	110
4.1.2.1 The metal in the active center	110
4.1.2.2 The characterization of the metal site in Zn(II)-isoDromeQC	111
4.1.2.3 The Zn(II) as Lewis acid activates the γ -carbonyl moiety of the N-terminal glutamine	112
4.2 The catalytic cycle of the cyclization reaction of substrates with N-terminal glutamine	113
4.2.1 Substrate binding	113
4.2.1.1 Mild alkaline pH supports the substrate affinity by deprotonation of the α -amino group of the substrate's N-terminal glutamine	115
4.2.2 Characterization of discrete mechanistic steps in the trajectory of QCs	115
4.2.2.1 Chemical activation of substrate moieties support the nucleophilic attack	116
4.2.2.2 The release of ammonia (deamination) is accompanied by the decomposition of the reaction intermediate	118
4.2.2.3 Proton transfer pathways are crucial for the release of ammonia	119
4.2.2.4 Release of pyroglutamic acid as final step of the catalytic cycle	120
4.3 QCs provide unfavorable conditions for conversion N-terminal glutamate substrates	121
4.3.1 N-terminal glutamate conversion lacks efficiency due to protonation conflict between crucial functional groups	121
4.3.2 N-terminal glutamine substrates assist the delineation of postulated amino acids as substrate binding motifs	123
4.3.3 The glutamyl cyclization requires protonation of the leaving group - a proposed proton transferring pathway	125
4.4 Investigation of the binding mode of enzyme inhibiting tripeptide AFA	127
6 OUTLOOK	131
BIBLIOGRAPHY	133
BIBLIOGRAPHY	133
8 SUPPLEMENTAL	143
8.1 Purification: final 15% Acrylamide SDS-Gel	143
8.2 Thermal stability study of the <i>iDQC</i> wild type and the variants	143

Table of Contents

8.3 CD spectroscopic spectra of the his ₆ -tagged Zn(II)isoDromeQC before and after the temperature treatment	144
8.4 Single measurements of the substrate specificity study	145
8.5 Catalytic efficiency in dependence of pH	147
8.6 Solvent Isotopic effect	152
8.7 Kinetic data Zn(II)-enzyme versus Co(II)-enzyme	152
8.8 β -Secondary isotopic effect measured by Dr. Franziska Seifert using Q-AMC and D5-Q-AMC	152
8.9 Determination of inhibition constant of the tripeptide AFA	153
8.10 Determination of product inhibition constant of pEFRH	153
8.11 Determination of product inhibition constant of pEFA	153
8.12 X-ray crystallography – Statistics	154
8.13 EPR spectra of Co(II)-isoDromeQC wild type with AFA and pEFA	158

List of Figures

Figure 1.1 Different pathways of amyloid precursor protein (APP) cleavage	18
Figure 1.2 Procession of full-length A β peptide into toxic A β -species	21
Figure 1.3 Conversion of N-terminal glutamate into pyroglutamic acid of N-truncated A β peptides	24
Figure 1.4 Peptides with N-terminal glutamine and glutamate can be converted by QC.....	26
Figure 1.5 Tertiary structures of animal and plant/bacteria QC	27
Figure 1.6 Structure alignment of mono-zinc animal QC and di-zinc bacterial aminopeptidase	28
Figure 1.7 Postulated reaction cycle of Zn(II) dependent QC in the active center [59]	30
Figure 2.1 Proportionality between the outer magnetic field (B_0) and the difference (ΔE) of the energy states.	57
Figure 3.1 Thermal denaturation curves of Zn(II)-isoDromeQC wild type and variants monitored by measuring the ellipticity employing CD spectroscopy at 196 nm	67
Figure 3.2 Kinetic constants of the Zn(II)-isoDrome wild type and the variants determined with several non-physiologic peptide and peptide surrogate substrates employing UV/Vis absorption and fluorescence spectroscopy e.....	69
Figure 3.3 Catalytic efficiencies (k_{cat}/K_M) of Zn(II)-isoDromeQC wild type and variants in dependence of the pH	74
Figure 3.4 UV/Vis absorption spectra of Co(II)-isoDromeQC wild type and variants in the resting state	76
Figure 3.5-1 UV/Vis absorption spectra of the Co(II)-isoDromeQC wild type and the variants during the reaction with the substrate QQ.....	78
Figure 3.5-2 Time resolved diagrams of the reaction of Co(II)-isoDromeQC wild type and variants with the substrate QQ	79
Figure 3.5-3 UV/Vis absorbance spectra recorded while the reaction of Co(II)-isoDromeQC wild type with the tetrapeptide QFRH	80
Figure 3.6 Stopped flow UV/Vis absorbance spectra of Co(II)-isoDromeQC wild type incubated with EFRH and EW	81
Figure 3.7 Stopped flow UV/Vis absorption spectra of Co(II)-isoDromeQC wild type and inhibitors.	83
Figure 3.9 The Overall structure of the Zn(II)-isoDromeQC wild type in the unit cell and the single molecule	84

List of Figures

Figure 3.10 Crystal structure of the active center of Zn(II)-iso <i>Drome</i> QC wild type aligned with the active center of the variants Zn(II)-iso <i>Drome</i> QC_E190Q and Zn(II)-iso <i>Drome</i> QC_D228N	85
Figure 3.11 Crystal structure of Co(II)-iso <i>Drome</i> QC wild type in complex with the substrate QFRH	88
Figure 3.12 Crystal structure of Co(II)-iso <i>Drome</i> QC wild type co-crystallized with the N-terminal glutamate substrate EFRH	90
Figure 3.13 Crystal structure of Co(II) iso <i>Drome</i> QC wild type in complex with the reaction product of pEFRH after the conversion of EFRH.	91
Figure 3.14 Crystal structure of two distinct conformations of the inhibitor AFA in complex with active center of Co(II)-iso <i>Drome</i> QC wild type.....	92
Figure 3.15 Co(II) EPR spectra of the Co(II)iso <i>Drome</i> QC wild type and variants in the resting state.....	95
Figure 3.17 EPR spectra of Co(II)iso <i>Drome</i> QC wild type and variants freeze quenched after defined incubation times with the substrate QQ	97
Figure 3.18 EPR spectra of Co(II)-iso <i>Drome</i> QC wild type and variants after incubation with N-terminal glutamine substrate and two N-terminal glutamate substrates	100
Figure 3.19-1 Manual freeze quench EPR experiments with inhibiting tripeptide AFA	103
Figure 3.20 Co(II) hyperfine structure measured in Co(II)-iso <i>Drome</i> QC E190Q and Co(II)-iso <i>Drome</i> QC_D228N incubate with AFA	104
Figure 3.21 Manual freeze quench EPR experiments of Co(II)(II)-iso <i>Drome</i> QC wild type and variants after incubation with the product analog pEFA	105
Figure 4.1 Electrostatic surface potential.....	108
Figure 4.2 Postulated substrate enzyme interaction in Zn(II)-iso <i>Drome</i> QC_E190Q.....	114
Figure 4.3 Postulated reaction cycle of Zn(II) dependent QC.....	116
Figure 4.4 Deuterated fluorogenic substrate Q-AMC and the postulated tetrahedral intermediate	118
Figure 4.5 Suggested proton transfer pathways in iso <i>Drome</i> QC while the catalysis.....	119
Figure 4.6 Suggested interactions between substrates and iso <i>Drome</i> QC wild type, iso <i>Drome</i> QC_D228N and iso <i>Drome</i> QC_E190Q in the active center	124
Figure 4.7 Postulated reaction cycle of N-terminal glutamate substrates.....	125
Figure 4.8 N-terminal glutamyl substrate in complex with Co(II) iso <i>Drome</i> QC wild type.....	126

Abbreviations

A/Ala	alanine
A β	Amyloid beta
AD	Alzheimers Disease
AFA	alanine-phenylalanine-alanine
AICD	APP intracellular domain
AMC	7-amino-4-methylcoumarine
ApAP	aminopeptidase of <i>Aeromonas proteolytica</i>
APP	Amyloid (-beta) Precursor Protein
approx.	approximately
BESSY II	Berliner Elektronenspeicherring-Gesellschaft für Synchrotronstrahlung
β NA	2-naphthylamine
C83	intracellular γ -secretase cleavage product of amyloid precursor protein in the non-amyloidogenic pathway
C99	intracellular γ -secretase cleavage product of amyloid precursor protein in the amyloidogenic pathway
CCL2	chemokine(C-C motif) ligand 2
CD	Circular Dichroism
<i>cf.</i>	confer (compare to)
Co(II)-isoDromeQC	Co(II) substituted (mitochondrial) isoform of <i>Drosophila melanogaster</i> glutaminyl cyclase
cos	cosinus
<i>C.papaya</i>	<i>Carica papaya</i>
D/Asp	aspartatic acid
Da	Dalton
<i>D. melanogaster</i>	<i>Drosophila melanogaster</i>
DMSO	Dimethylsulfoxid
E/Glu	glutamic acid
EC	enzyme classification
EFRH	glutamic acid- phenylalanine-arginine-histidine
EW	glutamic acid-tryptophane
EDTA	2({2[Bis(carboxymethyl)amino]ethyl}(carboxymethyl)amino)acetic acid
<i>e.g.</i>	exempli gratia lat. for example
EPR	Electron Paramagnetic Resonance spectroscopy
ESRF	European synchrotron radiation facility
F/Phe	phenylalanine

Abbreviations

G/Gly	Glycin
GDH	glutamate dehydrogenase
GDP	Gross domestic product
H/His	histidine
HIC	hydrophobic interaction chromatography
<i>hQC</i>	human glutaminyl cyclase
I/Ile	isoleucine
<i>i.e.</i>	id est lat. that is
IEC	ion exchange chromatography
IMAC	immobilized metal ion affinity chromatography
IPTG	isopropyl- β -D-thiogalactoside
<i>isohQC</i>	isoform of <i>human QC</i>
<i>isomQC</i>	isoform of <i>murine QC</i>
ITC	isothermal titration calorimetry
k_{cat}	rate constant
k_{cat}/K_M	catalytic efficiency
K_I	inhibition constant
K_M	Michaelis-Menten constant
LB	lysogeny broth (medium)
<i>mQC</i>	<i>murine</i> glutaminyl cyclase
N/Asn	asparagine
NADH/H ⁺ (NAD ⁺)	nicotinamide adenine dinucleotide reduced (oxidized)
NFT	Neurofibrillary tangles
Ni-NTA	nickel-nitrilotriacetic acid
OD	optical density
P	proline
p3	extracellular cleavage product of secretase α and γ in the non-amyloidogenic pathway
pEFA	pyroglutamic acid-phenylalanine-alanine
pEFRH	pyroglutamic acid-phenylalanine-arginine-histidine
PEG	polyethylene glycole
PETRA III	Positronen-Elektronen-Tandem-Ringbeschleuniger-Anlage
pGAP	pyroglutamyl aminopeptidase
pH	negative logarithm of H ⁺ concentration
pI	isoelectric point
pK_a	acid dissociation constant
PPG	polypropylene glycole
pyroGlu/pE	pyroglutamic acid

QC	Glutaminyl Cyclase
QFRH	glutamine-phenylalanine-arginine-histidine
Q/Gln	glutamine
QGP	glutamine-glycine-proline
QQ	glutamine-glutamine
R	arginine
RFQ	rapid freeze quenche
rpm	rounds per minute
[S]	substrate concentration
sAPP α	extracellular cleavage product of α -secretase in the non-amyloidogenic pathway
sAPP β	extracellular cleavage product of α -secretase in the amyloidogenic pathway
SEC	size exclusion chromatography
S _N 2 _t	nucleophilic substitution 2 nd order with a tetrahedral intermediate
T _M	melting point
TRH	thyrotropin releasing hormone
Tris	tris (hydroxymethyl)-aminomethan
Tyr	Tyrosin
US\$	currency of the United States of America, Dollar
UV/Vis	ultraviolet and visible fraction of electromagnetic radiation
W/Trp	tryptophane
Zn(II)-iso <i>Drome</i> QC	native (mitochondrial) isoform of <i>Drosophila melanogaster</i> Glutaminyl Cyclase

Acknowledgements

Acknowledgements

I would like to thank *Prof. Dr. Kai Tittmann* for the supervision of this thesis and for awarding me this interesting topic. I am indebted to him for all his support and advice and for many fruitful discussions. Further I am grateful that he gave me many opportunities to further my experience, in particular during the stay abroad.

I would like to thank *Dr. Franziska Seifert* for her supervision during the first two years of this project and the discussions and important support over the entire time-span of my work. In particular I am grateful for her practical and theoretical support during my stays in the Probiodrug laboratories and for the supply of experimental data, plasmids and protein samples.

I would like to thank *Prof. Dr. Franc Meyer* for his external co-supervision of this thesis and for taking part in my thesis committee. I also owe him my thanks for the many constructive discussions during the thesis meetings.

I would like to thank *Prof. Dr. Marina Bennati, Prof. Dr. Jörg Stülke* and *Prof. Dr. Ralf Ficner and Dr Manfred Konrad* for standing as members of my examination board.

I am much obliged to *Dr. Piotr Neumann* for his patient help in all aspects of X-ray crystallography. I want to thank him for his invaluable advice, for data collection at multiple synchrotron facilities and data processing for a multitude of data sets and for many, many jokes and amusing conversations.

My deep gratitude to *Prof. Dr. Brian Bennett* for inviting me to perform EPR experiments under his supervision in his laboratories at the Medical College of Wisconsin. Without his expertise in Co(II) EPR, an important part of the results would be missing in this work.

I am very thankful to *Dr. Florian Brodhun* for the feedback and the correction of this manuscript and for giving me valuable advice and essential support.

I am grateful to *Dr. Stefan Lüdtke* for helping me with different theoretical crystallographic aspects. I would like to thank him also for the practical support during our stays at BESSY II in Berlin.

I would like to thank *Florian, Danilo, Kathrin, Astrid, Stefan S. and Stefan L., Cindy, Michael, Viktor, Oliver, Sabin, Shao-Bo* and all former members of the Bioanalytics department for the constructive working atmosphere and the fruitful discussions.

In particular I would thank *Astrid Sitte* for joining me on various synchrotron trips and for her friendship during our time together in the group.

I am indebted to the Georg-August-University School of Science (GAUSS) and the International Research and Training Group 1422 (IRTG 1422). I would like to thank all persons who gave me assistance on administrative points. In particular I am grateful to Dr. Hanna Steininger for her administrative effort as coordinator of the IRTG 1422 and for her support in terms of organization and my research fellowship.

My thanks go to the IRTG 1422, the “Zentrales Innovationsprojekt des Mittelstandes” of the “Bundesministerium für Wirtschaft und Energie” for their financial support.

I am grateful to my friends, in particular to Anne, Alex and Lena who who took good care of my horse when I was absent due to the preparation of this work. I am thankful to Matthias and Julia for their long-term friendship and being available when necessary. I am grateful to the team of the “Antico & Abruzzo” in Hann. Münden for cheering me on and encouraging me over the entire time-span of this work.

My deepest gratitude to my parents, grandparents, my sister, aunts and uncles for their unlimited support in all fields of my life. Without their help, advice and sometimes pressure this work would never have come into being.

For his patience and for essential support I am much obliged to Nico.

1 Introduction

1.1 Alzheimer's Disease (AD) – a global challenge for a society in demographic transition - Current situation and future trends

Worldwide, approximately 35 million people suffer from a dementia disease. This chronic disease with a creeping deterioration of cognitive abilities leaves humans dependent on full time supervision by a care person. Increasing life expectancy caused by improvements in adult and child health along with decreasing mortality is doubtless the motor of a global demographic transition. In high-income countries of the northern American continent, Europe and Japan, 14 % of the population are aged 65 years and over. Sri Lanka, Brazil and China will reach these 14 % in the next 13 to 19 years [1]. A further example: In 2010, 4 % of people living in the OECD countries were aged 80 years and over. By 2050, 10 % of the population is expected to be older than 80 years [1]. Dementias, including Alzheimer's Disease (AD) are chronic diseases, which are strongly age-associated. The mean age of patients with diagnosed AD is 65 years [1]. Early onset of AD (*e.g.* at the age of 50 years) is often diagnosed in case of familial dementias but is of minor prevalence. The demographic transition to a high percentage of people aged 65 and over and a chronic age-associated disease is becoming a global challenge for care systems and politicians. In 2010, the estimated annual societal costs of dementia were US\$ 604 billion worldwide. This sum corresponds to 1 % of the aggregated Gross Domestic Product (GDP). Due to the demographic transition, the estimated number of dementia sufferers worldwide will have doubled by 2030 (70 million patients) and more than tripled by the year 2050 (115 million patients) [2]. For the year 2030, the cost increase is predicted to be around 85 %. This means that, instead of US\$ 604 billion, dementia including AD will cost approximately US\$ 1,117 billion [2].

1.2 The progress of Alzheimer's Disease –a brief clinical review in terms of pathohistological abnormalities and symptoms

The major changes in the brain of AD patients are cortical atrophy, neuron degeneration, extracellular and intracellular amyloid- β ($A\beta$) containing plaques and intracellular deposits of neurofibrillary tangles (NFT). Cellular abnormalities in the AD-affected brain are tortuous and dilated neurites with enlarged lysosomes, an increased number of mitochondria and paired helical filaments. In brains of AD patients, numerous neurons of many brain regions (hippocampus, parahippocampal gyrus, amygdala, frontal, temporal, parietal and occipital association cortices) are impaired by these $A\beta$ -plaques and NFTs [3]. The proceeding injuries of neuronal tissue lead to creeping loss of cognitive abilities. This includes, apart from numerous psychiatric traits *e.g.* behavioral changes, a progressive decrease in capacity for remembering and orientation. The stages of the progression of AD can be divided into early, middle and final stage. With the deterioration of the symptoms, the reliance on nursing increases continuously [4]. The life expectancy of AD patients after diagnosis is approx. 8 years in a range of 4-20 years [5].

1.3 Leading hypothesis of AD-causing molecular mechanisms

1.3.1 A brief historical outline of AD-related investigative milestones

Since Alois Alzheimer in 1906 first described a syndrome with symptoms similar to senile dementia, a time span of six decades elapsed until the advance of electron microscopy revealed two structurally distinguishable types of depositions in the brain of AD patients [3]. Postmortem analyses of brain tissues of AD patients uncovered the existence of $A\beta$ plaques and neurofibrillary tangles (NFT). In the 1970s, linkages between plaque and NFT depositions, neuronal dysfunction (*e.g.* decreased release of acetylcholine, acting as neurotransmitter) and the symptoms of senile dementia could be found. In the late 1980s, the molecular origin and the composition of these $A\beta$ -plaques and NFTs was unveiled, leading to first theories about the mechanism causing AD-related brain pathohistology. Recent investigations demonstrated that on the one hand, insoluble extracellular $A\beta$ aggregates and on the other hand, smaller and water-soluble intracellular $A\beta$ -oligomers cause brain related pathohistology [6-9]. Both soluble and insoluble $A\beta$ -aggregates appeared in sporadic (age-related) and inherited forms of AD. Today the most investigational effort in terms of the development of treatment strategies is related to the $A\beta$ hypothesis.

1 Introduction

1.3.2 On the molecular origin of A β plaques and NFTs

1.3.2.1 Neurofibrillary tangles – hyperphosphorylated Tau proteins form neurotoxic fibers

The microtubule-associated protein tau (MAPT) is involved in assembling and stabilizing neuronal microtubules. It is prevalently expressed in neurons of the central nervous system. In the brain of adults six isoforms of the protein Tau were found [10]. In AD, these isoforms become abnormally phosphorylated by phosphatases and protein kinases [11, 12] leading to the formation of paired helical filaments. This fibrous component is a general histopathological characteristic for neurofibrillary lesions [13].

1.3.2.2 Enzymatic cleavage of amyloid precursor protein (APP) provides fundamental aggregation seeds for neurotoxic plaque deposition

A β plaques in the brain of AD patients are composed of proteolytic cleavage products of the amyloid precursor protein (APP). APP is ubiquitously expressed in neuronal and non-neuronal tissues in different splicing forms (major isoforms 695, 751 and 770 residues) [3, 14-17]. The gene of this transmembrane protein is located on the chromosome 21. The physiological function has not yet been fully investigated. It is assumed that APP and its cleavage product act as autocrine, neuroprotective, neuritotropic and antimicrobial factors [18-20]. Three secretases (α -, β - and γ) are involved in its sequential cleavage yielding several fragments (*cf.* Figure 1.1). Depending on the type of secretases the products can be divided in non-amyloidogenic and amyloidogenic fragments. Both cleavage pathways release ectodomains, which differ in their biochemical properties *e.g.* solubility and propensity to form aggregates.

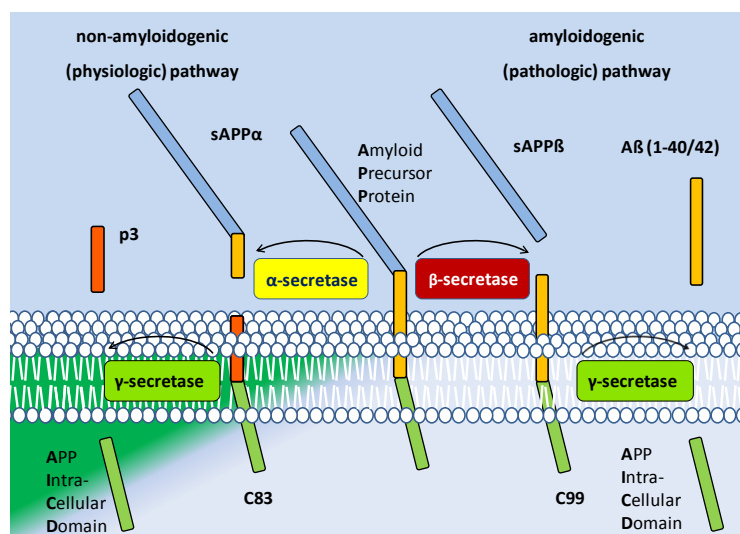


Figure 1.1 Different pathways of amyloid precursor protein (APP) cleavage

The transmembrane protein APP underlies two different degradation pathways. The APP cleavage by β - and γ -secretase liberates $A\beta$ -fragment in the cerebrospinal fluid that exhibits a high propensity to form insoluble $A\beta$ aggregates and soluble $A\beta$ -oligomers. Extracellular accumulation of insoluble $A\beta$ aggregates and enrichment of soluble $A\beta$ oligomers in brain tissue characterizes one type of neuronal lesions in AD-affected brain. The cleavage by α - and γ -secretase results in the release of soluble sAPP α and p3. Modified figure from Lichtenthaler *et al.* [21]

The first pathway can be assigned as the non-amyloidogenic pathway. In this case α -secretase cleaves APP within the $A\beta$ -domain yielding the soluble product sAPP α and the fragment C83. The γ -secretase cleaves the remaining membrane-bound fragment C83 into the product extracellular fragments p3 and APP intracellular domain (AICD). sAPP α was assumed to act as autocrine, neuroprotective and neuritotropic factor [18].

In the second case, β -secretase cleaves APP releasing the ectodomain product sAPP β and a membrane-bound fragment C99 [22]. Subsequently, the membrane-bound C99-fragment is cleaved by the γ -secretase into AICD and the fragment $A\beta$. The heterogenous C-terminal cleavage by the γ -secretase leads to the formation of $A\beta$ peptides containing 40 or 42 amino acids [23]. Due to the high propensity to form neurotoxic, soluble oligomers and insoluble aggregates, the formation of $A\beta$ -fragments is characterized as an amyloidogenic or pathophysiologic pathway.

A strong relation between APP and the occurrence of $A\beta$ peptides is noticeable in the brain tissue of persons suffering from Down's Syndrome. As mentioned above, the APP gene is located on chromosome 21. In Down's Syndrome the triplication of this particular chromosome thus leads to overproduction of APP. The increased amount of substrate for β - and γ -secretase might consequently result in a significantly higher $A\beta$ accumulation accompanied by an early (middle-age) onset of dementia symptoms [3].

1.3.3 Neuron toxicity of $A\beta$ peptides is mediated by posttranslational N-terminal and C-terminal modification steps

Nowadays it is well established that $A\beta$ -plaques consist of distinguishable forms of $A\beta$ peptides. Analysis of these components demonstrated that they consist of a spectrum of $A\beta$ -species containing $A\beta(1-40/42)$, $A\beta(3-40/42)$, $A\beta(11-40/42)$ [24]. The N-terminal truncated forms $A\beta(3-40/42)$, $A\beta(11-40/42)$ possess a glutamate in the first position that has undergone a chemical modification into pyroglutamic acid (pGlu or pE). These peptides are called $A\beta(pE3-40/42)$ and

1 Introduction

A β (pE11-40/42), respectively [25]. As previously mentioned, sequential modifications at the C-terminus occur by alternative γ -secretase cleavage at the C-terminus.

Modification of the N-terminal sequence proceeds stepwise. The first step is the removal of the first two or ten amino acids. The A β (11-40/42) is most likely processed by the β -secretase [26]. The processing of A β (3-40) is not fully elucidated yet. The second step is the chemical modification from glutamate into glutamic acid (pyroGlu) which is performed by the enzyme glutaminyl cyclase (QC) [27-30] (*cf.* Figure 1.2). *In vitro* experiments have shown that these distinct forms of A β peptides exhibit significant differences with regard to solubility in aqueous buffers, aggregation propensity and stability [23, 31-34]. A decreased solubility in aqueous solutions correlates with an accelerated formation of insoluble aggregates and soluble oligomers.

The most enhanced propensity to form aggregates accompanied by the lowest solubility in aqueous buffers was demonstrated for the N-terminally truncated and pyroGlu-modified A β (pE3-42) and A β (pE11-42) [23, 31, 32].

The reasons for decreased solubility are mainly due to the loss of the N-terminal basicity, which is accompanied by an increased hydrophobicity after the pyroGlu-modification. The isoelectric points (*pI*) of the peptides A β (3-42) (*pI* = 5.78) and A β (11-42) (*pI* = 6.02) are shifted into the neutral pH range A β (pE3-42) (*pI* = 6.3) and A β (pE11-42) (*pI* = 7.32) after the pyroGlu-modification. At the isoelectric point the surface of proteins or peptides carries no net electrical charge. Due to the missing electrical surface charge, interactions with solvent molecules (water) are minimized, leading to decreased solubility [31]. The shifted isoelectric points of pyroGlu-modified A β peptides are closer to the physiologic pH range (pH 7.36 – 7.44) in humans and depict a lower solubility accompanied by an accelerated amyloidogeneity *in vivo*. Schilling *et al.* [34] could demonstrate that the initial velocity of aggregate formation of A β (pE3-40/42) and A β (pE11-40/42) is increased 50-fold to 250-fold compared to the full length A β peptide. Those results indicate that these fast aggregating A β peptides might act as nucleation seeds for A β plaque formation *in vivo*. Piccini and co-workers found in their studies that both brains of healthy elderly and AD-patients contain A β plaque depositions. Interestingly, the composition of these plaques differ. The analysis by immunohistochemical staining of brains of healthy persons unveil three times higher amounts of plaques containing full-length A β peptides than plaques containing truncated and pyroGlu-modified A β peptides. The AD-affected brain shows an opposite ratio of the mentioned plaques [35]. Here the pyroGlu-modified A β (pE3-40/42) and A β (pE11-40/42) are clearly overrepresented.

This shows that the pathohistologic characteristics of AD are obviously due to the accumulation of plaques consisting predominantly of pyroGlu-modified A β peptides. The reasons for the neurotoxicity of these A β peptides seem to be various. First, the high aggregation velocity of A β (pE3-40/42) and A β (pE11-40/42) accelerates the progress of neuronal lesions. These peptides are protected against (enzymatic) degradation [36] due to the modified N-terminus; consequently the plaque accumulation is almost irreversible. Further, the toxicity of plaques containing pyroGlu-modified A β species seems to be higher compared to plaques containing lower amounts or no modified A β species. The latter were also found in normal-aged individuals showing no dementia-related symptoms. It is suggested that the A β (pE3-40/42) and A β (pE11-40/42) alters the membrane permeability of neurons by forming “pores” [37].

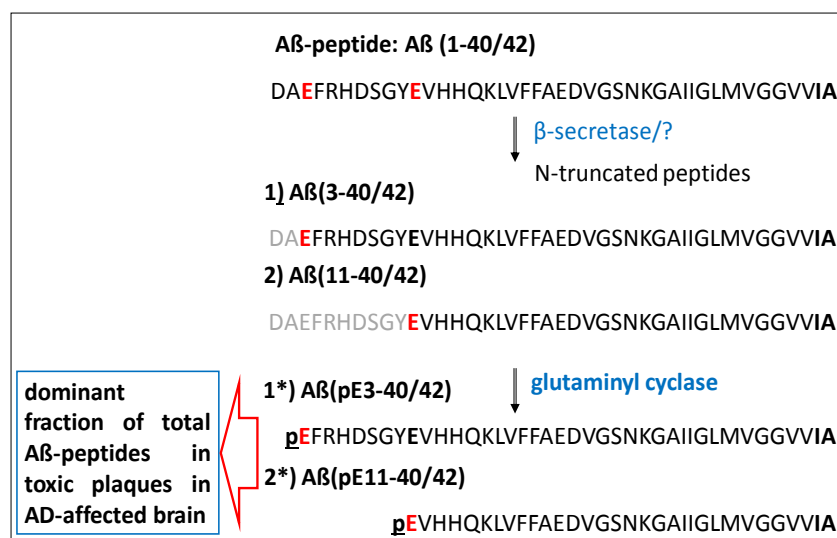


Figure 1.2 Procession of full-length A β peptide into toxic A β -species

The full-length A β peptide (sequence in one-letter-code) becomes N-terminally truncated by β -secretase and further unknown events. The resulting glutamate in the first position A β (3-40/42) and A β (11-40/42) is modified by the glutaminyl cyclase. The resulting A β peptides which possess an N-terminal pyroglutamic acid represent the main fraction in toxic plaques in the AD affected brain.

1.3.3 Deciphering pathoneurophysiological mechanisms unveils strategies for the treatment of AD

Currently no cure is available for AD or other chronic neurodegenerative disorders. Therapies and systemic medication for AD patients help to maintain the health-related quality of life. Due to numerous approaches, in this section only those strategies are described, which are related to the A β hypothesis and the recently applied therapy using an acetylcholinesterase inhibitor.

1 Introduction

1.3.3.1 Acetylcholinesterase inhibitor

As a consequence of the degeneration of basal forebrain in the course of AD, the level of some neurotransmitters *e.g.* acetylcholine is reduced. This lack of signaling molecules leads to impaired signal transmission accompanied by the progressive loss of cognitive abilities [38, 39]. To improve the cholinergic neurotransmission different therapeutic approaches were investigated in the past. The aim of these approaches was to increase the presynaptic release of acetylcholine and the deceleration of acetylcholine degradation by acetylcholinesterase within the synaptic space [38]. This approach shows only small beneficial effects on cognitive, functional and behavioral symptoms [40-42]. However, a minor beneficial effect was found for four acetylcholinesterase inhibitors: tacrine (1,2,3,4-tetrahydroacridin-9-amine), donezipil (1-Benzyl-4-[(5,6-dimethoxyindan-1-on-2-yl) methyl]piperidin), rivastigmine ({3-[α -(Dimethylamino)ethyl]phenyl}-N-ethyl-N-methylcarbamate) and galantamine (3-Methoxy-11-methyl-4a,5,9,10,11,12-hexahydro-6H-benzofurobenzazepin-6-ol). These are frequently applied in the therapy of AD patients with mild and moderate symptoms [43].

1.3.3.2 Inhibition of β - and γ -secretases can reduce A β peptide formation

The release of full-length A β peptides is mediated, as mentioned above, by the secretases β and γ (*cf.* Section 1.3.2, Figure 1.1) that catalyze the sequential proteolysis of APP. The β - and γ -secretase inhibition would lead to a reduced production of full-length A β peptide and consequently to a reduced formation of the truncated and pyroGlu-modified A β peptide (*cf.* Section 1.3.2).

The current state of drug development regarding β -secretase inhibitors is still in an early phase. Several companies *e.g.* Merck (Germany) and Eisai (Japan) are evaluating potential drug compounds in different clinical phases. In 2012 Merck could show that an inhibitor named MK-8931 can reduce the A β accumulation in the cerebral spinal fluid (CSF) of healthy (human) subjects by more than 90 % without dose-limiting side effects. Currently, clinical phases II and III are in progress to evaluate the efficacy of the mentioned drug candidate [published on Merck Newsroom Home (<http://www.mercknewsroom.com>) in March 2012]. A similar outcome of clinical phase I was reported by Eisai for the β -secretase inhibitor E2609 that reduced the overall

A β amount in the CSF in humans [published online in the Eisai News release <http://www.eisai.com/news/news201247.html>].

The investigation of γ -secretase as target protein in AD treatment is, due to its complexity, less advanced compared to the β -secretase. The inhibition of γ -secretase activity can reduce the A β amount in brain, cerebrospinal fluid and plasma [44, 45]. The application of γ -secretase inhibitors in transgenic mice with AD-like neuropathology reveals an improvement of A β induced cognitive deficits [44, 45]. Among others, one physiological function of the γ -secretase is the processing of the Notch protein. The unspecific inhibition of γ -secretase affects also the maturation of Notch protein that causes a dysregulated cellular homeostasis, organ side effects in the gastrointestinal tract. The development of specific γ -secretase inhibitors is still in the preclinical phase and requires further investigations [45].

1.3.3.3 Enhancing α -secretase activity can reduce A β formation in the human brain

A further therapeutic approach in the treatment of AD is the upregulation of α -secretase. As demonstrated in 1.3.2 (*cf.* Figure 1.1) this enzyme cleaves APP within the A β -domain. α -secretase is the body's own tool to diminish the A β production by reducing the amount of substrate for β -secretase.

It could be demonstrated that α -secretase cleaves APP constitutively and can be stimulated by different signaling molecules [46]. The stimulation of α -secretase is not yet fully understood. It is likely that the non-constitutional activation is linked to the activity of protein kinase C [47]. For clinical applications this matter has to be investigated and remains for now a theoretical approach in the treatment of AD.

1.3.3.4 Immunotherapy for AD leads to deaggregation of A β plaques

Extensive studies deal with the removal of already manifested A β depositions from neuronal tissue by immunoreactive mechanisms. Studies in 1999 and 2000 confirmed that the vaccination of mice (depicting A β induced AD-like pathology) with solubilized A β (1-42) or A β (1-40) lowers the A β accumulation in the brain by up to 50 – 60 % [48, 49]. Also passive immunization with monoclonal and polyclonal anti-A β antibodies leads to improvement of AD pathology in mouse models [50, 51].

Recent studies with humanized monoclonal anti-A β antibodies are actually in clinical phase III.

1 Introduction

1.3.3.5 Inhibition of N-terminal pyroGlu-modification of truncated A β peptides reduces the accumulation of neurotoxic A β -species

As mentioned above, the formation of pyroGlu-modified A β peptides (*e.g.* A β (pE3-40/42) and A β (pE11-40/42)) is a crucial step in the cascade of neuropathological progress. In this step N-terminal glutamate of previously truncated A β (1-40/42) into A β (E3-40/42) and A β (E11-40/42) is converted into pyroglutamic acid (pyroGlu or pE). The generated N-terminal lactam ring of the peptides A β (pE3-40/42) and A β (pE11-40/42) hallmarks A β peptides with high amyloidogenicity (propensity to form insoluble aggregates) and neurotoxicity (*cf.* Section 1.3.2). This chemical reaction is catalyzed by the enzyme glutaminyl cyclase (*cf.* Figure 1.3).

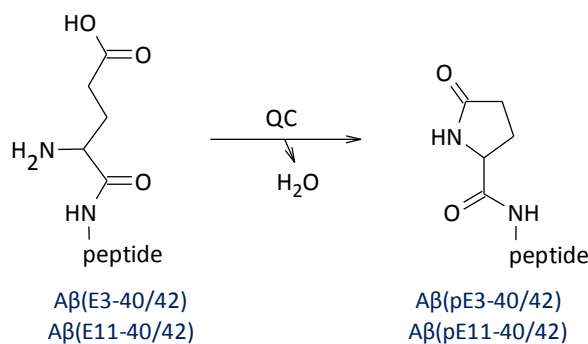


Figure 1.3 Conversion of N-terminal glutamate into pyroglutamic acid of N-truncated A β peptides Glutaminyl cyclase (QC) catalyzes the conversion of glutamate into pyroglutamic acid in the N-terminal position of truncated A β peptides. This pathophysiological side reaction of the QC provides highly amyloidogenic and neurotoxic A β species.

The interjection of this step constitutes a further strategy for the treatment of AD. The spontaneous cyclization reaction of glutamate into pyroglutamic acid at physiological pH exhibits a rate constant of 10^{-9} s^{-1} *in vitro*. QC mediated reaction enhances this reaction by a factor of five *in vitro* [52]. In experiments with rats it was demonstrated that an injection of A β (1-40) and A β (3-40) leads to a significant increase of pyroGlu-modified A β peptides in the cortex. Rats which received intracortical microinjection of QC inhibitors simultaneously with A β (1-40) and A β (3-40) showed significantly decreased formation of pyroGlu-modified A β peptides [53, 54]. Thus, these findings indicated that QC is involved in the initial pathoneurophysiological progress of the development of AD and represents a target enzyme concerning AD treatment.

The general physiological function of QC that is described in detail in the following section is the maturation of peptide hormones and several chemokines *e.g.* thyrotropin releasing hormone (TRH) or chemokine(C-C motif) ligand 2 (CCL2). The down-regulation of a constitutive enzyme contains severe risks with respect to regulatory dysfunctions. Interestingly, Schilling *et al.*

demonstrated that QC knock-out mice suffer from mild hypothyroidism. Those mice displayed no distinguishable changes in fertility, cognition and ingestion behavior compared to wild-type mice. Even blood glucose and glucose tolerance are comparable to wild-type animals. This is a significant contrast to TRH knock-out mice. Also (hypothalamic) pGlu-hormones are not significantly changed, implying the disposability of alternative hormone maturation (pyroGlu-modification) mechanisms. It is likely that an isoform of the QC fulfill hormone maturation processes (*cf.* Section 1.4.5) [55]. These results reveal that QC inhibition might be a promising strategy to reduce the formation of pyroGlu-modified A β peptides in the brain. Recent investigations have led to the development of a potent inhibitor compound (PQ912) whose harmlessness is proven. The efficacy of PQ912 has now to be tested in a phase 2 clinical study. [<http://www.probiodrug.de>].

1.4 Characterization of the QC as target protein in the treatment of AD

1.4.1 QC of animals and plants/bacteria – enzymes with convergent functionality but different archetypes – distribution, reaction, molecular 3D structure and evolutionary aspects

Glutaminyl cyclases (QC; EC 2.3.2.5) are assigned to the family of aminoacyltransferases and are widely distributed in vertebrates, plants, insects and bacteria.

The reaction catalyzed by QCs is the formation of pyroglutamic acid (5-oxoproline) from L-glutamine and L-glutamate residues at the N-terminal position of peptides or proteins. In contrast to plant and bacteria QCs, those from animals requires catalytically active Zn(II) ion for catalysis [56, 57].

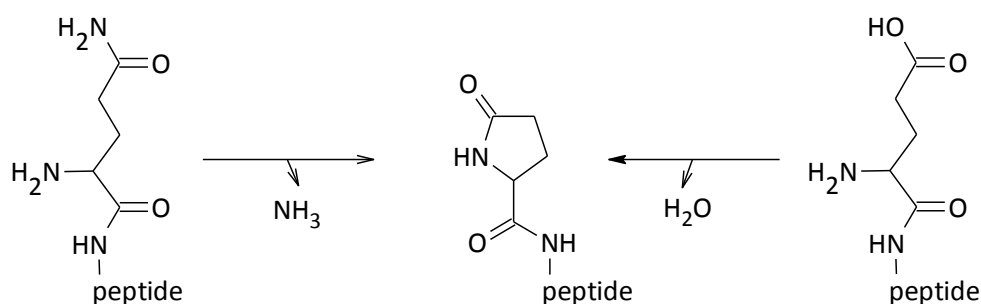


Figure 1.4 Peptides with N-terminal glutamine and glutamate can be converted by QC

The cyclization of N-terminal glutamine and glutamate residues into pyroglutamic acid (5-oxoproline) leads to the loss of N-terminal basicity. It should be noted here that substrates with N-terminal glutamine are preferred. The conversion velocity of these substrates is 10,000-fold faster compared to N-terminal glutamate substrates.

Studies on the structural and biochemical comparison between different animal QCs revealed that several amino acids in the active center and in the Zn(II) binding motifs are conserved (*cf.* Figure 1.5 B). Importantly, the removal of Zn(II) from the active site by dialysis against chelators leads to catalytic inactivation [56].

The most remarkable difference between animal and plant/bacterial QCs lies in the tertiary structure of these proteins. While animal QCs share the common globular α/β -hydrolase fold (*cf.* Figure 1.5 A) [58] plant and bacterial QC are defined by five-bladed β propeller (*cf.* Figure 1.5 C) with a central structure stabilizing Zn(II) ion [59]. The molecular weight difference between animal QC (38 kDa – 40 kDa) and plant and bacterial QC (approx. 31 kDa) is a further distinctive feature.

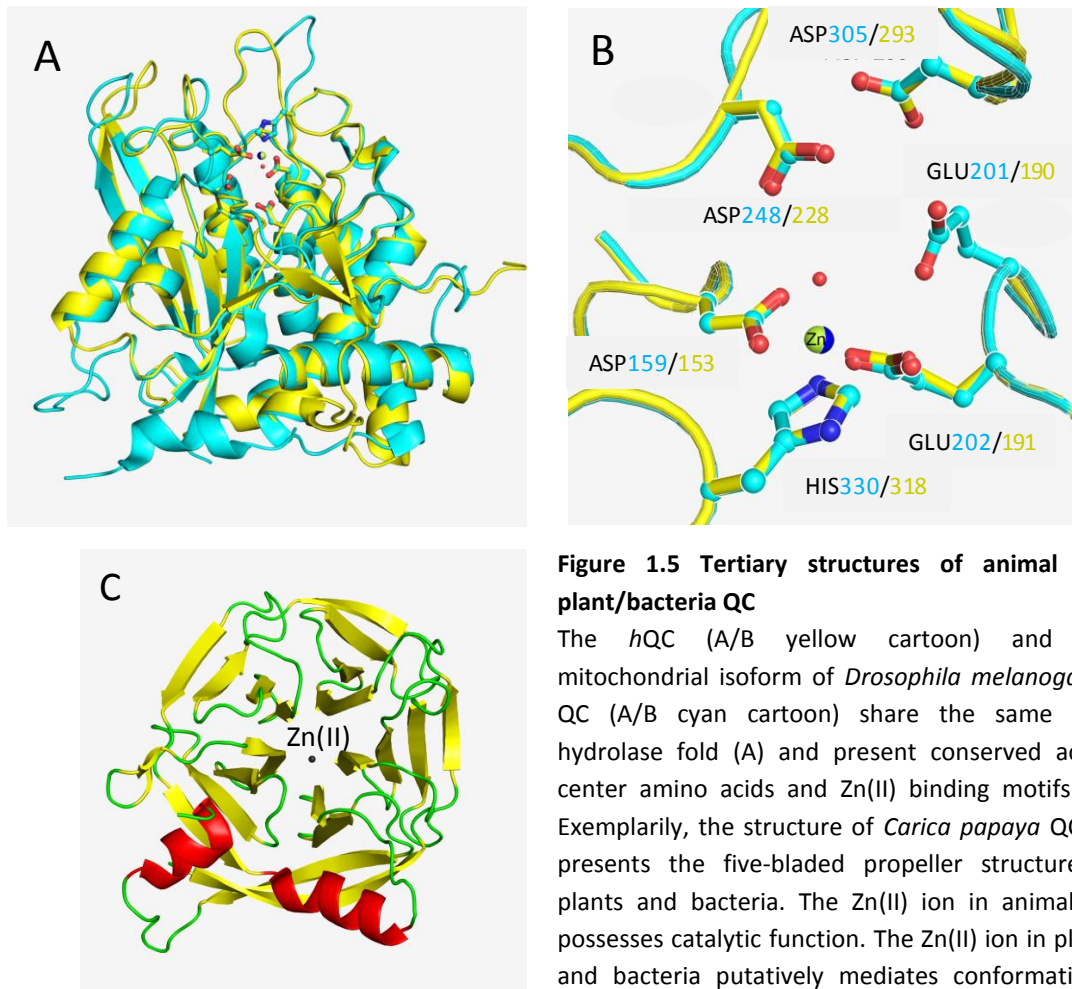


Figure 1.5 Tertiary structures of animal and plant/bacteria QC

The *hQC* (A/B yellow cartoon) and the mitochondrial isoform of *Drosophila melanogaster* QC (A/B cyan cartoon) share the same α/β -hydrolase fold (A) and present conserved active center amino acids and Zn(II) binding motifs (B). Exemplarily, the structure of *Carica papaya* QC (C) presents the five-bladed propeller structure of plants and bacteria. The Zn(II) ion in animal QC possesses catalytic function. The Zn(II) ion in plants and bacteria putatively mediates conformational stability.

hQC: pdb 2AFW, Huang *et al.* 2005; Res.1.56 Å

C. *papaya* QC: pdb 2FAW, Wintjens *et al.* 2006; Res.1.70 Å

D. *melanogaster* QC: own (unpublished) results (c.f. 3.5.2)

Interestingly, animal QCs exhibit also two conserved Zn(II) binding motifs and one disulfide bridge. The strong overall structural similarity with the bacterial aminopeptidase of *Aeromonas proteolytica* (*ApAP*) and the sequence homology of approx. 27 % [determined using Blast® online protein alignment service; <http://blast.ncbi.nlm.nih.gov/Blast.cgi>] indicate that the bacterial aminopeptidase is the evolutionary ancestor of animal QC [57, 60]. At this point it should be mentioned that animal QC requires only one Zn(II) ion for catalysis. The second Zn(II) binding motif is not occupied [61, 62]. However, *ApAP* requires both Zn(II) ions for catalytic activity. Both in QC and *ApAP* Zn(II) the substrate binding motives are identical [63], (cf. Figure 1.6).

The QC from *Carica papaya* and *Zymomonas mobilis* as representatives for plant and bacterial QC share the same tertiary structure [59, 64]. Both enzymes show an amino acid sequence

1 Introduction

identity of approx. 41%. Thus it can be hypothesized that bacterial QCs are evolutionary ancestors of plant QCs.

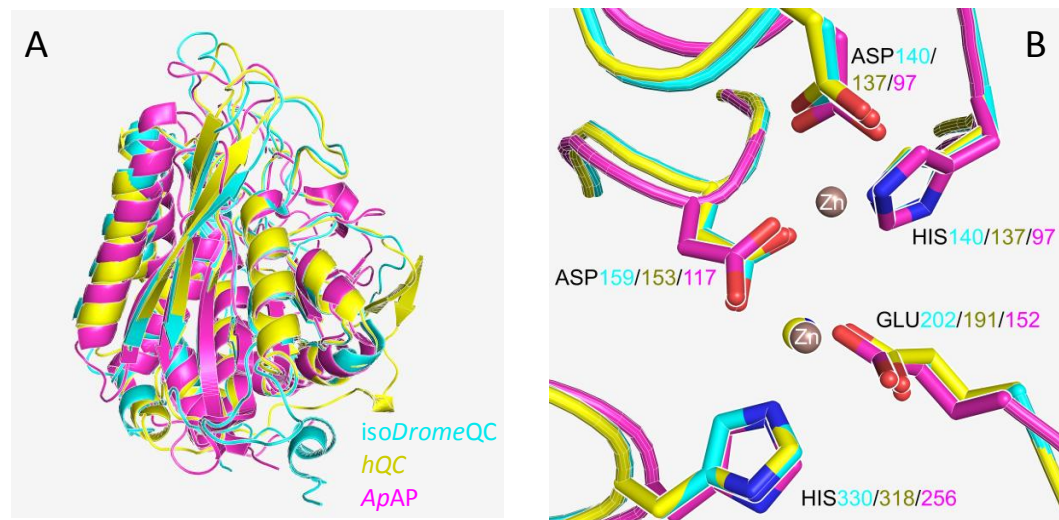


Figure 1.6 Structure alignment of mono-zinc animal QC and di-zinc bacterial aminopeptidase The overall structure of *isoDromeQC* (yellow cartoon), *hQC* (light blue) and *ApAP* (pink) share the common α/β -hydrolase fold. The active center (B) of these enzymes depict conserved Zn(II) binding motifs. The bacterial aminopeptidase requires two Zn(II) ions for catalysis, Whereas in QCs only one Zn(II) binding site is occupied. The structural homologies imply an evolutionary relationship of *ApAP* to QCs.

hQC: pdb 2AFW, Huang *et al.* 2005[62]; Res.1.56 Å; *ApAP*: pdb 3FH4 [65], Yong *et al.* 2009, Res.: 1.95 Å; *D. melanogaster* QC: own (unpublished) results (*c.f.* 3.5.2)

1.4.2 Discovering the physiological function of animal QC, posttranslational processing of peptide precursors by conversion of N-terminal glutamine into pyroglutamic acid

For the activation of signaling molecules such as hormones, often posttranslational modification steps are required [66]. These steps might include glycolization, C-terminal amidation, hydroxylation, proteolytic cleavages and N-terminal pyroglutamyl formation [30]. Fischer and Spiess described in 1986 for the first time that the formation of N-terminal pyroGlu from N-terminal glutamine in extracts from bovine pituitary is due to enzymatic activity. They observed the conversion of (Gln¹)gonadotropin-releasing hormone (Gln¹(GnRH)), (Gln¹,Gly⁴)thyrotropin-releasing hormone (Gln¹,Gly⁴(TRH)), and H-Gln-Tyr-Ala-OH to the respective pyroglutamyl peptides GnRH, Gly⁴(TRH) and pyroGlu-Tyr-Ala-OH [30]. Busby and Quackenbush observed in the same year this reaction in rat brain, porcine pituitary and human B-lymphocytes [28]. Pohl *et al.* showed that QC is predominantly expressed in brain and peripheral endocrine and exocrine glands [67]. Böckers *et al.* accumulated evidence that the peptide hormone maturation is processed within the regulated secretory pathway. He showed that GnRH and TRH, and QC are

co-localized in secretory vesicles in pituitary and hypothalamus [68]. A few years later Awadé *et al.* isolated numerous regulatory peptides containing N-terminal pyroglutamic acid [69]. Schilling *et al.* proved that numerous precursors of pyroGlu-peptides and pyroGlu-proteins with distinct physiologic functions can be converted by QC *in vitro*. [57].

The pyroGlu-modified N-terminus is crucial for receptor recognition [36, 70, 71]. The pyroGlu-modified peptides depict a prolonged half-life time. Due to the lacking N-terminal basicity these peptides lost an essential recognition signal for aminopeptidases. These investigations could clearly demonstrate the participation of QC in hormone anabolism [57].

A further physiological function of QC and a related isoform QC is the activation of chemokines *e.g.* CCL2 and monocyte chemoattractant protein 1 (MCP-1) [72].

The physiological function of QC in the fruit fly *Drosophila melanogaster* is unknown. It is suggested that *DromeQC* and *isoDromeQC* also play a role in the maturation of precursors of signal molecules or enzymes [73]

1.4.3 The postulated catalytic cycle of animal QCs

The catalytic cycle of the conversion of substrates with an N-terminal glutamine was postulated by Schilling *et al.* [60]. In this hypothetical catalytic cycle an acid base catalyst accepts a proton from the α -amino group of the glutamine substrate (*cf.* Figure 1.7 (2)). Structural analysis indicates that a glutamate residue in position 201 in *hQC* and 190 in *isoDromeQC*, respectively, abstracts this mentioned proton. Most likely in a concerted manner, the catalytically active Zn(II) ion acts as Lewis acid and accepts electrons from the γ -carbonyl oxygen accompanied by an increase in the electrophilicity of the γ -carbonyl carbon (*cf.* Figure 1.7 (2)). In this state, the α -amino nitrogen group can attack the γ -carbonyl carbon and would form a tetrahedral intermediate (*cf.* Figure 1.7 (3)). The proposed transfer of the proton from the protonated glutamate residue E201/190 to the γ -amino group enables the release of ammonia from the γ -carbonyl carbon. This proton transfer is putatively executed by the active center amino acids E201/190, D305/293 and D248/228. The formation of the 2-oxoproline ring is completed once the delocalized γ -oxygen electrons return to the oxygen carbon double bond (*cf.* Figure 1.7 (4)). This mechanistic cycle is discussed in detail in Section 4.2.2.

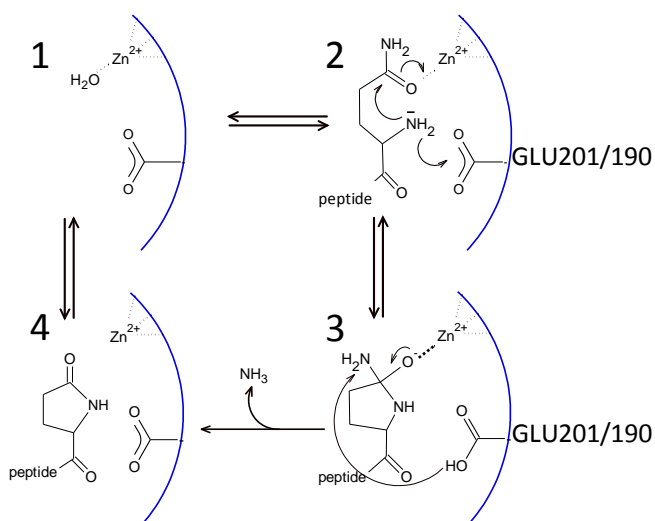


Figure 1.7 Postulated reaction cycle of Zn(II) dependent QC in the active center [60] The postulated catalytic cycle of glutaminyl cyclase depicts the formation of a tetrahedral reaction intermediate after the deprotonated α -amino group has attacked the γ -carbonyl nucleophilically. This intermediate breaks down into ammonia and pyroglutamic acid.

1.4.4 Structural characterization of *human* and *Drosophila melanogaster* QC

As described in Section 1.4.2, *hQC* and *isoDromeQC* show a strong structural and sequence homology (*cf.* Figure 1.5 A). Both share the α/β -hydrolase fold. The center of the QC overall structure consists of a β -sheet, which is composed of five parallel (β_1, β_3 - β_6) and one antiparallel β -strand (β_2). This twisted β -sheet is coated by nine α -helices. In *hQC* six helices (α_2 - α_5 , α_8 and α_{10}) encircle the convex face of the β -blade. Three further helices (α_6 , α_7 and α_9) are positioned on the concave face of the β -blade. One further helix (α_1) is situated at the N-terminus. In *isoDromeQC* seven helices (α_1 – α_5 , α_8 and α_9) encircle the convex side of the β -sheet. Hence, two α -helices (α_6 and α_7) flank the concave side. [74]. In addition to that common overall structure, the *isoDromeQC* is hallmarked by two further N-terminal, antiparallel β -strands β_{-1} and β_0 .

In both enzymes the active center with the catalytic Zn(II) ion is located in a loop region (*cf.* Figure 1.5 B). The distance between Zn(II) ion and the surface is approx. 8 Ångström. The catalytically active Zn(II) ion in the resting state is tetrahedral coordinated by two conserved carboxylic moieties and an imidazole group (D159 (OD2), E202 (OE2) and H330 (NE2) in *hQC* and D153 (OD2) and E191 (OE2) and H318(NE2) in *isoDromeQC*) [75]. The fourth coordinative position of Zn(II) is occupied by a water molecule. This water molecule acts as placeholder in the resting state and will be replaced by the substrate molecule. The water molecule is in hydrogen bond distance to the residue E201/E190. Two further aspartate residues (D305 and D248 in *hQC* and D293 and D228 in *isoDromeQC*) in the second shell around the Zn(II) may play a role in substrate and product binding and the suggested proton transfer during the reaction trajectory. The human enzyme presents N-linked glycosylation at D49 which indicates no influence on the catalytic activity [75]. Glycosylation sites in *isoDromeQC* are not described [74].

A further characteristic is the existence of a disulfide bond in both *hQC* and *isoDromeQC*. The enzymes present two conserved cysteines H139 and H164 in *hQC*, and H136 and H158 in *isoDromeQC*, forming a disulfide bond [75].

1.4.5 Distinct isoforms of mammalian and insect QCs are differently distributed in tissues and cell compartments

In animals (man, mice and fruit fly), at least two isoforms of QC exist [73, 76-78]. In humans and mice (*mQC* and *isomQC*), QCs were found which show similarities in terms of substrate specificity pattern, Zn(II) dependence and inhibitor sensitivities [78]. Biochemical analysis of the amino acid sequence revealed that *isohQC* and *isomQC* possess an N-terminal anchor sequence

1 Introduction

that mediates the retention of this isoform in the Golgi complex [77]. Contrarily, *hQC* and *mQC* exhibit an N-terminal secretion signal sequence and are targeted to the endoplasmatic reticulum [67]. Investigations concerning the transcript concentration of *mQC* and *isomQC* of several organs of mice, as a mammalian model system, showed that secretory *mQC* is preferentially expressed in the neuronal tissue and in a minor extent in intestines [77]. The Golgi-localized sister enzyme (*isomQC*) was ubiquitously expressed in an almost equal extent in brain and intestine tissues.

The sequence identity of *hQC* and *isohQC* is approx. 45 % [77]. The 3-D stucture analysis reveals differences in terms of overall structure and architecture of the active centers [76]. These differences between *hQC* and *isohQC* likely cause weaker (2–15-fold) QC activities on different synthetic substrates in comparison with *hQC* activities [77].

Nevertheless, similarities of catalytic properties and distinct subcellular and tissue distribution of both isoforms unveil a new strategy in terms of QC-inhibition based AD treatment. The development of *hQC* specific inhibitors might help to down-regulate the levels of pathoneurological pyroGlu-A β -procession in the brain without an impairment of physiological functions. At least in the above-mentioned mouse model, the respective QC knock-out mutants show no severe phenotypical changes. Thus it is likely that the lack of one QC isoform can be compensated by its second isoform [55].

Analogously to mammals, in *Drosophila melanogaster* different isoforms also exist with distinct subcellular localization. While *DromeQC* possesses an N-terminal secretion signal peptide, the *isoDromeQC* contains either an N-terminal mitochondrial targeting signal or a secretion signal due to alternative splicing. Alongside structural aspects, kinetic and inhibition constants as well as pH behavior of the mitochondrial *isoDromeQC* are highly similar to the *hQC* [73, 74].

1.5 Aim of the work, strategy and motivation

1.5.1 Aim of the work

A reason for the necessity of enzyme-specific inhibition is that many inhibitors investigated so far interact with the catalytically active Zn(II) ion in the active center of the QC. Those inhibitors might interfere with other Zn(II)-dependent enzymes (*e.g.* dipetidyl peptidase 4) and thus might cause severe side effects [unpublished data of the Probiodrug Company].

The long-term goal of this field of investigation is the development of enzyme-specific and mechanism-based *h*QC inhibitors. Most enzyme-specific inhibitors would adopt a molecular structure that occurs in the trajectory of the QC catalysis – a reaction intermediate or a transition state. Transient intermediate states such as the postulated tetrahedral intermediate (*cf.* Section 1.4.3) are frequently highly energetic and short-lived entities whose decomposition results in the formation of further intermediate states or in the release of the reaction product and the (regenerated) enzyme. The enzyme-specific binding of inhibitors, which mimic sterical and conformational features (*e.g.* bond length, bond angles) of the reaction intermediate or a transition state might interrupt the catalytic cycle and thus act as suicide substrate. Therefore, the structural characterization of intermediate states motivates this project.

In this regard, the main goal of this work is the elucidation of the glutaminy cyclization mechanism of *h*QC. This includes the definition of discrete mechanistic steps, *e.g.*, substrate binding, formation and decomposition of postulated tetrahedral intermediate states and product release. In addition, microscopic reaction rates of these single steps and the definition of postulated proton transferring pathways is in the focus of interest.

Furthermore, in this work it is attempted to delineate peculiarities of the glutamyl cyclization reaction that is involved in the pathoneurological process inducing dementia disorders.

1.5.2 Strategy and motivation

In the planning phase of this project the heterologous expression of *hQC* yields insufficient amounts of protein lacking adequate conformational stability. For this reason the mitochondrial isoform of the well studied model *Drosophila melanogaster* QC (*isoDromeQC*) was expressed in *Escherichia coli*. The sequence identity with *hQC* (cf. Section 1.4.5), conserved amino acid residues in the active center and nearly equal kinetic and inhibitory properties and pH behavior imply analogous mechanistic features.

In order to investigate the role of certain amino acid residues in the active center and their involvement in substrate binding and further catalytic steps, e.g. deamination or proton transfer, the following variants were used. Zn(II)-*isoDromeQC*_E190Q, Zn(II)-*isoDromeQC*_D293N, Zn(II)-*isoDromeQC*_D293A and Zn(II)-*isoDromeQC*_D228N. In these variants acidic (electrically negatively charged) γ -carboxylate moieties were substituted for polar and uncharged carboxamide groups with isosteric conformation. In case of Zn(II)-*isoDromeQC*_D293A, this variant possesses an uncharged non-polar methyl group with altered steric properties instead of acidic carboxylate.

In the case that these amino acid residues play a role in the enzymatic reaction cycle, their substitution would lead to significant effects on the kinetic constants. The Michaelis-Menten constant (K_M) as a measure of affinity between substrate and enzyme would be altered in the event that one of these substituted reactive groups mediates the substrate binding. For the kinetic investigations, several synthetic N-terminal glutamine substrates were used with the Zn(II)-*isoDromeQC* wild type and the variants to determine alterations in terms of kinetic constants e.g. Michaelis-Menten constant (K_M), the turnover rate (k_{cat}) and the catalytic efficiency (k_{cat}/K_M).

Former investigations displayed that the deprotonation of the α -amino group of the N-terminal glutamine of the substrate peptide is crucial for the required proton abstraction by an acid/base-catalyst. Further, the γ -amino group has to be protonated in order to be released as free ammonia. In order to determine both the mentioned acid/base catalyst as well as the proton transferring groups, the catalytic efficiency of Zn(II)-*isoDromeQC* wild type and the variants was measured as a function of the pH. This method allows the determination of pK_a values of functional groups that are involved in these proton abstracting or transferring steps.

Substitution of pivotal amino acid residues in the variants would result in altered pH/catalytic-efficiency profiles.

The detection of (tetrahedral) reaction intermediates was the predominant aim of this work. For that purpose, two spectroscopic methods were chosen which allow the observation of the electronic environment of the catalytic active metal ion. UV/Vis stopped-flow analysis using the photodiode array and electron paramagnetic resonance spectroscopy (EPR). This analysis requires the substitution of diamagnetic and UV/Vis and EPR silent Zn(II) into paramagnetic Co(II). The metal replacement has no significant influence on the catalytic properties or the conformational stability of the QC. Co(II)-*isoDromeQC* and the variants Co(II)-*isoDromeQC_E190Q*, Co(II)-*isoDromeQC_D293N* and Co(II)-*isoDromeQC_D228N* were incubated with different synthetic N-terminal glutamine and glutamate substrates. This enables the detection of changes in the electronic environment of the catalytically active Co(II) during the catalysis with the intention of detecting the accumulation of intermediate reaction states. Further, an inhibitor was incubated with the Co(II) substituted enzymes to investigate the nature of the inhibitor-metal interactions.

X-ray crystallography was a further biochemical approach used to visualize intermediate states.

2 Materials and methods

2.0 Materials

Compound	Supplier
Acetic acid	Carl Roth GmbH & Co KG, Karlsruhe
Acrylamid/Bisacrylamide (30 %,Mix 37.5:1)	Carl Roth GmbH & Co KG, Karlsruhe
Agar Agar	AppliChem GmbH, Darmstadt
Agarose	AppliChem GmbH, Darmstadt
Ammonium chloride	Carl Roth GmbH & Co KG, Karlsruhe
Ammonium peroxide disulfate (APS)	AppliChem GmbH, Darmstadt
Ammonium sulfate	AppliChem GmbH, Darmstadt
Ampicillin	AppliChem GmbH, Darmstadt
Baysilone paste	GE Bayer Silicones GmbH & Co. KG, Leverkusen
Bis-(2-hydroxyethyl)-imino-tris-(hydroxymethyl)-methan (Bis/Tris)	AppliChem GmbH, Darmstadt
Bromophenol blue (sodium salt)	AppliChem GmbH, Darmstadt
Calcium chloride	Carl Roth GmbH & Co KG, Karlsruhe
Chelex 100 Resin 100-200 Mesh size	Bio-Rad Laboratories GmbH; München
cobalt chloride anhydrous, beads, 99.999 % trace metal basis	Sigma-Aldrich Chemie GmbH, Deisenhofen
Coomassie Brilliant blue G-250	AppliChem GmbH, Darmstadt
Dimethyldichlorsilane	AppliChem GmbH, Darmstadt
Ethanol (96 %, denatured 1 % MEK)	Carl Roth GmbH & Co KG, Karlsruhe
Ethylenediaminetetraacetic acid (EDTA)	AppliChem GmbH, Darmstadt
Glycerol (96 %)	Carl Roth GmbH & Co KG, Karlsruhe
Glycine	Carl Roth GmbH & Co KG, Karlsruhe
Guanidine Hydrochloride	AppliChem GmbH, Darmstadt
Hydrochloric acid (37%)	Th. Geyer GmbH & Co. KG, Renningen
Histidine	AppliChem GmbH, Darmstadt
Kanamycin sulfate	Carl Roth GmbH & Co KG, Karlsruhe
α -Ketoglutarate	Sigma-Aldrich Chemie GmbH, Deisenhofen
Magnesium chloride, hexahydrate	Carl Roth GmbH & Co KG, Karlsruhe
Magnesium sulfate	Carl Roth GmbH & Co KG, Karlsruhe
β -Mercaptoethanol	Carl Roth GmbH & Co KG, Karlsruhe
2-(N-morpholino)ethanesulfonic acid hydrate (Mes)	AppliChem GmbH, Darmstadt
Nickel sulfate hexahydrate	AppliChem GmbH, Darmstadt
Nicotinamide adenine dinucleotide, reduced (NADH)	Sigma-Aldrich Chemie GmbH, Deisenhofen
Parafin oil	Hampton Research Corp., USA
1,10-phenanthroline	Sigma-Aldrich Chemie GmbH, Deisenhofen
Phenyl phosphorodiamidate	Sigma-Aldrich Chemie GmbH, Deisenhofen
Phosphoric acid (85 %)	Carl Roth GmbH & Co KG, Karlsruhe
Potassium chloride	Fluka Chemie GmbH, Switzerland
Potassium dihydrogen phosphate	Carl Roth GmbH & Co KG, Karlsruhe
Potassium hydroxide	AppliChem GmbH, Darmstadt
Polyethylene glycol (PEG) 200, 1000, 4000	6000 Fluka Chemie AG, Buchs, Switzerland
Polypropylene glycol (PPG) 400	400 Fluka Chemie AG, Buchs, Switzerland

2-Propanol	AppliChem GmbH, Darmstadt
Sodium acetate, trihydrate	AppliChem GmbH, Darmstadt
Sodium chloride	AppliChem GmbH, Darmstadt
Sodium dodecylsulfate (SDS)	AppliChem GmbH, Darmstadt
Sodium hydroxide	AppliChem GmbH, Darmstadt
N,N,N',N'-Tetramethylethylenediamin (TEMED)	Carl Roth GmbH & Co KG, Karlsruhe
Tris-(hydroxymethyl)-aminomethane (Tris)	AppliChem GmbH, Darmstadt
Tryptone	AppliChem GmbH, Darmstadt
Yeast extract	AppliChem GmbH, Darmstadt
Zinc chloride (hexahydrate)	AppliChem GmbH, Darmstadt
Peptides	Supplier
AFA	Probiodrug AG, Halle (Saale); Bachem
H-E-F-R-H-OH	Probiodrug AG, Halle (Saale); Innovagen, Sweden
H-E-W-OH	Bachem AG, Switzerland
H-Q-aminomethyl coumarine (Q-AMC)	Bachem AG, Switzerland
H-Q-F-R-H-OH	Probiodrug AG, Halle (Saale); Innovagen, Sweden
H-Q-G-P-OH	Probiodrug AG, Halle (Saale)
H-Q-Q-OH	Bachem AG, Switzerland
H-Q- β naphthylamine (Q- β NA)	Bachem AG, Switzerland
pyroglutamyl-F-A-OH	Probiodrug AG, Halle (Saale)
pyroglutamyl-F-R-H-OH	Probiodrug AG, Halle (Saale); Innovagen, Sweden
Enzymes and Marker	Supplier
DNase	AppliChem GmbH, Darmstadt
Glutamate dehydrogenase	Sigma-Aldrich Chemie GmbH, Deisenhofen
pyroglutamyl aminopeptidase	Probiodrug AG, Halle (Saale)
Plasmid preparation QIAprepR Spin Miniprep kit (50)	Qiagen GmbH, Hilden
Lysozyme	AppliChem GmbH, Darmstadt
Unstained protein molecular weight standard Gene Ruler™ 1 kb DNA ladder 0,5 μ g/ μ l	Fermentas GmbH, St.Leon-Rot
<i>E. coli</i> strains	Supplier
<i>E. coli</i> -M15	Invitrogen
Plasmids	Supplier
pQE31	Probiodrug AG
Devices/Materials	Supplier
AKTA <i>purifier</i> , AKTA <i>prime</i> plus	GE Healthcare Europe
Circular dichroism spectropolarimeter, Chirascan	Applied Photophysics Ltd., UK
Centrifuges,	
AvantiJ-20XPI	Beckmann Coulter GmbH, Krefeld
AvantiJ-30I	Beckmann Coulter GmbH, Krefeld
Biofuge Pico	UniEquip GmbH, Martinried
Universal 320R	Hettich AG, Bach, Switzerland
Centrifuge tubes (50, 500, 1000 ml)	Beckmann Coulter GmbH, Krefeld
Hydrophobic Interaction Chromatography 200 ml	GE Healthcare Bio-Sciences GmbH, Munich
Butylsepharose in a XK16/20 column provided	

2 Materials and Methods

HiPrep™ 26/10 Desalting UnoQ6- column HisPrep FF 16/10 HiLoad 16/600Superdex 75 pg	GE Healthcare Bio-Sciences GmbH, Munich Bio Rad Laboratories GmbH, Munich, Germany GE Healthcare Bio-Sciences GmbH, Munich GE Healthcare Bio-Sciences GmbH, Munich
Concentrator, Vivaspin 0.5 ml, 15 ml, 20 ml (10.000 MWCO) Vivaspin Gap	Sartorius AG Göttingen Sartorius AG Göttingen
Cover plates, 18 mm Crystallization plates (24 well), costar Electrophoresis device, EV 231 Electroporator, MicroPulser electroporator EPR-spectrometer EleXsys E600 Gel documentation chamber Incubation shaker ITC system, ITC200 pH electrode Precision cuvettes, suprasil Sterile filters, 0.20µm Stopped-flow system, SX.20 MV Superloop (10 ml, 50 ml, 150 ml) Thermoblock, Digital Dry Bath 3721D Fisher Bioblock UV-Vis Spectrometer, V-650	VWR International GmbH, Darmstadt Corning, Inc., USA Consort nv, Belgium Bio-Rad Laboratories GmbH, Munich Bruker BioSpin Corporation, Billerica, USA Raytest Ida Herolab, Wiesloch Unitron Infors AG, Bottmingen, Switzerland GE Healthcare Hettler Toledo, Giesen Hellma GmbH & Co. KG, Muhlheim VWR International GmbH, Darmstadt Applied Photophysics Ltd., UK GE Healthcare Europe GmbH, Freiburg Scientific, UK Jasco GmbH, Groß-Umstadt
X-ray MM-007 rotating-anode generator, Micromax 007-HF X-stream 2000, R-AXIS IV++ imaging-plate system	Supplier Rikagu Corp., USA Rikagu Corp., USA
Software Blast <i>ClustalW2</i> <i>CCP4 suite</i> <i>Expasy, ProtParam</i> <i>Kaleidagraph</i> <i>SigmaPlot Version 11.0</i> <i>Origin-7</i> <i>Phenix suite</i> <i>PYMOL</i> <i>SigmaPlot Version 11.0</i> XDS	Supplier Online alignment service http://blast.ncbi.nlm.nih.gov/Blast.cgi http://www.ebi.ac.uk/Tools/msa/clustalw2/ (Larkin et al., 2007) Bailey, 1994 http://web.expasy.org/protparam/ Synergy Software, USA Systat Software, Inc OriginLab Corporation, USA (Adams et al., 2010 a) <i>DeLano Scientific LLC</i> Systat Software, Inc Kabsch, W. (1993). <i>Automatic processing of rotation diffraction data from crystals of initially unknown symmetry and cell constants. J. Appl. Cryst.</i> 26, 795-800

2.1 Expression of the mitochondrial isoform of glutaminyl cyclase from *Drosophila melanogaster* in *Escherichia coli*

An untagged as well as the N-terminal His₆-tagged version of wild-type QC and the variants were expressed heterologously in *Escherichia coli* under identical conditions. Plasmids bearing either the *Drosophila-melanogaster* QC isoenzyme gene (CG 5976 - PB) or the different genetically modified QC constructs were provided by the Probiodrug Company. After transformation in *Escherichia coli* M15 cells by electroporation, the cells were plated on lysogeny broth (LB) plates containing 2 % agar, 100 µg/ml ampicillin and 50 µg/ml kanamycin, and cultivated at 37°C. One single colony was used to inoculate 100 ml LB medium containing ampicillin and kanamycin as selection markers. After cultivation at 37°C for approximately 16 h, the cell culture was centrifuged for 10 minutes at 3320 g and re-suspended in fresh LB medium. A main culture (6 x 1 l LB medium in 2 l chicane shaking flasks) was inoculated with these cells so that the start OD₆₀₀ was approx. at 0.1. The incubation was carried out at 37°C at 200 rpm until the OD₆₀₀ had reached 0.8. Then 200 µM IPTG were added and the temperature was set to 20°C. After 14 – 16 hours, the cells were harvested by centrifuging for at least 30 minutes at 5749 g.

2.2 Cell disruption

Cell lysis was performed by two freeze thaw cycles: For this purpose harvested cells were pre-incubated with lysozyme in lysis buffer (*cf.* Table 2.2). The suspension was slowly frozen at – 80°C and subsequently thawed at room temperature. A repetition of the freeze and thaw disruption procedure was performed to ensure the complete cell lysis.

2.3 Purification

The original protocols for QC purification were established by the Probiodrug Company. During the practical phase of preparing the present doctoral thesis, various steps were optimized or omitted, resulting in highly modified protocols.

The adequate conformational stability of the QCs allows that all purification steps could be performed at room temperature. All buffers were filtered and degassed before use. The

2 Materials and Methods

chromatography columns which were used are listed in Table 2.1, including the applied flow rates if these are not mentioned in the text.

2.3.1 Purification of His₆-tagged QC

Immobilized metal ion affinity chromatography (IMAC) was used to obtain high amounts of purified QC.

After cell disruption the supernatant obtained by centrifugation of the raw extract at 36,000 g for 30 minutes at 4°C was diluted to a protein concentration of approximately 10 – 15 mg/ml. The resulting protein solution was applied on a nickel-nitrilotriacetic acid (Ni-NTA) chelating column (GE Healthcare Bio-Sciences GmbH, Munich, Germany) equilibrated with Ni-NTA-buffer-A, (*cf.* Table 2.2) by using an Äkta FPLC system (GE-Healthcare). Since imidazole is a potent inhibitor of QC [79], histidine was used for the following washing and elution steps. The column was washed with elution buffer containing 1 mM histidine (Ni-NTA-buffer *cf.* Table 2.2) until the absorption at 280 nm reached the baseline. A second wash step was performed by using the elution buffer containing 17 mM histidine. Protein elution was achieved by applying a gradient in which the histidine concentration was constantly increased to 100 mM histidine within 120 ml (6 column volumes). A good peak separation was assured by using flow rates that did not exceed 5 ml/min. In most cases SDS-PAGE with 15 % acrylamide/bisacrylamide gels showed protein fractions with high homogeneity. It should be noticed, however, that in some batches minor impurities were visible in the gel. In that case, a further run with the size-exclusion chromatography (SEC) column was used to eliminate the impurities and to transfer the protein to the storage buffer (*cf.* Table 2.2). If this gel filtration was not necessary, the pure protein was concentrated and desalted by membrane filtration (Vivaspin concentrators, 10 kDa MWCO, Sartorius, Göttingen, Germany). Typically QC was concentrated to 10 – 35 mg/ml before freezing it in liquid nitrogen.

2.3.2 Purification of untagged QC

As described above, cobalt-substituted QC was used for experiments employing UV/Vis and EPR spectroscopy. In order to perform successful experiments in that direction, it is a strict requirement to avoid any metal chelating substances in the samples. Since the affinity of a His₆ tag to metal ions might disturb these measurements in an incalculable manner, it was necessary to express and purify QC without an additional His₆ tag.

The purification of the untagged protein was done by the consecutive use of hydrophobic interaction chromatography (HIC), ion exchange chromatography and, if required, a size-exclusion chromatography step. The HIC column was equilibrated with HIC-buffer-A (*cf.* Table 2.2). The protein raw extract from cell lysis (*cf.* Section 2.2.) was diluted with HIC-buffer-A to a protein concentration of 10 – 12 mg/ml. To ensure that the QC binds to the column, it is important to adjust the ionic strength of the protein sample before it is loaded on the HIC-column. The ionic strength of the protein sample has to be equal to that of the HIC buffer-A. The ionic strength was measured by using a conductometer. HIC-buffer-A with 1.2 M ammonium sulfate has a conductance of approximately 160 mS/cm. Loading was achieved with a peristaltic pump and a flow rate of 5 – 6 ml/min. Unbound impurities were removed by washing the column with HIC buffer A. The second wash step included a decrease of the ammonium sulfate concentration to 1.0 M (17 % HIC-buffer-B) to elute unspecific bound proteins. Subsequently the ammonium sulfate concentration was gradually set to zero (100 % HIC-buffer-B) and the eluate was collected in 10 ml fractions. The QC-containing fractions were concentrated and desalted three times (“Vivaspin” concentrators, 10 kDa MWCO) to change the buffer into the low-salt IEC-buffer-A. The binding capacity of the applied ion exchange column amounts to 80 mg protein. Therefore, in order to get an optimal separation profile, the QC-containing protein solution was loaded in portions of 60 mg to the equilibrated column. The increase of the sodium chloride concentration from 0 mM to 300 mM (100 % IEC-buffer-B) with a flow rate of 2.5 ml/min in 24 min led to base-line-separated elution peaks. Similar to the purification of the His₆-tagged QC, in some cases, a size-exclusion chromatography step was required to yield QC with high homogeneity. This step was performed under the same conditions as described above. The storage conditions were identical to the His₆-tagged QC. After all purifications, the enzyme activity was proven by the GDH-coupled assay described below [80].

2 Materials and Methods

Table 2.1 Column specifications and applied flow rates

Purification step	Commercial name	Column volume ^E	Flow rates ^F
IMAC ^A	His-Prep Fast Flow 16/10	20	4.0 – 5.0
HIC ^B	Butylsepharose Fast-Flow	200	10 – 20
IEC ^C	UnoQ	6	2.0 – 2.5
SEC ^D	Superdex 75, 16/60,	120	1.0 – 1.3

^A) Immobilized Metal ion Affinity Chromatography – provided by GE-Healthcare

^B) Hydrophobic Interaction Chromatography – Butylsepharose in a XK16/20 column provided by GE-Healthcare

^C) Ion Exchange Chromatography – provided by Bio Rad Laboratories GmbH, Munich, Germany

^D) Size Exclusion Chromatography – provided by GE-Healthcare

^E) Total volume of medium (ml)

^F) Flow rate (ml/min)

Table 2.2 Utilized buffers for preparation, storage and activity test

Buffer	Compounds	pH
lysis	50 mM Bis/Tris, 1 mg/ml lysozyme	6.8 – 7.0
Ni-buffer-NTA-A	50 mM phosphate based saline (PBS), 1 mM histidine	7.2 – 7.4
Ni-buffer-NTA- B	50 mM Na ₂ HPO ₄ /NaH ₂ PO ₄ , 100 mM histidine	6.8
HIC-buffer-A	50 mM Na ₂ HPO ₄ /NaH ₂ PO ₄ , 1.2 M ammonia sulfate	6.8
HIC-buffer-B	50 mM Na ₂ HPO ₄ /NaH ₂ PO ₄	6.8
IEC- buffer-A	25 mM Bis/Tris	6.8
IEC- buffer-B	25 mM Bis/Tris, 300 mM NaCl	6.8
Gel-filtration/storage buffer	25 mM Bis/Tris, 100 mM NaCl	6.8
activity assay	50 mM Tris/HCl	8.0

2.4 Determination of protein concentration

The concentrations of all QC constructs were determined via UV/Vis spectroscopy at a wavelength of 280 nm. At this wavelength, aromatic amino acids and cysteine can be detected. The content of these amino acids leads to the extinction coefficient of the entire protein. A theoretical extinction coefficient was calculated with the online program “ProtParamTool” [<http://web.expasy.org/protparam/>]. The extinction coefficient for the native QC was calculated as 46,870 M⁻¹ cm⁻¹ (1 g/l = 1.237), while that of the His₆-tagged is 46,995 M⁻¹ cm⁻¹ (1 g/l = 1.241).

2.5 Preparation of Cobalt (II) substituted QC

A modified protocol provided by Probiodrugs [56] was used to exchange the metal ions in the active center of the QC. Recombinant QC (≈ 25 mg/ml) was dialyzed against 1 l chelating buffer containing 50 mM sodium phosphate and 100 mM sodium chloride 5 μ M 1,10-phenanthroline and 5 μ M EDTA, pH 6.8 in order to remove the Zn(II) catalytically and to generate the apoenzyme. After 4, 8 and 14 h the chelating buffer used was exchanged for fresh buffer. Three additional dialyzing steps with 2,5 l 50 mM sodium phosphate buffer containing 100 mM NaCl, 25 g/l Chelex-100, pH 6.8 were performed (buffer exchange after 4 h, 8 h, 14 h) and the apoenzyme was tested for QC activity. For a typical apoenzyme preparation, a residual activity of $<1\%$ (compared to the holo-enzyme) was observed. The absorption of 1,10-phenanthroline at 260 nm was used to ensure the complete removal. Chelex-100 is insoluble and can be eliminated by filtering the buffer.

2.5.1 Cobalt (II) insertion

In order to reconstitute QC with Co(II) ions the apoenzyme was incubated with a substoichiometric amount (0.95 equivalents) of CoCl_2 . The mixture was incubated for 15 minutes on ice. During that time the resulting solution changed optically from colorless to pinkish. The cobalt QC should show 95 % of the specific enzyme activity compared to the zinc enzyme.

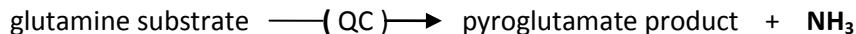
2.6 Enzyme activity assays

In order to determine QC activity, two different assays were performed according to Schilling and co-workers [80]. The underlying principles of those experiments will be described briefly in the following:

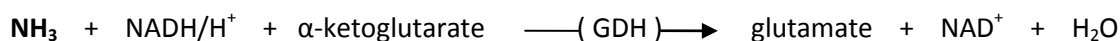
2.6.1 UV/Vis absorption spectroscopic assay

Glutamate dehydrogenase (GDH) is used as an auxiliary enzyme in this spectrophotometric assay. GDH catalyzes the reductive amination reaction of ammonia generated during the QC reaction and exogenously added α -ketoglutarate yielding glutamate. The electrons are derived from the oxidation of NADH/H⁺ to NAD⁺. The NADH/H⁺ consumption can be monitored by UV/Vis spectroscopy at 340 nm.

Cyclization reaction:



Detection reaction:



Experiments were performed at 30°C for 10 min. Except for GDH, all compounds used were dissolved in activity assay buffer (*cf.* Table 2.2). 150 μ l of α -ketoglutarate (50 mM) and 150 μ l NADH/H⁺ (1 mM) were mixed with 30 U/ml glutamate dehydrogenase 50 μ l substrate (50 mM), and 100 μ l activity assay buffer (50 mM Tris/HCl, pH 8.0) was added and incubated for 15 minutes. The reaction was started by adding 50 μ l of the enzyme with a final enzyme concentration of 10 – 20 μ g/ml for the Zn(II)-iso*Drome*QC wild-type QC. Due to their low residual activity, variants were used with higher concentrations in a range of about 1-6 mg/ml.

The time-resolved change of extinction (ΔE) was measured with the Jasco UV- VIS spectrometer V-650 or in the Probiobdrug labs with the microplate reader (POLARstar optima, BMG Labtech

GmbH, Ortenberg, Germany). When the UV/Vis spectrometer (UV/Vis spectrometer, V-650, Jasco GmbH Groß-Umstadt, Germany) was used, the specific activity was calculated from the slope of the progressive curve ($\Delta E/\text{min}$). This slope correlates with the NADH/ H^+ consumption. While the QC reaction converts one molecule substrate, one molecule NH_3 will be released. In the GDH reaction NH_3 will be used for the oxidation of one molecule NADH/ H^+ . The direct proportional relation of QC reaction and the detection reaction allows the determination of the specific activity using the equation based on the Lambert-Beer Law (1).

$$A_{\text{specific}} \left[\frac{U}{\text{mg}} \right] = \frac{-\frac{\Delta E}{\text{min}} \cdot V_{\text{total}} \cdot 1000}{d \cdot \epsilon_{\text{NADH}} \cdot V_{\text{enzym}} \cdot c_{\text{enzym}}} \quad (\text{equation 1})$$

A_{specific}	=	specific activity (U/mg)
$\Delta E/\text{min}$	=	extinction change per minute at $\lambda = 340 \text{ nm}$
V_{total}	=	total volume in the cuvette (μl)
1000	=	translation factor
d	=	path length (1 cm)
ϵ_{NADH}	=	extinction coefficient of NADH/ H^+ at 340 nm ($6220 \text{ M}^{-1} \text{ cm}^{-1}$)
V_{enzyme}	=	applied volume of QC (μl)
c_{enzyme}	=	QC concentration (mg/ml)

This assay served as the basic activity test and was used after each purification or cobalt reconstitution procedure in order to test for enzymatic activity. Further, it was also used for the investigation of the substrate specificity. For this purpose, the microplate reader was applied. In this case the data were evaluated with a standard curve measured with ammonia under assay conditions. A limiting factor for the GDH assay is that ammonia contaminations disturb the activity determination [80].

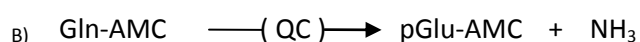
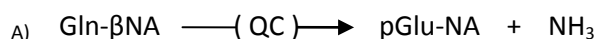
2.6.2 Fluorescence spectroscopic assay

The bacterial pyroglutamyl aminopeptidase (pGAP) is the auxiliary enzyme used in the coupled fluorescence assay. As substrates artificial dipeptides, L-glutaminy-2-naphtylamine (Gln- β NA) and L-glutaminy-4-methylcoumarinylamide (Q-AMC) were used. These substrates are converted by QC to pyroglutamyl-2-naphtylamine (pGlu- β NA) or pyroglutamyl-4-methylcoumarinyl-amide

2 Materials and Methods

(pGlu-AMC) and stoichiometric amounts of NH_3 . In the following cleavage reaction catalyzed by pGAP, pyroglutamic acid (pGlu) and 2-naphthylamine (βNA) and 7-amino-4-methylcoumarine (AMC), respectively, are formed. βNA and AMC are used as fluorophores that can be observed at excitation/emission wavelengths 320 nm/410 nm in the case of βNA and 380/465 nm in the case of AMC [80, 81].

Cyclization reaction:



Detection reaction:



For this approach, 197.5 μl substrate (2.5 mM), 2.5 μl pGAP (0.25 U) and 40 μl activity assay buffer were mixed (*cf.* Table 2.2). After 15 minutes incubation, the reaction was started by adding 10 μl enzyme (typically 20 $\mu\text{g}/\text{mL}$ for Zn(II)-*isoDromeQC* wild type). Data evaluation was performed using a calibration curve which was measured for the fluorescence signal at different β -naphthylamine concentrations.

pGAP shows robust qualities regarding its tolerance of a wide pH range and its long term stability [80]. For this reason, this assay was chosen for the investigation of the pH dependence of the Zn(II)-*isoDromeQC* wild type and variants.

Since this fluorescence assay is not sensitive to ammonia formed during reaction, it could be used for detection of QC activity in raw extracts or other ammonia-containing solutions [80]. These experiments were performed in the Probiobdrug Company laboratories.

2.7 X-ray crystallography

2.7.1 Protein crystallization

The crystallization protocol which was typically used in the present work was slightly modified from that provided by Probiodrugs AG. For the hanging-drop vapor diffusion method, common 24-well cell culture plates were used. In most cases, two droplets were set on a self-silanized cover glass. The well was sealed with the medium viscose silicone.

QC that was stored in the storage buffer (*cf.* Table 2.2) at -80°C was thawed and centrifuged for 12 minutes at 21,000 g (Hettich AG, Bach, Switzerland) in order to remove protein precipitate. The resulting protein solution was adjusted to a protein concentration of 10 mg/ml, or 15 mg/ml if a co-crystallization attempt was planned. The reservoir buffer contained 200 mM MgCl_2 , 100 mM Tris/HCl. The concentration of PEG 4000 varied from 20 % to 25 %, and the pH values covered a range from 8.0 to 8.7. If no ligands were added, the protein solution and the reservoir were mixed in a ratio of 1:1 (1 μl : 1 μl) yielding a final protein concentration of approximately 5 mg/ml.

In case of a co-crystallization experiment, the ligands were dissolved in reservoir buffer (100 mM Tris/HCl, 200 mM MgCl_2 , 20 % PEG 4000, pH 8.0). Ligand stock solution (*cf.* Table 4) and protein were pre-mixed in a ratio 1:2 and incubated on ice. Subsequently protein-ligand-solution and reservoir were mixed as described above. While the final protein concentration was set to 5 mg/ml the ligand concentrations were variable (*cf.* Table 3) and were adjusted with respect to the Michaelis-Menten constant (K_M) or the inhibition constant (K_I), respectively.

It should be emphasized that the two buffers used for crystallization had different pH values (enzyme storage buffer pH 6.8, reservoir buffer 8.0 – 8.7). The final pH of the droplets in each well led to the optimal crystal growth condition. It should also be noted that QC precipitates when mixing with the reservoir buffer containing 100 mM Tris/HCl. The incubation was carried out at 6°C , 20°C , and 25°C . Depending on the QC variant, the ligand and the incubating temperature, the crystal grew within two days or two weeks.

2.7.2 Crystal harvesting and cryo-protection

To the droplets containing protein crystals 250 – 500 nl cryo-solution (100 mM Tris/HCl, 200 mM MgCl_2 , 10 % glucose, 7 % glycerol, 5 % PPG 400, 3 % PEG 1000, pH 8.0) and 500 nl soaking solution were added. The incubation time is depicted in Table 2.3. A 2 μl droplet of paraffin oil

2 Materials and Methods

was set next to the reservoir droplet. With the help of a micro-needle or a cryo-loop, the crystal of interest was transferred through the phase boundary into the oil droplet without contact to the gas phase. Finally the crystals were frozen in liquid nitrogen.

Table 2.3 Ligands for co-crystallization and soaking experiments

Ligand	Stock concentration ^A	Droplet concentration ^B	Soaking time ^C
QQ	<i>60</i>	<i>10</i>	10 – 20
QFRH	60	10	10 – 20
QFA	60	10	10 – 20
EW	<i>60</i>	<i>10</i>	300 – 600
EFRH	30	5	300 – 600
pEFRH	60	10	600
AFA	60	10	600

^A) Concentration (mM) of the stock solution which was used for co-crystallization or soaking attempts, *italics*: approx. for slightly oversaturated solutions

^B) Final ligand concentration (mM) in the droplet in case of co-crystallization attempts

^C) Incubation of the crystals in the soaking/cryo-protection solution (s)

2.7.3 Data collection

To test crystals for diffracting properties, an in-house facility was utilized. Structural data were collected in different synchrotron radiation facilities (ESRF Grenoble (beam-line ID14-1), Frankreich, BESSY II Berlin (beam-line BL 14-1), Germany and PETRA III (beamline B13, B14) Hamburg, Germany).

2.7.4 Data processing, structure refinement and modelling

The sets of data were processed with XDS [Kabsch 2010]. Data processing was accomplished by Dr. Piotr Neumann (Department for Molecular Structural Biology, University Göttingen). Whereas the PHENIX software [82] was used for the structure refinement, the WinCoot software [83] was employed for model building. Structures from the isoenzyme of *Drosophila melanogaster* had been solved previously by the Probiodrugs Company. Hence, the initial molecular replacement for the structure data of the obtained isomorphous crystals was already done. A rigid body refinement fitted the model to the recorded density map using the provided pdb file of the pdb entry 4FAI [74].

2.8 Protein stability study based on circular dichroism spectroscopy

The conformational stability of protein molecules is mediated by numerous intra-molecular interactions such as hydrogen bonds between different amino acid residues or disulfide bridges between cysteins. Substitution of different amino acids by site-directed mutagenesis may change the scaffold of hydrogen bonds and sterical situation, and thus might affect the overall conformational stability. In terms of the QC variants, it was important to exclude that a possible decrease of the stability brings about changes of the kinetic properties.

The stability of the variants was studied using circular dichroism spectroscopy (CD-spectroscopy). The CD-signal arises if the absorption of the left- and the right-circular polarized light of an asymmetric optical center are unequal. In the far UV range (170 – 250 nm) the secondary structure elements of the protein composition can be determined.

A protein which undergoes an unfolding transition loses its secondary structure elements. The CD signal identifying α -helices or β -sheets disappear with the ongoing denaturation [84]. In this study the unfolding transition was induced by a continuous temperature ramp (“thermal denaturation”) starting at 283 K (10 °C) to a final temperature of 367 K (94 °C). The settings of the CD spectrometer are listed in Table 2.4.

Table 2.4 Settings of the CD spectrometer for the thermal denaturation

Setting	
Temperature ramp start	10 °C
Temperature ramp end	94 °C
Data interval	0.5 °C
Heating rate	2.0 °C/min
Tolerance	0.2 °C
Wavelength (λ)	196 nm
Time per point	12 s
Path length	1 mm

QC was concentrated to 0.1 mg/ml in 10 mM potassium phosphate buffer at pH 6.8. To compare the native and denaturated enzyme, CD spectra were taken before and after the temperature ramp (settings: 190 nm – 260 nm at 10 °C and 94 °C, step 1.0 nm, time per point 1 s)(*cf.* Supplemental 8.3)

2 Materials and Methods

Thermal denaturation was monitored by spectral changes at 196 nm. At this wavelength the maximum change of the signal was observable. All measurements were performed in triplicates.

2.8.1 Data analysis

The data were normalized with respect to the slight variance in the protein concentration. The start point of all unfolding curves at 10°C was aligned. For a comparison in terms of conformational stability, the wild type and all variants, the midpoint (T_m) was calculated by fitting the curve to equation (2) [84].

$$y = \frac{\{(y_f + m_f \cdot T) + (y_u + m_u \cdot T) \cdot \exp\left[\left(\frac{\Delta H_m}{RT}\right) \cdot \left(\frac{T - T_m}{T_m}\right)\right]\}}{1 + \exp\left[\left(\frac{\Delta H_m}{RT}\right) \cdot \left(\frac{T - T_m}{T_m}\right)\right]} \quad (\text{equation 2})$$

y	=	Circular dichroism signal at 196 nm
y_f, y_u	=	Intercepts of pre- and post-transition baselines
m_f, m_u	=	Slopes of pre- and post-transition baselines
T	=	Temperature in Kelvin
T_m	=	Midpoint of the thermal unfolding curve
ΔH_m	=	Enthalpy change for unfolding at T_m
R	=	Gas constant

The curve fitting was done with the SigmaPlot 11 software.

This equation is valid for the determination of the midpoint for reversible unfolding transitions. The thermal unfolding transition of the QC is irreversible. So the unfolding transition depends on the heating rate and exposure time at a certain temperature. The observed midpoints may differ from the real transition midpoints. Nevertheless the midpoints are adequate measures for a comparative examination.

2.9 Substrate specificity of the His₆-tagged isoenzyme of the *Drosophila melanogaster* QC

In order to analyze the effect of the amino acid exchange on the kinetic parameters, the variants were incubated with five different substrates. These measurements were executed applying the photospectroscopic and the fluoroscopic activity assay described above (*cf.* Section 2.6.1 and

Section 2.6.2). In the focus of interest were the K_M value, the turnover number (k_{cat}) as well as the catalytic efficiency (k_{cat}/K_M). The K_M value or Michaelis – Menten constant of a substrate reflects the affinity between an enzyme and a substrate. The turnover number specifies the number of conversions per second per active center. A further important measure for enzyme reactions is the catalytic efficiency k_{cat}/K_M . The catalytic efficiency considers both values k_{cat} and K_M . In some cases, it was not possible to measure under substrate saturation. This means, the applied substrate concentration is much smaller than the K_M . The k_{cat}/K_M is a suitable value for comparing the preference of the enzyme for a particular substrate [85].

When QQ, QGP or QFRH were used as substrates, the measurements were performed by employing the UV/Vis absorption spectrophotometric assay (*cf.* Section 2.6.1). On the other hand, the substrates Q- β NA and Q-AMC were studied with the fluorescence spectroscopic assay (*cf.* Section 2.6.1). In both cases the experiments were measured with the microplate reader. The substrate specificity was determined by measuring the reaction rates subject to substrate concentration. From the obtained velocity/substrate concentration characteristic the kinetic constants were derived by fitting these curves according to equation 3. It should be noted that the respective measurements for the *isoDromeQC* wild type enzyme have been performed by the Probiodrugs company.

For some variants it was important to adjust the protein concentration according to Table 2.5. Due to the low solubility of the substrates in aqueous solution the maximum concentration used in those experiments was limited to 1.5 mM for Q- β NA and Q-AMC and 3 – 4 mM for QQ, QGP and QFRH.

2.9.1 Data analysis

The kinetic constants K_M and V_{max} were calculated by fitting eight data points (measured in triplicates) to the Michaelis-Menten equation (3).

$$v = V_{max} \cdot \frac{[S]}{K_M + [S]} \quad (\text{equation 3})$$

v = enzyme reaction velocity (U/mg)

V_{max} = enzyme reaction velocity under substrate saturation (U/mg)

$[S]$ = substrate concentration (mM)

K_M = Michaelis - Menten constant (substrate concentration at half of V_{max} (mM))

V_{max} can be converted into k_{cat} by applying the following equation 4.

$$k_{cat} = \frac{V_{max} \cdot MW}{60000} \quad (\text{equation 4})$$

k_{cat} = turnover number (s^{-1})

MW = molecular weight of the QC (37883.3 g/mol, 38706.2 g/mol with His₆ tag,)

60000 = conversion factor

Division of k_{cat} by K_M results in the catalytic efficiency k_{cat}/K_M .

Table 2.5 Applied enzyme concentrations for the determination of substrate specificity.

Variant	QQ	QGP	QFRH	Q-βNA	Q-AMC
D228N	2.12	--	0.50	1.05	1.05
D293N	2.25	0.73	0.60	1.50	1.50
D293A	1.78	1.77	0.60	--	--
E190Q	5.59	--	--	3.00	3.00

Concentrations (mg/ml) of the variants depending on the used substrate.

2.10 pH Dependence of the isoenzyme of the *Drosophila melanogaster* QC and their variants

In order to identify amino acids that might act as acid-base catalysts during reaction, the catalytic efficiency (k_{cat}/K_M) of different QC variants was determined at varying pH values using the substrate Q- β NA. These measurements were performed under first-order reaction conditions at which the applied substrate concentration is significantly (10 fold) lower than the respective K_M value ($[S] \ll K_M$). The auxiliary enzyme pGAP has been tested and found to be stable at pH values from pH 5.5 to pH 8.5 by Tsuru and co-workers [81].

To ensure, that the buffer covers the whole pH range from 5.3 to 9.0 the variants were transferred in a three-component-buffer-system which provides a constant ionic strength [86]. This buffer system contains 100 mM Tris/HCl, 50 mM Mes and 50 mM sodium acetate. The applied microplate reader was set to a temperature of 30°C. The reaction was started by adding the enzyme after an incubation time of 15 minutes.

2.10.1 Data analysis

The bell-shaped curves were analyzed with the KaleidaGraph software. The rates were fitted to the nonlinear regression equation (5).

$$\frac{k_{cat}}{K_M} = [k_{cat}/K_M]_{\max} \cdot \frac{1}{1 + 10 \exp(\text{p}K_{a1} - \text{pH}) + 10 \exp(\text{pH} - \text{p}K_{a2})} \quad (\text{equation 5})$$

k_{cat}/K_M	=	catalytic efficiency ($\text{s}^{-1}\text{mM}^{-1}$)
$[k_{cat}/K_M]_{\max}$	=	pH-independent maximum rate constant
$\text{p}K_{a1/2}$	=	dissociation constants of the catalytically important functional groups

2.11 Fast Kinetics applying the stopped-flow UV/Vis absorbance method

For the UV/Vis spectroscopic investigation of the electronic environment of the substituted Co(II) ion, the stopped-flow method was used in combination with the photo diode array. The rapid mixing of the stopped-flow device monitors the enzymatic reaction with a dead-time of 1.5 milliseconds. The upcoming signal can be followed via UV/Vis absorbance. The photo diode array enables the detection of all wavelengths of the UV/Vis-spectra simultaneously allows the acquirement of multiple spectra within a defined time range. For the stopped-flow experiments, the Co(II)-*isoDromeQC* wild type and variants Co(II)-*isoDromeQC_E190Q*, Co(II)-*isoDromeQC_D228N* and Co(II)-*isoDromeQC_D293N* were used. The enzyme was dissolved in 50 mM sodium phosphate buffer containing 100 mM sodium chloride at pH 6.8. Data acquisition was accomplished with settings shown in Table 2.7.

Table 2.6 Compound concentrations in the detection chamber after rapid mixing

Co(II)- <i>isoDromeQC</i> ...d/ compound	c^A
Wild type	0.106
E190Q, D293N	0.09
D228N	0.076
QQ, EW, EFRH	8.00
AFA	7.50
pEFRH	15.0

^{A)} Molar concentration of the variants or the compounds in mM.

Table 2.7 Stopped-flow data acquisition with the photo diode array

Setting	
Temperature	10.0 °C
Wavelength	190 nm – 750 nm
Split time base	0.10 s 10 points
	150 s 200 points
Stop syringe volume	150 µl
Path length	1.00 cm

After a baseline measurement, the spectrum of the used buffer was acquired. Subsequently the spectrum of the resting enzyme was recorded before the enzyme was rapidly mixed with the substrate or the inhibitor AFA. The stopped-flow-syringes were filled with QC and the respective substrate or imidazole. In the detection chamber the compounds were mixed in a ratio of one to one. The final concentrations are given in Table 2.6.

2.11.1 Data analysis

The spectra were normalized by setting the absorbance at a wavelength of 750 nm to zero utilizing the software “SX-Prodata Viewer”. Single spectra were assessed with SigmaPlot 11 software.

2.12 Electron paramagnetic resonance spectroscopy (EPR)

2.12.1 Fundamental aspects of EPR spectroscopy and special details regarding the utilized techniques

The electron paramagnetic resonance spectroscopy delivers insights into the nature of interactions between an unpaired electron and its environment. In biological systems unpaired electrons appear in bioorganic radicals and in numerous biological active metal centers. An electron with the spin quantum number $S = \frac{1}{2}$ has the magnetic components $m_s = +\frac{1}{2}$ and $m_s = -\frac{1}{2}$. In a magnetic field the magnetic moments adopt a parallel ($m_s = +\frac{1}{2}$) or anti-parallel orientation ($m_s = -\frac{1}{2}$) to the magnetic field. According to the Zeeman Effect (Pieter Zeeman 1882) the energy states of both orientations diverge equidistantly around the zero-field energy ($E = 0$) and are proportional to the effective magnetic field (B_{eff}) (cf. Figure 2.1). The proportionality between the magnetic field and the energy difference is described by the factor g [97].

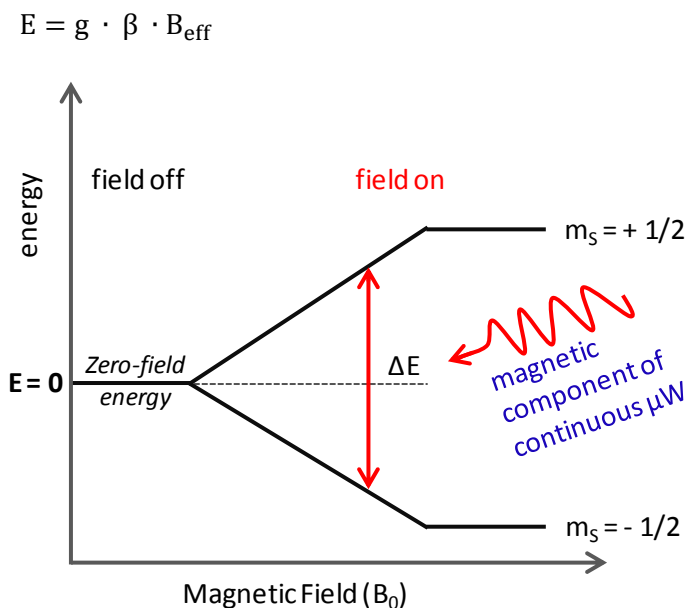


Figure 2.1 Proportionality between the outer magnetic field (B_0) and the difference (ΔE) of the energy states.

An unpaired electron can switch between both orientations or rather between both energy states by absorbing or emitting energy.

2 Materials and Methods

In EPR spectroscopy techniques, the absorption of the magnetic component of microwave radiation is exploited to change the spin into the high-energy state. The resonant absorption of energy can be monitored as an EPR spectrum.

$$E = h \cdot \nu = g \cdot \beta \cdot B_{\text{eff}} \quad (\text{equation 7})$$

E	=	energy difference of the spin orientations
h	=	Planck's constant
ν	=	microwave frequency
g	=	constant of proportionality
β	=	Bohr magneton
B_{eff}	=	effective magnetic field

The resulting EPR spectrum is rich in information about the compound of interest. The spectrum delivers compound specific g values. But the information cannot be read out directly for the following reasons:

The applied magnetic field (B_0) and the effective magnetic field B_{eff} which affects the unpaired electron are divergent. The g value for a free electron *in vacuo* was determined to be $g_e = 2.00232$ in a resonance field of 3390 Gauss and a microwave frequency of 9500 MHz (X-band). In a molecule an electron is exposed to a couple of magnetic interactions. Among others, interactions occur between electron spins and nuclear spins (S*I) or between electron spins and electron spins (S*S). These additional compound-internal magnetic fields (δB) change the equation for the resonance condition as follows (equation 8) [97]:

$$E = h \cdot \nu = g_e \cdot \beta \cdot (B_e + \delta B) \quad (\text{equation 8})$$

g_e	=	g value of the free electron <i>in vacuo</i>
B_e	=	external magnetic field
δB	=	internal magnetic field

The unknown quantity δB is reflected by the g value. So the condition for the resonant absorption is now (9):

$$E = h \cdot \nu = (g_e + \delta g) \cdot \beta \cdot B \quad (\text{equation 9})$$

Finally δg is the value which holds the whole information of a molecule. This quantity contains the information of the electronic structure of a molecule [97].

2.12.2 Anisotropy

Caused by randomly oriented molecules in a powder or frozen liquid EPR sample, the molecules have different orientations to the external field vector. If one imagines a molecule in Cartesian diagram with the magnetic field vector along the z axis, in the EPR spectrum a certain g-value (g_z) appears. If the molecule rotates along the x or y axis, the molecule changes its orientation with respect to the field vector. In the resulting EPR spectra there are two further possible g values g_y and g_x . Depending on the molecule's symmetry, the three g values can have three different relations to each other. In an isotropic molecule all g values are equal ($g_x=g_y=g_z$). In the case of $g_x=g_y \neq g_z$ the molecule is axial, and it is rhombic if all three g-values are unequal ($g_x \neq g_y \neq g_z$). From these g values one can read out information regarding bond angles and bond length as well as the coordination number [97].

2.12.3 System parameters

2.12.3.1 Temperature and Power

In accordance with the Boltzmann distribution (equation 10), at a thermal equilibrium a certain number of molecules (n_0) are in the lowest energy state and a certain number of molecules (n_1) are in the highest energy state.

$$n_0 = n_1 \cdot \exp(-\Delta E/k \cdot T) \quad (\text{equation 10})$$

ΔE = energy difference between highest and lowest energy state

k = Boltzmann constant ($0.695 \text{ cm}^{-1} \text{ K}^{-1}$)

K = absolute Temperature in Kelvin

At $T = 0 \text{ K}$ all molecules are in the ground state. With increasing temperature the number of molecules in the highest energy state increases. At an infinite high temperature n_1 and n_0 become equal. To facilitate the absorption of the magnetic component of the microwave

2 Materials and Methods

radiation, a certain difference between both populations ($n_1 < n_0$) has to be available in the EPR sample. The smaller the differences between n_1 and n_0 , the smaller becomes the signal intensity. Further, the velocity of the energy transfer from the high-energy-state molecules to the environment (spin-lattice relaxation) decreases with decreasing temperature. The slower the spin-lattice relaxation rate the longer the life-time of a molecule in the high energy state (excited state). From the Heisenberg uncertainty principle it is known that the longer the life-time of the excited state, the higher is the accuracy of the excited state energy. This accuracy of the excited state energy narrows the EPR linewidth and increases the signal amplitude. On the other hand, higher temperature would broaden the band linewidth.

The optimal power of the applied microwave interacts with the temperature and has to be determined experimentally. The aim of this optimization procedure is to obtain a sharp EPR spectrum with a high signal-to-noise ratio. Too low microwave power at a certain temperature changes the signal-to-noise ratio to the worse. If the microwave power is too high, the spin-lattice relaxation at a certain temperature becomes the limiting factor and saturation effects would deform the EPR spectra. In this case, an increase in temperature could improve the shape of the EPR bands but also could lead to homogenous band broadening [97].

The microwave power and the temperature need to be adjusted carefully for each system.

The experiments were carried out at three different temperatures. To yield a proper $S = 3/2$ EPR signal, the temperature was set to 4 K. Occurring $S = 1/2$ signals were observed at 10 K or 25 K. The power of the microwave was set 20 mW.

2.12.3.2 Continuous wave X-band EPR

To fulfill the resonance condition given in equation 7, there are two possibilities. The first is to keep the magnetic field (B) constant and change the frequency (ν) of the microwave. The second, and for technical reasons favored, possibility is a continuous frequency and a variable magnetic field. The designation X-band stands for a frequency of 9500 MHz [97].

2.12.4 EPR-experiments with Co(II)-substituted enzymes

The Zn(II)-dependent glutamyl cyclase does not bear any spectroscopically detectable feature which allows the observation of single mechanistic steps *e.g.* by the accumulation of reaction

intermediates. The catalytically active Zn(II) is a diamagnetic transition metal and EPR and UV/Vis spectroscopic inactive.

With Co(II) as a virtually equivalent substitute for Zn(II), a spectroscopically detectable probe can be inserted into the active center of the QC molecule. Zn(II) and Co(II) exhibit comparable atomic properties. The ionic radii for octahedral Zn(II) and Co(II) ions are nearly the same (Zn(II) 0.88 Å and Co(II) 0.89 Å). Further the electro-negativities according to the Allred-Rochow scale are similar (Zn(II) 1.66 and Co(II) 1.70). Both transition metals can adopt a four- or five-fold coordination [87]. In some proteins the five- or six-coordinated Co(II) replaces tetrahedral coordinate Zn(II). In these cases, often the resulting EPR spectra lead to an incorrect interpretation [87] [63] [88, 89]. Co(II) substituted enzymes exhibit a high-spin EPR signal of $S = 3/2$. To obtain reliable signals these measurements have to be accomplished at very low temperatures and high microwave power. This is due to the very fast relaxation of the excited state [87]. A further challenge is the high protein concentration which is required in the high-spin cobalt EPR experiments, especially for the Rapid-freeze-quench-EPR experiments. A characteristic of the $S = 3/2$ EPR signals is that they are broad and small in intensity. For proper signals and an adequate signal-to-noise ratio, concentrations of at least 0.2 mM are necessary.

2.12.5 Experimental procedures and methods

All EPR experiments were accomplished under the supervision of Prof. Dr. Brian Bennett in the Department of Biophysics of the Medical College of Wisconsin (USA).

The goal of these experiments was to investigate the coordination sphere of the substituted and the catalytic active Co(II) ion in the active center of the Co(II)-isoDromeQC wild type and the variants Co(II)-isoDromeQC_E190Q, Co(II)-isoDromeQC_D228N plus Co(II)-isoDromeQC_D293N. The proteins were analyzed in their resting state and with the addition of glutamyl substrates, glutamyl substrates as well as an inhibitor and a pyroglutamyl compound. Along with the coordination number of the coordination sphere, the changes in the geometry of the Co(II) ion was a matter of interest in this examination.

2.12.5.1 Sample preparation

The different freeze-quench techniques described below require different protein concentrations to obtain adequate signal-to-noise ratios. Further it was necessary to perform these experiments with multiple protein preparation batches. The applied concentrations as well

2 Materials and Methods

as the incubation times of the protein and the reaction partners are presented in the Results section. For the measurements the EleXsys E600 (Bruker BioSpin Corporation, Billerica, USA) spectrometer was applied. The cooling to the very low temperature was achieved utilizing liquid helium.

2.12.5.2 Samples which require a long reaction time

To observe the Co(II) coordination when the formation of intermediates or product was suggested to be very slow, the equilibration time was prolonged to minutes or hours.

Samples that should be scanned after such a long reaction time (substrates) or incubation time (inhibitors and product) were pipetted in an EPR quartz tube. After the desired incubation time the tube was transferred in liquid nitrogen to stop the reaction.

2.12.5.3 Manual freeze-quench EPR

For a reaction time in the seconds range, the first component (enzyme) was poured into an EPR tube. The rapid mixing of the two components was achieved by emptying a syringe filled with the second component (*e.g.* substrate) in the EPR tube. The mixture was freeze-quenched in cryogenic isopentane (153 K).

2.12.5.4 Rapid freeze-quench EPR

To examine the cobalt coordination in the pre-steady-state phase, the reaction has to be stopped as early as possible. A pre-experiment showed that an incubation time of 20 milliseconds led to reliable signals. For these rapid freeze-quench trials a self-made device was available. Here the enzyme and the substrate were filled in separate syringes. The automated drain of the syringes into a mixing chamber and the liberation of the mixture into isopentane guaranteed the observance of the desired reaction time. The samples were stored in liquid nitrogen.

2.12.5.5 Sample concentration

The concentrations of protein stock solutions were in a range of 600 μM in some cases higher. The accurate concentrations were specified in the results section. The ligand stock solutions were concentrated as follows: for the slow freezing and manual freezing technique the substrate QQ, QFRH, EFRH, EW and the product pEFA were concentrated to 30 mM. The inhibitors were

2 Materials and Methods

used in a concentration of 15 mM for AFA. For the RFQ technique QFRH was concentrated to 10 mM and QQ to 30 mM.

For the measurements the proteins and the ligands were mixed in a ratio of 1:1. For the RFQ technique a higher protein concentration was required. In these cases the mixing ratio was 2 (protein):1 (ligand).

2.12.6 Data analysis

For data analysis the software XSophe was utilized for computer simulations. The g values were calculated using equation 7.

3 Results

3.1 Thermal stability study of His₆-tagged Zn(II)-isoDromeQC wild type and the variants employing CD-spectroscopy

3.1.1 Substitution of active center residues as a tool for structure-function analysis

Crystal structures of former investigators [74, 75] and structural comparison of QCs with the putatively evolutionary ancestor - a bacterial aminopeptidase [60] - implicates that particular amino acid residues are involved in discrete mechanistic steps of catalysis.

To explore the role of active center amino acid residues in the native enzyme (Zn(II)-isoDromeQC wild type) in detail, they were substituted by utilizing site-directed mutagenesis. The plasmid DNA of the variants Zn(II)-isoDromeQC_D228N, Zn(II)-isoDromeQC_E190Q, Zn(II)-isoDromeQC_D293A and Zn(II)-isoDromeQC_D293N was provided by the Probiodrugs Company. The recombinant expression and purification of these variants was accomplished according to the previously described protocols (*cf.* Section 2.1 – 2.3).

Electronically negatively charged, amino acid residues were exchanged for uncharged but isosteric residues (Zn(II)-isoDromeQC_E190Q, Zn(II)-isoDromeQC_D228N and Zn(II)-isoDromeQC_D293N) and uncharged and non-isosteric amino acid residue (Zn(II)-isoDromeQC_D293A).

3.1.2 Amino acid substitution may influence the structural stability

The examination of the conformational stability is in most cases the initial work on an enzyme after the preparation. In particular, when working with different enzyme variants which are created by site directed-mutagenesis, it is important to assure that substitution of a single amino acid residue does not impair the conformational stability of the enzyme. Along with the chemical unfolding achieved by adding guanidinium hydrochloride or urea, the unfolding transitions can be induced by the pH and ionic strength. In this work, the choice fell on heat-induced unfolding. The thermal denaturation is in case of Zn(II)-isoDromeQC an irreversible process as has been determined in initial pre-experiments (*cf.* Supplemental 8.3). Nevertheless the merit lies in the

3 Results

straightforwardness of this approach. The reversibility is not essential if one only wants to compare the midpoints (melting point (T_M)) of the unfolding transition curves. The melting point correlates with the inflection point of the unfolding transition curve and can be calculated by a curve fit based on equation 2 (*cf. Section 2.8.1*).

The thermal denaturation (unfolding) experiment was done by measuring changes in the composition of secondary structure elements (*e.g.* α -helices, β -sheets, etc.) with circular dichroism spectroscopy in the far UV range. In this wavelength range, absorption occurs due to the peptide bond with its $n \rightarrow \pi^*$ transitions in the region around 220 nm and around 190 nm. In this experiment the maximum change of absorption was determined at 196 nm. While observing the CD signal at this wavelength, the protein sample (0.1 mg/ml in 10 mM potassium phosphate buffer at pH 6.8) was heated gradually from 283 K to 360 K (*cf. 2.8*)

Figure 3.1 and Table 3.1 present the results of these experiments. The curves show three distinct phases. The first linear phase in the low temperature region from 283 K to approximately 310 K. The second phase describes a sigmoid shaped decay from 310 K to 340 K. The third phase is again linear and comprises the temperature range between 340 K and the 360 K.

This study shows that the decay of the curves of the Zn(II)-isoDromeQC wild type and the variants Zn(II)-isoDromeQC_E190Q and Zn(II)-isoDromeQC_D228N starts at higher temperatures compared to those of the variants Zn(II)-isoDromeQC_D293A and Zn(II)-isoDromeQC_D293N (*cf. Figure 3.1*). Hence, the determined midpoints of the transition curves of Zn(II)-isoDromeQC wild type and Zn(II)-isoDromeQC_E190Q and Zn(II)-isoDromeQC_D228N can be found at higher temperatures compared to those of Zn(II)-isoDromeQC_D293A and Zn(II)-isoDromeQC_D293N (*cf. Table 3.1*).

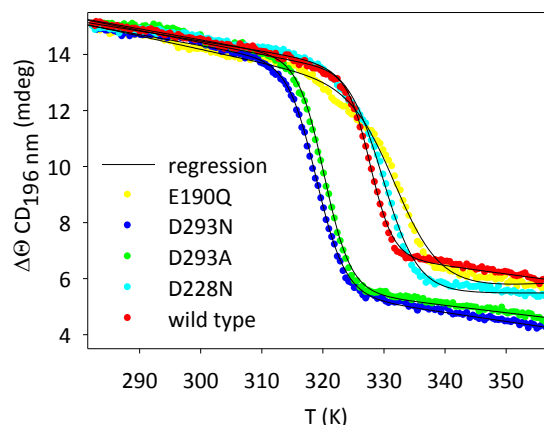


Figure 3.1 Thermal denaturation curves of Zn(II)-isoDromeQC wild type and variants monitored by measuring the ellipticity employing CD spectroscopy at 196 nm The temperature ramping from 283 K to 360 K of the protein samples (approx. 0.1 mg/ml) leads to different transition (denaturing) curves. The decay of the curves of Zn(II)-isoDromeQC wild type (red dots), Zn(II)-isoDromeQC_E190Q (yellow dots) and Zn(II)-isoDromeQC_D228N (cyan dots) starts at higher temperatures than for the variants Zn(II)-isoDromeQC_D293A and Zn(II)-isoDromeQC_D293N. The regression curve (continuous line) is based on equation 2 (cf. 2.8.1) and allows the calculation of the theoretical midpoints of the thermal transition (cf. Table 3.1). Measurements were performed in 10 mM phosphate buffer at pH 6.8.

Table 3.1 Midpoints (T_M) of the thermal unfolding transition curves The ellipticity was measured by using CD-spectroscopy at 196 nm in 10 mM phosphate buffer at pH 6.8 in a temperature range between 283 K (10° C) and 360 K (87° C). The calculated midpoints of transition (cf. equation 2 and Section 2.8.1) are converted in °C. Standard deviations of the triplicates are in brackets.

variant	T_M [°C]
wild type (His ₆)	55 (± 2.00)
E190Q (native)	59 (± 0.00)
D293N (His ₆)	46 (± 1.73)
D293A (His ₆)	48 (± 1.00)
D228N (His ₆)	57 (± 1.53)

3.2 Kinetic investigation of His₆-tagged Zn(II)-isoDromeQC wild type and variants using photospectroscopic methods indicate a distinct substrate specificity pattern

The preference of a substrate can be investigated by determination of the kinetic constants K_M (Michaelis-Menten constant), the turnover number k_{cat} and the catalytic efficiency k_{cat}/K_M . From the structure, steric properties and partial charges of a highly preferred substrate, conclusions can be drawn about the architecture of an enzyme binding pocket, or the active center.

The kinetic constants K_M and k_{cat} were determined under steady state conditions (substrate concentrations beyond K_M , $[S] > K_M$). For that purpose, the reaction velocity was measured subject to substrate concentration $[S]$. The K_M and k_{cat} were obtained by fitting the resulting velocity/substrate concentration dependence curve ($v/[S]$ -characteristic) to equation 3 (cf. Section 2.9.1). Applying equation 4 (cf. Section 2.9.1) k_{cat} can be calculated. The catalytic efficiency was calculated by division of k_{cat} by K_M . Due to the low solubility of the peptide substrates, in many cases the applied substrate concentration was equal or slightly below the K_M . In case of Zn(II)-isoDromeQC_D293N/A with the substrate QGP and Zn(II)-isoDromeQC_D293A with QQ, the k_{cat}/K_M was assessed under first order rate conditions with substrate concentrations of one tenth of the K_M .

This substrate specificity study was carried out by utilizing UV/Vis absorption spectroscopy (cf. Section 2.6.1) and fluorescence spectroscopy (cf. Section 2.6.2). All measurements were done using the microplate reader (POLARstar optima, BMG Labtech GmbH, Ortenberg, Germany) at 30° C in 50 mM Tris/HCl, pH 8.0.

The substrate specificity pattern of the Zn(II)-isoDromeQC wild type was investigated in the past by the Probiobdrug Company [73]. It has been shown that for Zn(II)-isoDromeQC wild type, the efficiency of substrate conversion increases with the peptide length. Further, the catalytic efficiency increases if the substrate contains a positively charged residue. In contrast, a negative charge leads to higher K_M values and a reduction of the catalytic efficiency. Along with these observations it could be demonstrated that the turnover number increases and K_M value decreases if the second N-terminal position of the substrate is occupied by an aromatic amino acid [73].

According to these findings, the following peptides and peptide surrogates were chosen to carry out analogous investigation of the corresponding variants of the active center amino acid residues D228, E190, D293 (cf. Section 3.1).

QQ and QGP represent uncharged di- and tripeptides, respectively. QFRH as a tetrapeptide consists of a hydrophobic and aromatic system in the second position and a positively charged arginine at position three. The dipeptide surrogates Q- β NA and Q-AMC also represent substrates with an aromatic system in the second position.

Figure 3.2 and Table 3.2 depict the kinetic constants of the Zn(II)-isoDromeQC wild type and the variants. The substrate specificity study points out a dramatically impaired catalysis if one of the amino acid residues as outlined above has been exchanged. The variants exhibit catalytic efficiencies below one per mill in comparison to the wild type. Nevertheless, the variants exhibit a wild type-like substrate specificity pattern. The ranking of the substrates with reference to rate constant and the K_M value is similar to that of the Zn(II)-isoDromeQC wild type enzyme. Measurements with shorter peptides QQ and QGP show the highest K_M values except for the E190Q variant. Significantly declined Michaelis-Menten constants are observed in the case of the substrates QFRH and both peptide surrogates Q-AMC and Q- β NA.

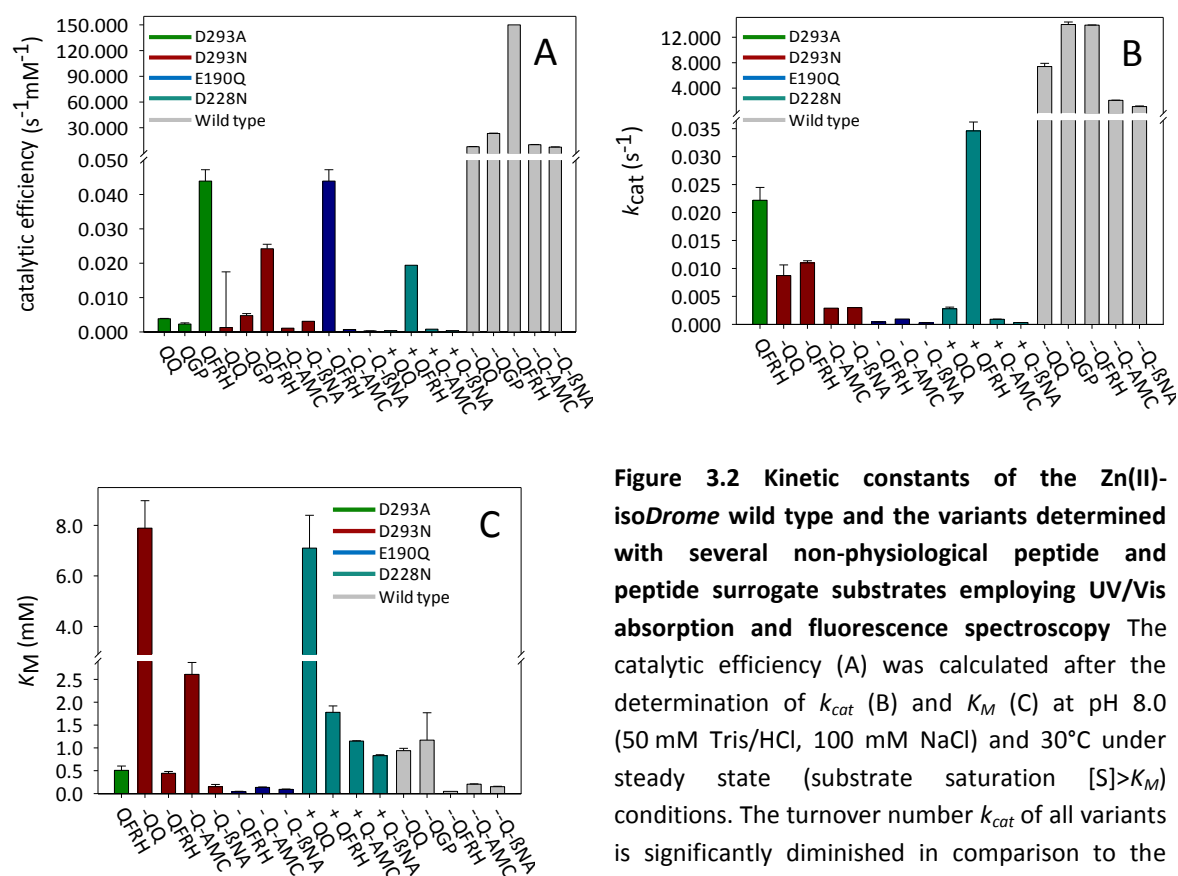


Figure 3.2 Kinetic constants of the Zn(II)-isoDrome wild type and the variants determined with several non-physiological peptide and peptide surrogate substrates employing UV/Vis absorption and fluorescence spectroscopy The catalytic efficiency (A) was calculated after the determination of k_{cat} (B) and K_M (C) at pH 8.0 (50 mM Tris/HCl, 100 mM NaCl) and 30°C under steady state (substrate saturation $[S] > K_M$) conditions. The turnover number k_{cat} of all variants is significantly diminished in comparison to the Zn(II)-isoDromeQC wild type.

However, when QQ, QGP and QFRH were used as substrate, higher turnover numbers with a rough tendency of longer peptides showing higher k_{cat} could be observed. The peptide

3 Results

surrogates show better K_M values than QQ and QGP. Conversely, measurements with peptide surrogates Q-AMC and Q- β NA yield worse rate constants.

In general, the longest peptide with the aromatic system and the electronically positively charged residue QFRH shows the highest catalytic efficiency in reaction with the wild type as well as the variant. The high catalytic efficiency is also a result of the very low K_M value of this substrate.

Side chain substitution of D293 leads to higher Michaelis-Menten constants. In case of D293A, the K_M value is too high for a reliable determination with low-solubility substrates. A more moderate but also low substrate affinity was observed if D293 was replaced by an isosteric asparagine (Zn(II)-isoDromeQC wild type_D293N).

The D228N variant yielded similar results. For all tested substrates K_M values were determined that were at least five-fold higher than that of Zn(II)-isoDromeQC wild type. Along with the Zn(II)-isoDromeQC_D228N, Zn(II)-isoDromeQC_E190Q shows k_{cat} and k_{cat}/K_M values that are reduced by the factor of 10,000 compared to the values determined for the Zn(II)-isoDromeQC wild type. Conversely, the measurements with the Zn(II)-isoDromeQC_E190Q variant yield lower K_M values for all measured substrates.

Table 3.2. Kinetic constants of the Zn(II)-isoDromeQC wild type and the variants measured with diverse substrates The kinetic constants K_M and k_{cat} were determined using UV/Vis absorption (cf. 2.6.1) and fluorescence (cf. 2.6.2) spectroscopy at pH 8.0 and 30 °C under steady state conditions ($[S] > K_M$).

	K_M (mM)		k_{cat} (s ⁻¹)		k_{cat}/K_M (mM ⁻¹ s ⁻¹)	
wild type						
QQ	0.94	± 0.05	7.4	± 0.5	7.9	± 0.2 ^A
QGP	1.17	± 0.6	14.0	± 2	23.4	± 0.4 ^A
QFRH	0.048		13.9		150.0	
Q-AMC	0.205	± 0.008	2.09	± 0.03	10.2	± 0.3 ^A
Q-βNA	0.15	± 0.01	1.1	± 0.1	7.4	± 0.3 ^A
D293A						
QQ	<i>n.d.</i>		<i>n.d.</i>		3.8 *10 ⁻³	± 0.1*10 ⁻³ ^B
QGP	<i>n.d.</i>		<i>n.d.</i>		2.3 *10 ⁻³	± 0.3*10 ⁻³ ^B
QFRH	0.51	± 0.09	22.2*10 ⁻³	± 2.3*10 ⁻³	43.5 *10 ⁻³	
D293N						
QQ	7.9	± 1.1	8.7*10 ⁻³	± 1.9*10 ⁻³	1.1*10 ⁻³	
QGP	<i>n.d.</i>		<i>n.d.</i>		4.8*10 ⁻³	± 0.6*10 ⁻³ ^B
QFRH	0.45	± 0.04	11.0*10 ⁻³	± 0.4*10 ⁻³	24.2*10 ⁻³	
Q-AMC	2.61	± 0.26	2.9*10 ⁻³	± 0.2*10 ⁻³	1.1*10 ⁻³	^C
Q-βNA	0.97	± 0.05	3.0*10 ⁻³	± 0.1*10 ⁻³	3.1 *10 ⁻³	^C
E190Q						
QQ	0.04	± 0.01	0.43*10 ⁻³	± 0,03*10 ⁻³	10.75*10 ⁻³	^C
Q-AMC	0.14	± 0.008	0.97*10 ⁻³	± 0.02*10 ⁻³	6.9*10 ⁻³	^C
Q-βNA	0.085	± 0.008	0.27*10 ⁻³	±0.03*10 ⁻³	3.0*10 ⁻³	^C
D228N						
QQ	7.1	± 1.3	2.80*10 ⁻³	± 0.29*10 ⁻³	0.40*10 ⁻³	^C
QFRH	1.78	± 0.14	34.6*10 ⁻³	± 1.6*10 ⁻³	19.4*10 ⁻³	^C
Q-AMC	1.15	± 0.065	0.92*10 ⁻³	± 0.03*10 ⁻³	0.80*10 ⁻³	^C
Q-βNA	0.83	± 0.02	0.333*10 ⁻³	± 0.003*10 ⁻³	0.40*10 ⁻³	^C

^A) Results from the Probiodrugs Company [73]

^B) k_{cat}/K_M calculated by division of k_{cat} by K_M which were determined under steady state conditions ($[S] > K_M$).

^C) k_{cat}/K_M determined under first-order rate conditions ($[S] \ll K_M$).

n.d. not determinable

3.3 Catalytic efficiency measurements as a function of the pH

Concerted acid-base catalysis is a common enzymatic mechanism. Many amino acid side chains are enabled to donate (acidic) or to receive (alkaline) protons from a functional group of the substrate or a proximate amino acid side chain. These proton transferring steps are able to reduce the free enthalpy of a transition state of an enzymatic reaction. Subsequently these steps become accelerated compared to the uncatalyzed reaction. To find out whether acid-base catalyzing amino acids are involved in the QC reactions, pH titration is a tool used to determine the pK_a values of such amino acid residues. To identify a putative acid-base catalyst, the amino acid residue of interest can be substituted by site-directed mutagenesis. In the event that the substituted amino acid is involved in proton transferring steps, we would expect a change in the pK_a values.

For this purpose, the catalytic efficiencies (k_{cat}/K_M) of the Zn(II)-isoDromeQC wild type and all variants were determined as a function of the pH using the fluorescence spectroscopy method (*cf.* Section 2.6.2). The catalytic efficiency was determined in equidistant steps from the mild acid to moderate alkaline pH range at 30° C utilizing the microplate reader (POLARstar optima, BMG Labtech GmbH, Ortenberg, Germany). From the resulting curve of the pH dependence, it is possible to obtain parameters like pK_{a1} (inflection point of the ascending branch), pK_{a2} (inflection point of the descending branch) as well as the maximum catalytic efficiency (k_{cat}/K_{Mmax}) by fitting this curve to equation 5 (*cf.* Section 2.10.1).

In a second experiment it was investigated whether different protonation states of functional groups of the substrate have effects on the catalysis. Therefore, K_M values as a measure for the substrate affinity were determined at three different pH values.

For this purpose, the reaction velocity under steady state (substrate saturation $[S] > K_M$) conditions was measured as a function of the concentration of Q-βNA as a dipeptide surrogate at 30°C using the fluorescence spectroscopic assay (*cf.* Section 2.6.2). Finally, the K_M was obtained by fitting the obtained velocity/substrate concentration dependence curve ($v/[S]$ -characteristic) to equation 3 (*cf.* Section 2.9.1).

The pH dependence of the catalytic efficiency of the Zn(II)-isoDromeQC wild type (*cf. Figure 3.3 A*) exhibits a relatively narrow and symmetric bell-shaped curve with a maximum of catalytic efficiency ($k_{cat}/K_{M\ max}$) between 7.5 and 8. The determined pK_a values around pH 6.56 and pH 9.10 (*cf. Table 3.2*) are reproducible. This result tallies well with a former study carried out by the Probiobdrug Company [73]. The pH profiles of the variants (*cf. Figure 3.3 B – E*) do not reveal any outstanding changes. The observed maximum of k_{cat}/K_M varies in small ranges around pH 7.9. The pK_a values of the acid-base catalysts remain almost equal.

Table 3.3-1 Catalytic efficiency subject to the pH

Calculated parameters of Zn(II)-isoDromeQC wild type and variants. The pH optimum corresponds to the maximum catalytic efficiency ($k_{cat}/K_{M\ max}$). $k_{cat}/K_{M\ max}$ and the pK_{oa} values were determined by fitting the obtained pH dependence curves (*cf. Figure 3.3*) to equation 5 (*cf. 2.10.1*).

	pH optimum	$k_{cat}/K_{M\ max}$ ($\text{mM}^{-1}\ \text{s}^{-1}$)	pK_{a1}	pK_{a2}
Zn(II)-isoDromeQC wild type	7.93	11.21 ± 0.78	6.56 ± 0.06	9.1 ± 0.02
Zn(II)-isoDromeQC_D228N	7.90	$0.747 \cdot 10^{-3} \pm 0.065 \cdot 10^{-3}$	6.33 ± 0.06	9.49 ± 0.07
Zn(II)-isoDromeQC_D293A	7.8	$3.37 \cdot 10^{-3} \pm 0.26 \cdot 10^{-3}$	6.79 ± 0.10	9.09 ± 0.15
Zn(II)-isoDromeQC_D293N	7.82	$1.08 \cdot 10^{-3} \pm 0.08 \cdot 10^{-3}$	6.38 ± 0.06	9.39 ± 0.04
Zn(II)-isoDromeQC_E190Q	8.10	$1.10 \cdot 10^{-3} \pm 0.16 \cdot 10^{-3}$	6.82 ± 0.04	9.45 ± 0.14

Table 3.3-2 K_M values determined under steady state conditions at different pH values The K_M values were determined by fitting the obtained $v/[S]$ -characteristic (*cf. text*) to equation 3 (*cf. 2.9.1*). The K_M values are given in mM of the used substrate Q- β NA employing the fluorescence spectroscopic assay (*cf. 2.6.2*) at 30° C in 100 mM Tris/HCl, 50 mM Mes and 50 mM sodium acetate.

Zn(II)-isoDromeQC ...						
pH	wild type K_M (mM)	pH	E190Q K_M (mM)	D293N K_M (mM)	D293A K_M (mM)	D228N K_M (mM)
5.24	2.6 ± 0.4	5.80	<i>n.d.</i>	2.02 ± 0.66	<i>n.d.</i>	1.20 ± 0.2
7.00	0.73 ± 0.03	7.00	0.43 ± 0.011	1.83 ± 1.25	4.35 ± 0.70	0.34 ± 0.02
8.39	0.60 ± 0.05	8.39	0.31 ± 0.025	1.60 ± 0.18	3.42 ± 0.30	0.56 ± 0.09

n.d. not determinable

The results of the second part of the experiment show that the K_M values determined from $v/[S]$ -characteristic at different pH conditions decrease with rising pH (*cf. Table 3.3*).

Notwithstanding the extremely decreased catalytic deficiency, the pH profiles of the variants are nearly equal to the wild type.

3 Results

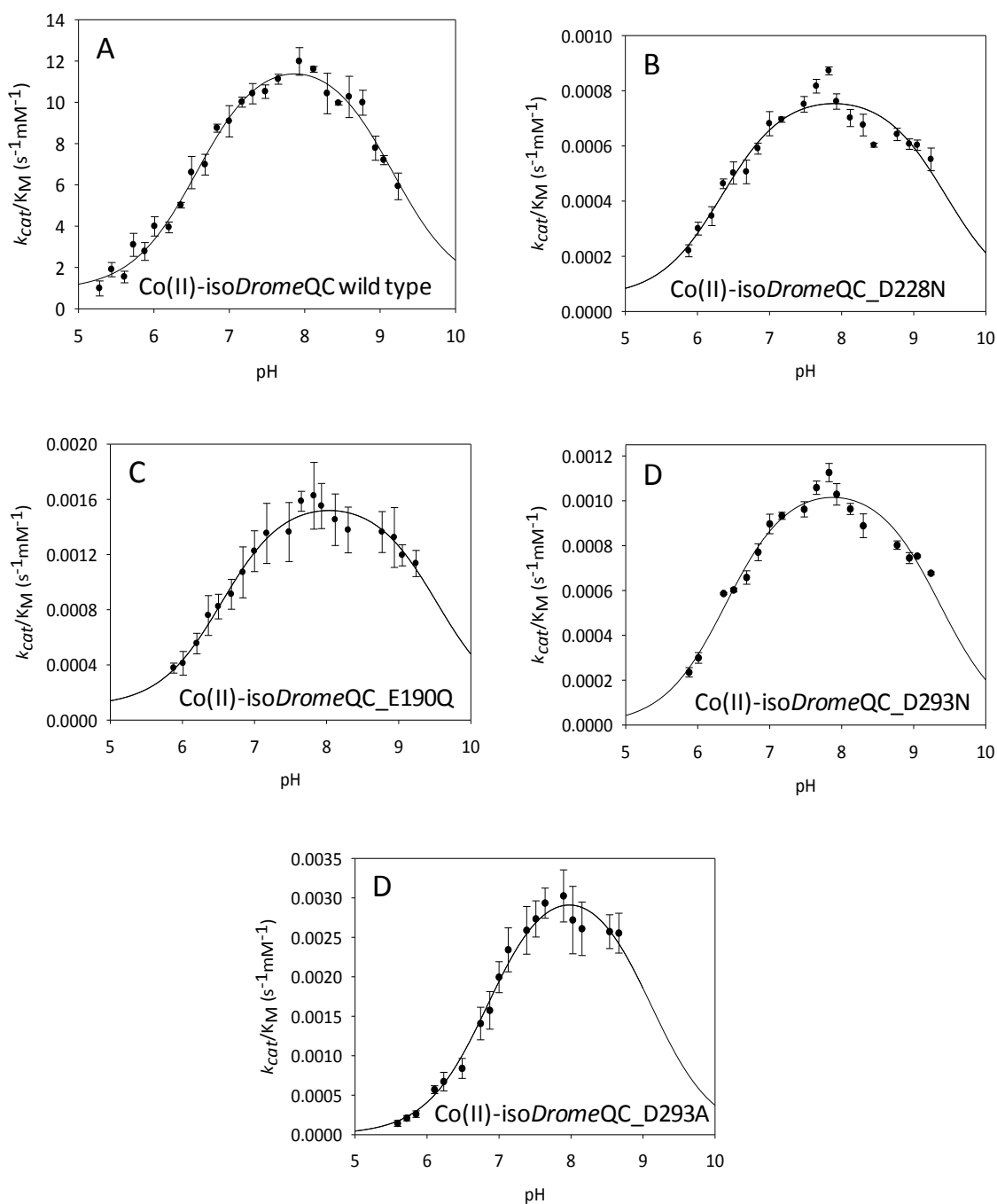


Figure 3.3 Catalytic efficiencies (k_{cat}/K_M) of Zn(II)-isoDromeQC wild type and variants as a function of the pH The catalytic efficiency of Zn(II)isoDromeQC wild type (A) and the variants (B-E) was measured under first-order law conditions ($[S] \ll K_M$), i.e. that the Q- β NA concentration was around one tenth of the pre-experimentally determined K_M (Zn(II)-isoDromeQC wild type: 11.85 μ M, (Zn(II)-isoDromeQC_D228N: 43.50 μ M, (Zn(II)-isoDromeQC_E190Q: 19,75 μ M, (Zn(II)-isoDromeQC_D293N: 99.5 μ M and (Zn(II)-isoDromeQC_D293A: 320 μ M). The error bars reflect the standard deviation, conveyed from multiple determinations. Measurements were executed in 100 mM Tris/HCl, 50 mM Mes and 50 mM sodium acetate at varying pH values at 30 °C. The calculated pK_a values (cf. Table 3.2) and the obtained pH optimum (pH at maximum k_{cat}/K_M) of the variants do not vary significantly from that of the Zn(II)-isoDromeQC wild type. The k_{cat}/K_M of the variants is significantly diminished.

3.4 Stopped-flow UV/Vis absorption analysis of Co(II)-*isoDromeQC* wild type and variants

In order to detect direct interactions between the catalytically active metal ion and several components including substrates, reaction intermediates, reaction products and inhibitors, the stopped-flow technique was utilized. The stopped-flow device mixes the enzyme and the component of interest together within milliseconds. That allows the observation of the reaction after a very short dead time of 1.5 milliseconds. As the detecting device, the photo diode array was utilized in order to observe all wavelengths spontaneously in a range of 185 nm – 723 nm by UV/Vis absorption spectroscopy.

In this experiment the Co(II)-substituted *isoDromeQC* has to be used because the native Zn(II)-*isoDromeQC* shows no band transitions in the UV/Vis absorption spectra. d-d Band transition of Co(II) in the active center of the QC allows photospectroscopic detection in a wavelength range of approx. 400 nm to 650 nm. The way to detect metal interaction in this experiment with the ligands described above is to observe changes in the UV/Vis absorption spectra due to distortions in the electronic environment of the enzyme bound Co(II). If the component is a substrate, it is possible to detect short-lived transition states during the catalysis.

The Co(II)-*isoDromeQC* wild type and the variants Co(II)-*isoDromeQC*_E190Q, Co(II)-*isoDromeQC*_D228N, Co(II)-*isoDromeQC*_D293N and all used ligand components were dissolved in 50 mM Tris/HCl, 100 mM NaCl, pH 6.8. All experiments were carried out at 10° C to slow down chemical reactions according to the correlation between reaction velocity and temperature. For the detailed experimental setup, see Section 2.11, Tables 2.6 and 2.7. For this purpose, the enzymes were shot together in two-fold concentration with buffer (50 mM Tris/HCl, 100 mM NaCl, pH 6.8). Due to mixing in a ratio of 1:1, the enzyme concentration (see below) is divided by a factor of two.

3.4.1 Stopped-flow UV/Vis absorption analysis of the resting state

The first step of all measurements was to monitor the enzyme in the resting state. The UV/Vis absorbance spectra of the Co(II)-*isoDromeQC* wild type (0.106 mM) and the variants Co(II)-*isoDromeQC*_E190Q (0.090 mM), Co(II)-*isoDromeQC*_D228N (0.076 mM), Co(II)-*isoDromeQC*_D293N (0.090 mM) indicate differences in the coordination sphere of the Co(II) ion. The Co(II)-*isoDromeQC* wild type (*cf.* Figure 3.4 A) exhibits three absorption bands at

3 Results

517 nm, 550 nm and 570 nm. Further, two small peaks can be observed in the range between 410 nm and 450 nm.

The E190Q (B) variant shows two distinct absorption bands at 513 nm and 571 nm. The absorption band at 550 nm, which was observed in the Co(II)-isoDromeQC wild type spectrum, is not clearly pronounced. In the range of 400 nm to 500 nm, different absorption bands become more prominent (e.g. 435 nm and 471 nm). In general, this range reveals higher absorbance as the wild type.

The major absorption bands in the spectrum of variant Co(II)-isoDromeQC_D293N (C) appear at 517 nm and 560 nm. In contrast to the Co(II)-isoDromeQC wild type and the Co(II)-isoDromeQC_E190Q and Co(II)-isoDromeQC_D228N, the peak at 517 nm is the dominant one. Two further defined peaks appear at 420 nm and 470 nm.

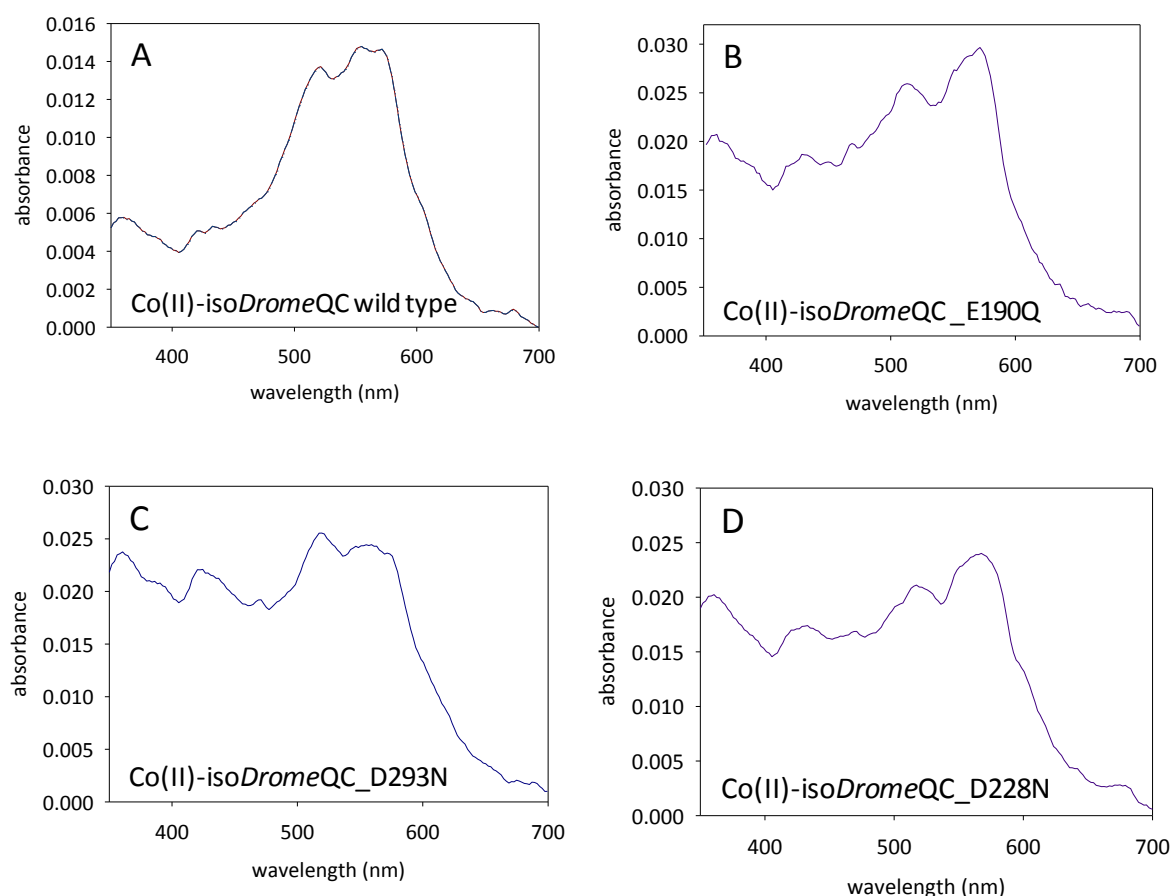


Figure 3.4 UV/Vis absorption spectra of Co(II)-isoDromeQC wild type and variants in the resting state The monitored resting state of the Co(II)-isoDromeQC wild type (A) and the variants (Co(II)-isoDromeQC_E190Q (B) Co(II)-isoDromeQC_D293N (C) and Co(II)-isoDromeQC_D228N (D)) reveal distinct absorption spectra. The measurements were carried out in 50 mM Tris/HCl, 100 mM NaCl, pH 6.8 at 10 °C using the stopped-flow device combined with the photo diode array. The molar concentration after mixing the proteins amounts to (Co(II)-isoDromeQC wild type) 0.106 mM, (Co(II)-isoDromeQC_E190Q, Co(II)-isoDromeQC_D293N) 0.09 mM and (Co(II)-isoDromeQC_D228N) 0.076 mM.

The absorption spectrum of the Co(II)-isoDromeQC_D228N variant (D) is comparable to the variants Co(II)-isoDromeQC_E190Q, Co(II)-isoDromeQC_D293N. Absorption bands can be observed at 431 nm, 471 nm, 517 nm and 567 nm. In general, all variants demonstrate a higher absorption in the region between 400 nm and 500 nm compared to the wild type.

3.4.2 Stopped-flow analysis of Co(II)-isoDromeQC wild type and the variants incubated with the substrate QQ

In this experiment, the focus of interest is on the detection of (short-lived) intermediates states during the enzyme reaction. According to the expectations that the substrate would interact with the catalytically active Co(II) ion, this interaction would lead to changes in the UV/Vis absorption spectra.

Therefore, the dipeptide substrate QQ was mixed with the Co(II)-isoDromeQC wild type and the variants. The enzyme concentrations are described above (*cf.* Section 3.4.1). The concentration of QQ was 8.0 mM after mixing. This substrate concentration assures steady state conditions (K_M approx. 1.00 mM QQ, *cf.* Table 3.2).

The spectrum which was monitored first (*cf.* Figure 3.5-1 A spectrum 2, after approx. 0.01 s reaction time) depicts increased absorption signals at 515 nm and 555 nm. These absorption signals reach a maximum within approx. 0.1 s (*cf.* Figure 3.5 A spectrum 3). After approx. 25 s the absorption signals begin to decrease (*cf.* Figure 3.5 A spectrum 4). The signals at both wavelengths have almost completely disappeared after approx. 55 s (*cf.* Figure 3.5 A spectrum 5). Spectra monitored after 55 s remain constant and they are similar to that of the resting state (*cf.* Figure 3.5 A spectrum 1), which was recorded as described in Section 3.4.1. The spectrum contains two isosbestic points at the wavelengths 525 nm and 571 nm.

Analog experiments with the different variants mentioned above revealed that only minor spectral changes can be observed (*cf.* Figure 3.5-1 B – D). Thus, only small time-dependent changes at 420 nm – 435 nm, 471 nm, 517 nm and 560 nm – 571 nm could be observed.

3 Results

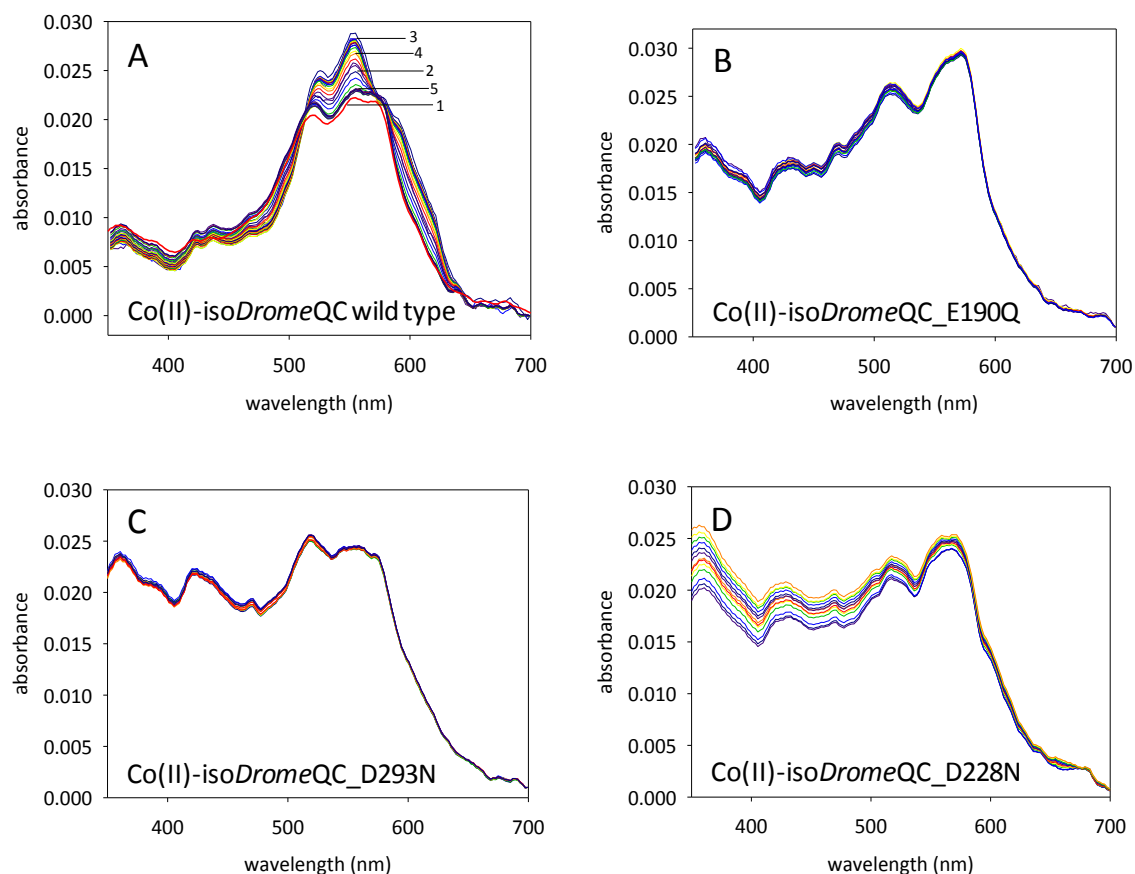


Figure 3.5-1 UV/Vis absorption spectra of the Co(II)-isoDromeQC wild type and the variants during the reaction with the substrate QQ The diagrams depict the UV/Vis absorption spectra of the Co(II)-isoDromeQC wild type (A) and the variants Co(II)-isoDromeQC_E190Q (B), Co(II)-isoDromeQC_D293N (C) and Co(II)-isoDromeQC_D228N (D) measured after rapid mixing in the stopped-flow device and monitored with the photo diode array in the wavelength range from 350 nm to 700 nm. Only in the case of Co(II)-isoDromeQC wild type are clear changes in the absorbance spectra observable during the reaction with the substrate.. The variants do not exhibit prominent photospectroscopic changes in the course of the reaction. The measurements were carried out in 50 mM Tris/HCl, 100 mM NaCl at 10 °C.

Observing the band wavelengths of Co(II)-isoDromeQC wild type in a time-resolved diagram (*cf.* Figure 3.5-2 A), one can observe a significant increase of the mentioned signals at the wavelengths 525 nm and 555 nm within the 1.5 ms (dead-time of the stopped-flow device). This increase can be assigned to the pre-steady state. The absorption at this wavelength remains nearly constant for approx. 25 s. This phase correlates to the steady state of the reaction and is followed by the substrate consumption phase lasting approx. 20 s in which the absorption signals decrease.

The time-resolved diagrams of the analog experiments with the variants depict only a slight increase of absorbance. In case of Co(II)-isoDromeQC_E190Q (*cf.* Figure 3.5-2, B) the absorbance maxima at the wavelengths at 435 nm, 471 nm, 513 nm and 571 nm was detected after approx.

four s. In the experiment with Co(II)-isoDromeQC_D293N, the maximum absorbance at the wavelengths 420 nm, 470 nm, 517 nm and 560 nm was reached after 40 s (cf. Figure 3.5-2, C). In the case of Co(II)-isoDromeQC_D228N, the reaction has to be detected for about 400 s (cf. Figure 3.5-2, D) to observe also marginal changes in the absorbance at the wavelengths of 431 nm, 471 nm and 517 nm.

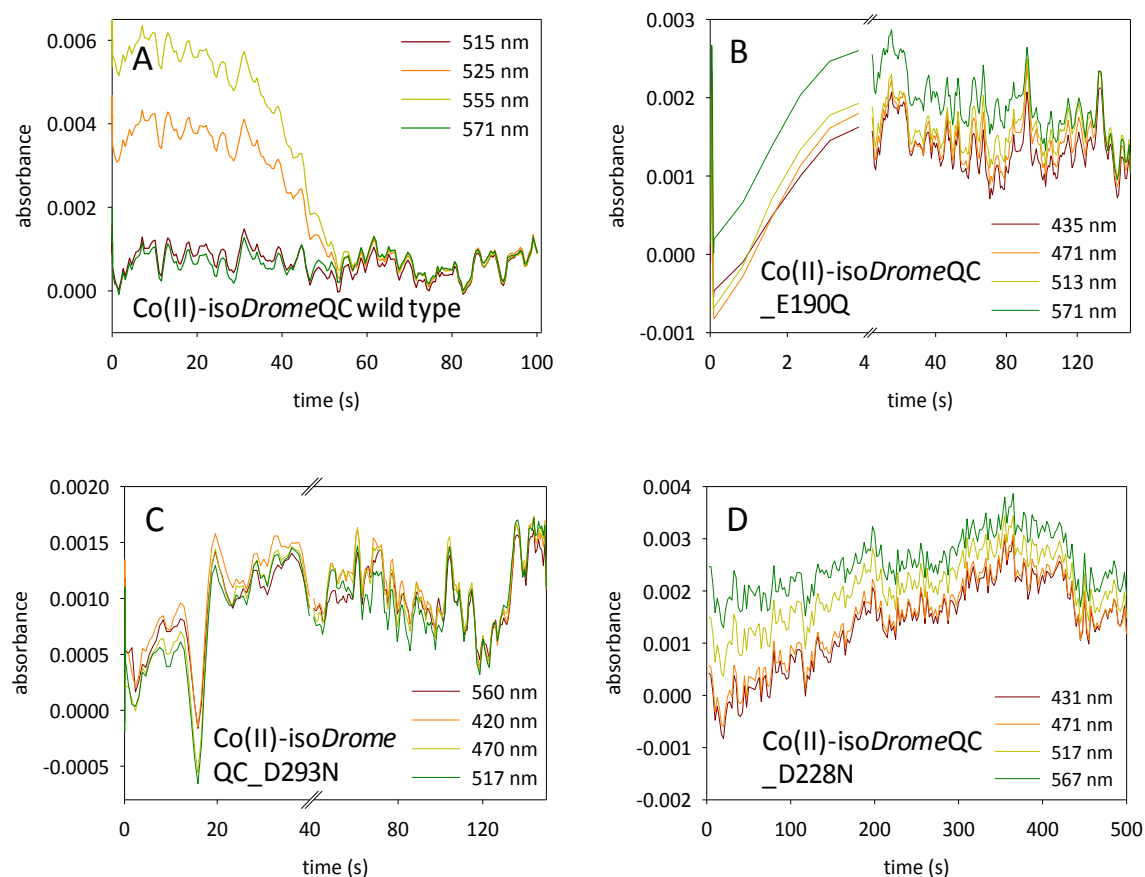


Figure 3.5-2 Time-resolved diagrams of the reaction of Co(II)-isoDromeQC wild type and variants with the substrate QQ The time-resolved diagrams reflect the reaction under steady state conditions. Only the Co(II)-isoDromeQC wild type show distinct phases of the reaction. These phases can be divided into pre-steady state, which shows an increase of absorbance signals within the dead time of the stopped-flow device (not detectable) and the steady state lasting approx. 20 s showing constant absorbance at the specified wavelengths. The following phase depicts an decrease of absorbance signals that correlates to the substrate consumption. In contrast, the variants yielded only marginal increases in absorbance during the incubation. Measured in 50 mM Tris/HCl, 100 mM NaCl at 10°C using the stopped-flow device in combination with the photo diode array.

3.4.3 Stopped-flow analysis of Co(II)-isoDromeQC wild type incubated with the substrate QFRH

The measured K_M value with QFRH and Zn(II)-isoDromeQC wild type is 0.048 mM. This measure for the affinity between substrate and active center is 20-fold lower than the K_M of QQ.

Interestingly, when Co(II)-isoDromeQC wild type was incubated with the tetrapeptide QFRH stronger changes in the absorption band, especially at 525 nm and 555 nm, could be observed compared to the resting state (*cf.* Figure 3.5-3). According to the experiment with QQ, several absorbance spectra were recorded in the different phases of the reaction progress (*cf.* Section 3.4.2). Two isosbestic points are observable at wavelengths around 515 nm and 575 nm. The time-resolved diagram points out progression curves, which are similar to the conversion of QQ.

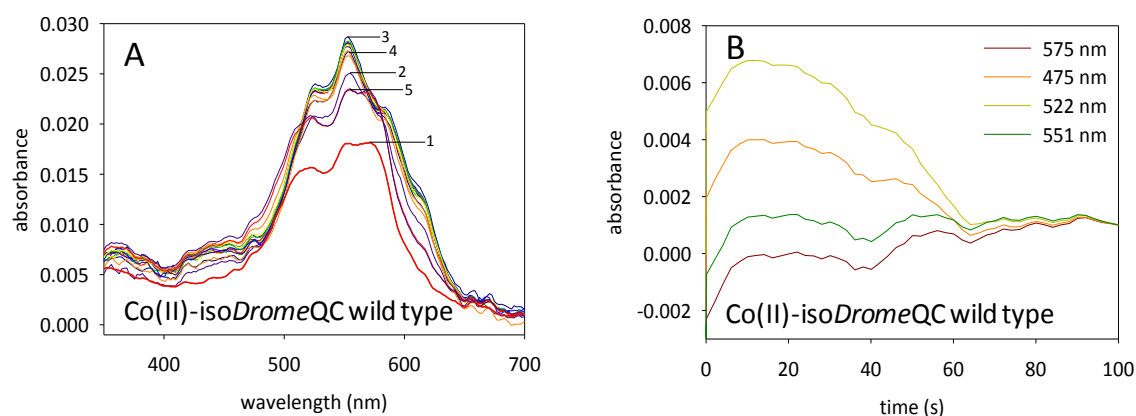


Figure 3.5-3 UV/Vis absorbance spectra recorded during the reaction of Co(II)-isoDromeQC wild type with the tetrapeptide QFRH Analogously to the experiment with Co(II)-isoDromeQC wild type and QQ UV/Vis, absorbance spectra were recorded as a function of wavelength (A) and time (B) using the stopped-flow device under the same conditions (*cf.* Section 3.5.1) The resting state (figure A, spectrum 1) was recorded with buffer. Approximately 0.01 s after mixing with QFRH, a spectrum during the pre-steady state (figure A, spectrum 2) could be recorded. After approx. 0.1 s the spectra show the maximum absorbance at the mentioned wavelength (figure A, spectrum 3). After approx. 30 s the spectra show decreased absorption bands (*cf.* Figure A, spectrum 4). In this phase the substrate concentration decreases continuously. One minute after the reaction starts, the intensities of the absorption bands remain constant (*cf.* Figure A, spectrum 5).

3.4.4 Stopped-flow analysis of Co(II)-isoDromeQC wild type incubated with substrates possessing an N-terminal glutamate

As mentioned earlier, truncated A β peptides consisting of an N-terminal glutamate are converted by QCs [54]. Evidence could be mounted that the resulting highly amyloidogenic

products are involved in neurodegenerative processes leading to dementia diseases such as Alzheimer's. [25].

In the following experiments, the analysis of the QC catalyzed pathophysiological conversion of N-terminal possessing glutamate substrates is in the focus of investigation.

In order to detect changes in the coordination sphere of the catalytically active Co(II) when Co(II)*isoDromeQC* was incubated with substrate harboring an N-terminal glutamate, stopped-flow experiments were executed in the same manner as described in Section 3.4.1. EFRH and EW possess an aromatic system in the second position. According to the results of the substrate specificity (*cf.* Section 3.2), such substrates show higher catalytic efficiencies compared to substrates lacking aromatic amino acids in the second positions. For Zn(II)-*isoDromeQC* there are hitherto no kinetic data collected with substrates bearing N-terminal glutamate.

Interestingly, the monitored stopped-flow UV/Vis absorbance spectra of Co(II)-*isoDromeQC* wild type incubated with the substrate EW or EFRH showed no significant spectral changes compared to the spectra of the resting state (*cf.* Figure 3.6 A/B). The slight spectral changes derive most likely from a general increase of absorbance at shorter wavelengths.

It should be noted that the EW substrate exhibits an intrinsic absorption in the range around 490 nm (*cf.* Figure 3.6 B).

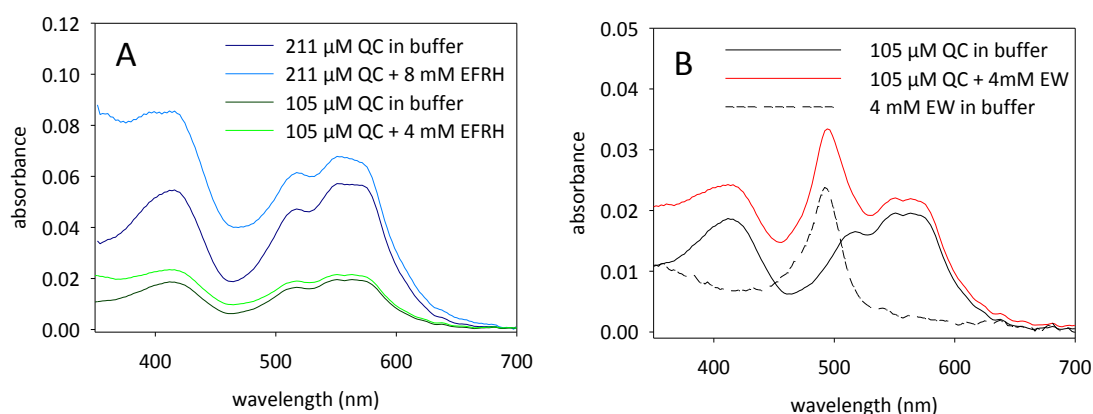


Figure 3.6 Stopped-flow UV/Vis absorbance spectra of Co(II)-*isoDromeQC* wild type incubated with EFRH and EW The absorbance spectra display the Co(II)*isoDromeQC* wild type in resting state and incubated with EFRH (A) and EW (B). Significant spectral changes are not detectable. The diagram (B) additionally displays the UV/Vis spectrum of pure EW (dashed line). The measurements were carried out in 50 mM Tris/HCl, 100 mM NaCl at 10 °C. The reactions were detected employing the stopped-flow device in combination with the photo array detector.

3.4.5 Stopped-flow analysis of Co(II)-isoDromeQC wild type incubated with competitive inhibitors

Enzyme-specific inhibition of QC plays a role in treatment of AD. Inhibition of QC reaction leads successfully to a reduction of A β -plaque deposition in mouse models [54]. The interference of many inhibitors investigated so far with other Zn(II)-dependent enzymes requires further investigations regarding inhibitor-metal interaction (unpublished data, Probiodrugs).

In order to analyze the effect of different inhibitors on the spectral properties of Co(II)-isoDromeQC, analogous experiments were performed using the following compounds. These peptides show competitive inhibition effects on the reaction of hQC and isoDromeQC (kinetic measurements were accomplished by Dr. Franziska Seifert using Zn(II)-isoDromeQC wild type, unpublished data, cf. Supplemental 8.9 and 8.10).

As inhibitors the following substances were used: The tripeptide alanine-phenylalanine-alanine (AFA), and the reaction product pyroglutamic acid-phenylalanine-arginine-histidine (pEFRH).

The tripeptide AFA exhibits an inhibition constant (K_i) of 0.6 mM. This peptide possesses neither glutamine nor glutamate in the first N-terminal position. However, this compound inhibits the QC activity. This experiment should show whether the inhibitor binding is mediated by interaction with the catalytically active metal. The UV/Vis spectrum of Co(II)-isoDromeQC wild type incubated with AFA showed an increased absorption in the range from 350 nm and 570 nm. In particular around 555 nm the signal seems to indicate a slightly increased absorption band. However, from 570 nm to 700 nm the absorption was similar to that of Co(II)-isoDromeQC incubated with buffer as control. In general, the spectrum demonstrates a rise of absorbance at lower wavelengths.

It was also kinetically determined that peptides bearing pyroglutamic acid in the first position exhibit an inhibition constant of $K_i=1.8$ mM (pEFRH). These peptides are products of the QC reaction. In general, product inhibition indicates that the product release is likely the rate limiting catalytic step in the catalytic cycle. Under this aspect, it could be possible to demonstrate the interaction of the product and the Co(II) ion in this experiment. When Co(II)-isoDromeDQC wild type is incubated with synthesized pEFRH, a slightly increased absorption at 560 nm and decreased absorption at 517 nm and 570 nm are detectable.

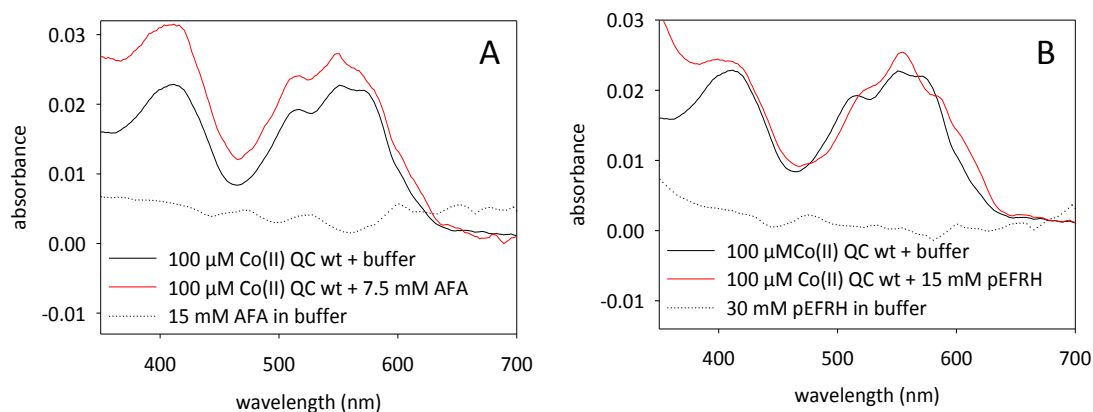


Figure 3.7 Stopped-flow UV/Vis absorption spectra of Co(II)-isoDromeQC wild type and inhibitors Here the UV/Vis spectra of Co(II)-isoDromeQC wild type incubated with AFA (A) and pEFRH (B) are shown. The UV/Vis spectra of the respective inhibitors (dotted lines) and enzyme (black line) are shown as controls. Co(II)-isoDromeQC wild type shows slight changes of the absorbance spectra at 555 nm. Significant differences in the shape of the spectra are observable with the product pEFRH. The measurements were executed in 50 mM Tris/HCl, 100 mM NaCl at 10 °C. The reactions were detected employing the stopped-flow device in combination with the photo array detector.

3.5 Protein crystallization – X-Ray structure of Zn(II)- and Co(II)-isoDromeQC wild type and the variants Zn(II)-isoDromeQC_E190Q and Zn(II)-isoDromeQC_D228N

A high-resolution crystal structure of an enzyme is rich in information about the nature of its biological and mechanistic functionality. The overall structure of a single molecule provides information about the composition of secondary structure elements (*e.g.* α -helices, β -sheets or loops). Furthermore, the exploration of an enzyme's crystal structures can reveal binding sites for substrates or regulatory biomolecules (*e.g.* inhibitors) as well as binding sites for cofactors. Especially the architecture of the active center plays a central role if the issue of interest lies in mechanistic considerations. Mechanistic insights can be obtained by the resolution of structures of crystallized substrates, reaction intermediates, products or inhibitors in complexes with the active center.

To accumulate information about the structural and mechanistic features of the QC, overall crystal structures of Zn(II)-isoDromeQC wild type, Zn(II)-isoDromeQC_E190Q and Zn(II)-isoDromeQC_D228N were resolved. Interestingly, Co(II)-isoDromeQC wild type could be crystallized in complex with the substrates QFRH and EFRH and their product pEFRH. Further, a crystal structure could be obtained by crystallization of Co(II)-isoDromeQC wild type in complex with the competitive inhibitor AFA.

3.5.1 Overall crystal structure of Zn(II)-isoDromeQC and variants

Crystallizing attempts of Zn(II)-isoDromeQC wild type, Zn(II)-isoDromeQC_E190Q and Zn(II)-isoDromeQC_D228N leads to crystals with the space group P1. Those crystals diffract between resolutions of 1.12 and 2.23 Å if the data collection was accomplished at a synchrotron facility (ESRF, Grenoble, France; BESSYII, Berlin/Adlershof or PETRAIII, Hamburg, Germany). The asymmetric unit comprises two autonomic molecules (*cf.* Figure 3.9 A). In most cases, both molecules are different with respect to the isotropic displacement parameter (B-factor). Currently, no crystallization conditions were found to yield crystals of Zn(II)-isoDromeQC_D293A and Zn(II)-isoDromeQC_D293N with a resolution better than 4 Å.

The center of the QC overall structure consists of a β -sheet, which is composed of five parallel (β_1, β_3 - β_6) and one antiparallel β -strand (β_2). This twisted β -sheet is coated by nine α -helices (*cf.* Figure 3.9). Seven helices (α_1 – α_5 , α_8 and α_9) encircle the convex side of the β -sheet. Hence, two α -helices (α_6 and α_7) flank the concave side. This tertiary structure of the isoDromeQC is characteristic for the globular α/β -hydrolase fold superfamily [58, 74]. In addition to this common overall structure, the isoDromeQC is hallmarked by two further N-terminal, antiparallel β -strands β_{-1} and β_0 . The active center with a Zn(II) ion is located in a loop region. The distance between Zn(II) ion and the surface is approximately eight Ångström.

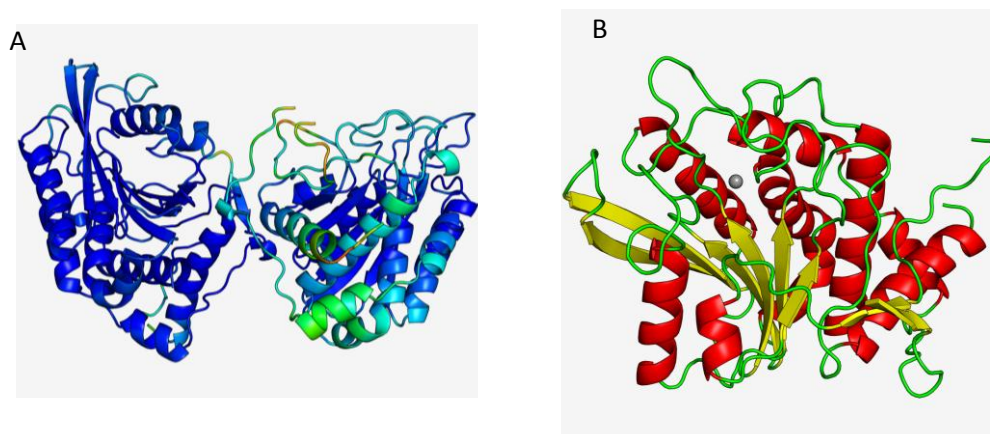


Figure 3.9 The Overall structure of the Zn(II)-isoDromeQC wild type in the unit cell and the single molecule Figure A illustrates two molecules in one asymmetric unit. Both molecules exhibit variant B-factors (blue-colored segments correspond to very rigid structure elements, red-colored segments reflect highly flexible regions). The overall structure of the monomer resembles the α/β hydrolase fold with nine α -helices (red), eight β -sheets (yellow) and several loops (green). The catalytically active zinc ion is embedded in a loop region near the protein surface. Resolutions: wt 1.12 Å, R-work = 0.155, R-free = 0.179, $B_{\text{averaged}} = 20.6 \text{ \AA}^2$.

3.5.2 The crystal structure of the active center in the resting state of the Zn(II)-isoDromeQC wild type and the variants Zn(II)-isoDromeQC_E190Q and Zn(II)-isoDromeQC_D228N

The catalytically active Zn(II) ion in the resting state is tetrahedrally coordinated by two carboxylate moieties (D153 and E191) and an imidazole group (H318) (*cf.* Figure 3.10). The fourth position is occupied by a water molecule. This water molecule acts as placeholder in the resting state and will be replaced by the substrate molecule. The water molecule is in hydrogen bond distance to the residue E190. Two further acidic aspartate residues (D293 and D228) in the second shell around the Zn(II) may play a role in substrate and product binding and the suggested proton transfer that is part of the reaction trajectory.

The variants Zn(II)-isoDromeQC_E190Q and Zn(II)-isoDromeQC_D228N were crystallized in order to investigate the influence of the amino acid substitution on the structural feature of the active center.

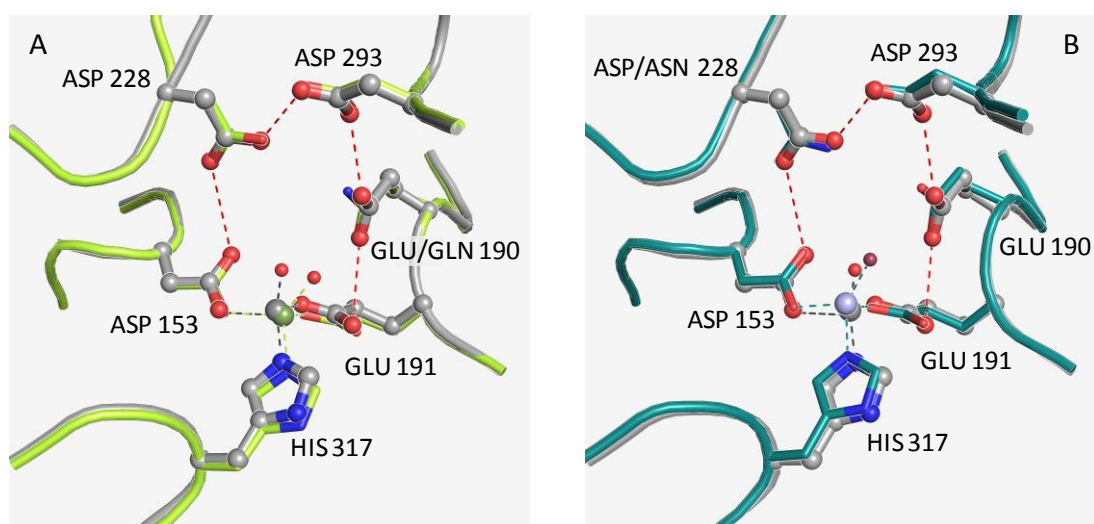


Figure 3.10 Crystal structure of the active center of Zn(II)-isoDromeQC wild type aligned with the active center of the variants Zn(II)-isoDromeQC_E190Q and Zn(II)-isoDromeQC_D228N These structure images demonstrate the aligned active centers of the Zn(II) isoDromeQC wild type (grey) and Zn(II) isoDromeQC_E190Q (A, lemon) as well as Zn(II) isoDromeQC_D228N (B, deep cyan). The active center is characterized by three zinc-coordinating residues (D153, H317 and E191) and at least three catalytic obligate acidic residues (D228, D293 and E190). The hydrogen bond lengths (red dashes) between the residues are in a range between 2.6 -3.6 Å. The substitution of the acidic side chain against uncharged side chains results in a distorted tetrahedral coordination of the zinc ion along with changed bond angles in particular with respect to the coordinated water molecule. Resolutions: wt 1.12 Å, R-work = 0.155, R-free = 0.179, D228N 2.23 Å, R-work = 0.183, R-free = 0.243, E190Q 1.70 Å, R-work = 0.146 R-free = 0.204

The substitutions of the amino acid E190 to glutamine in the active center (*cf.* Figure 3.10 A) lead to slight distortions of the residues H317, and E191 compared to the Zn(II)-isoDromeQC wild type. In the case of the variant Zn(II) isoDromeQC_D228N, the Zn(II) ion coordinating residues

3 Results

are also marginally distorted. In this structure the catalytically active Zn(II) ion is shifted approximately 0.2 Å.

Remarkable is the clear change of the bond angles of the tetrahedron in Zn(II)-iso*DromeQC*_E190Q and Zn(II)-iso*DromeQC*_D228N. This significant distortion of the bond angles (*cf.* Table 3.4) in comparison to the Zn(II)-iso*DromeQC* wild type is mainly due to the dislocated water molecule that occupies the fourth ligand binding position.

Table 3.4 Bond angles between Zn(II) coordinating residues, the Zn(II) ion and the water molecule
The bond angles were determined using the Pymol program version 1.3 based on the structures shown in Figure 3.10.

bond angles	D153/OD2-Zn(II)-H ₂ O	E191/OE1-Zn(II)-H ₂ O	H318/NE2-Zn(II)-H ₂ O
Zn(II)-iso <i>DromeQC</i> wild type	108.0 °	115.1 °	112.5 °
Zn(II)-iso <i>DromeQC</i> _E190Q	124.8 °	98.4 °	112.7 °
Zn(II)-iso <i>DromeQC</i> _D228N	129.5 °	113.6 °	110.8 °

3.5.3 The crystal structure of Co(II)-iso*DromeQC* wild type soaked with the substrate QFRH

In this experiment the aim was to obtain a structure of the QC in complex with a substrate or an intermediate state of the glutaminy cyclization reaction. As mentioned in the introduction, the glutaminy cyclization correlates to the physiological function of QCs. No other substrate possessing an N-terminal glutamine leads to analyzable structure data. This substrate shows high affinity to the Zn(II)-iso*DromeQC* wild type and reveals a high catalytic efficiency (*cf.* Section 3.2). The crystallization attempts with QFRH and Zn(II)-iso*DromeQC* were without success. Interestingly, the Co(II)-substituted iso*DromeQC* provides analyzable crystal structures of the enzyme substrate complex.

The analysis of Co(II)-iso*DromeQC* wild type crystals soaked with substrate QFRH showed that varying ligand orientations in both the molecules of the unit cell are possible. In one of the molecules the γ -amido oxygen of the first-position glutamine acts as the fourth coordination partner of the Co(II) ion (*cf.* Figure 3.11 A, B and C). Different structure refinements show coordinative bond lengths around 2.0 ± 0.1 Å.

In this orientation (*cf.* Figure 3.11 B), the γ -carbonyl oxygen of E190 is in hydrogen bond contact with the α - and γ -amino nitrogen of the N-terminal glutamine. The γ -carboxylate oxygen atoms of D228 may form a hydrogen bond to the γ -amino nitrogen of the N-terminal substrate glutamine. The backbone of D292 (not shown) acts as a further binding motif. The main chain nitrogen of D292 interacts with the main chain oxygen of the second amino acid in the substrate sequence and the main chain oxygen from D292 interacts with the main chain nitrogen from the phenylalanine via hydrogen bond. This binding motif occurs also when an N-terminal glutamate (*cf.* Figure 3.12 B) or pyroglutamic acid (*cf.* Figure 3.13 B) is bound to the active center. Even if the inhibitor AFA is bound (*cf.* 3.14 B), both hydrogen bond interactions occur.

An alternative orientation of the substrate is shown in Figure 3.11 (D: view from above, and E: side view). In this position, the hydrogen bond mediated contact between the substrate and the enzyme is bridged by six water molecules. The distance between the γ -amido moiety of the N-terminal glutamine and the metal ion is too large for chemical bonding.

Nevertheless, the N-terminal glutamine residue of the substrate is directed into the acidic binding pocket of the QC molecule. The measured electron density for residues in the second shell around the metal ion is barely perceptible.

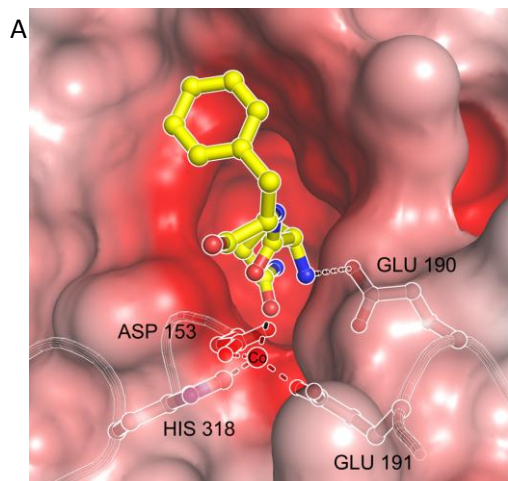
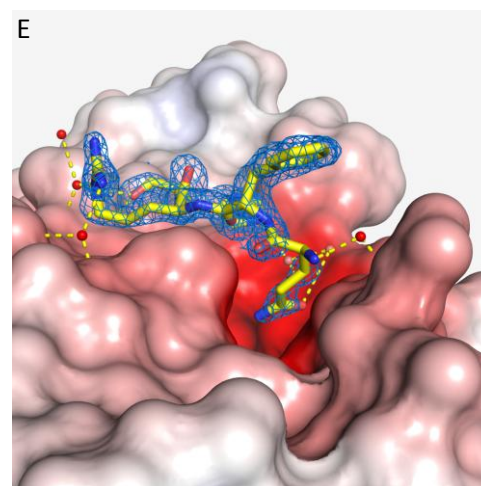
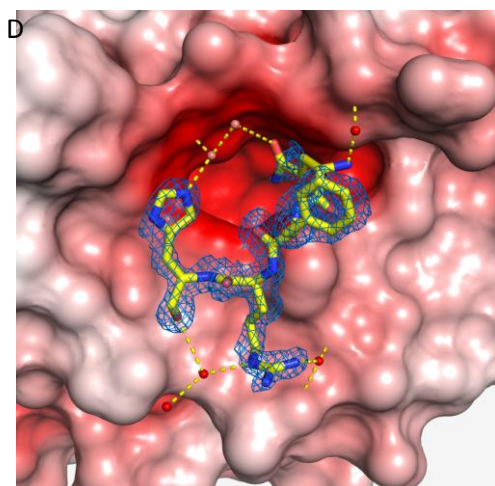
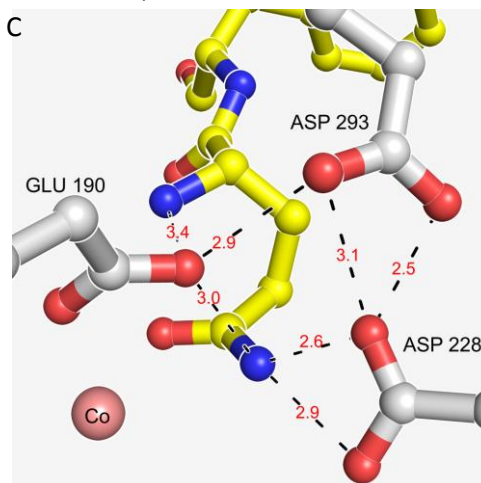
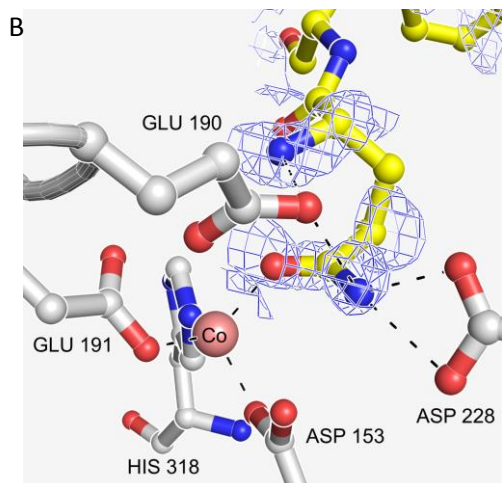


Figure 3.11 Crystal structure of Co(II)-isoDromeQC wild type in complex with the substrate QFRH The soaked synthetic substrate QFRH (surrounded by a $2F_o-F_c$ electron density map (sigma contour level = 1.0σ)) (yellow) was found in two different localizations. The first exhibits the γ -amido oxygen of the N-terminal glutamine in a cobalt-bound state along with potential hydrogen bond interactions (dashed line) (A, B and C). The monodentate ligand coordinates a tetrahedral Co(II) ion. The second position of the substrate shows an outlying ligand (D and E). The contact between substrate and QC is mediated by water molecules. The resolution of this structure is 1.31 (R-work = 0.143, R-free = 0.182).



3.5.4 Co-crystallization of Co(II)-isoDromeQC wild type with the substrate EFRH

The following crystallization attempt was performed to analyze the structure of the complex between the Co(II)-isoDromeQC wild type and a substrate containing an N-terminal glutamate. Substrates with N-terminal glutamate are involved in the pathophysiological side reaction leading to neurodegenerative process in the brain of humans [23].

In this experiment again, the use of Co(II)-substituted isoDromeQC wild type leads to analyzable structure data.

The analysis of the XDS-processed and Phenix-refined structure data showed an observed electron density, which indicates that the active center might be occupied by EFRH as well as by the reaction product pEFRH (*cf.* Figure 3.12 A). The appearance of the product in this structure is obviously due to the substrate conversion during the co-crystallization-procedure. Despite the minimal rate constant for this substrate ($k_{cat} = 1/10000 \text{ s}^{-1}$, measured with *hQC*), apparently the high concentration of EFRH (approx. 7.5 mM) and the typical high QC concentration in the crystal lattice has led to sufficient product conversion. The most reliable statistic values, such as the R-work and R-free factors, were obtained when the PHENIX refinement definitions were assessed to an occupancy $n_{\text{EFRH}} = n_{\text{pEFRH}} = 0.5$. This indicates that the ratio of the protein-bound substrate and product molecules, respectively, is one to one.

The Co(II)-isoDromeQC in complex with the product pEFRH is described in a separate Section below (*cf.* Section 3.5.5). In this section, only the binding mode of EFRH will be described.

The flexibility of the side chain of phenylalanine (the second residue of EFRH) is apparently too high. This leads to a lack of electron density (B). The corresponding averaged B-factor of the phenylalanine side chain is approx. 45 \AA^2 and is hence increased by a factor of two compared to the N-terminal glutamate residue ($B_{\text{averaged}} = 25 \text{ \AA}^2$). If a substrate with an N-terminal glutamine is bound to the active center (*cf.* Section 3.5.3), the Co(II) ion is four-coordinated. In stark contrast thereto, in this structure the Co(II) ion is five-coordinated (*cf.* Figure 3.12. B). This is the result of the bidentate coordination of the γ -carboxylate moiety belonging to the N-terminal glutamate side chain. The coordinative bond lengths between the Co(II) ion and both oxygen atoms is 2.2 \AA . Further substrate protein interactions are displayed in Figure 3.12 B. Next to possible polar contacts between the γ -carboxylate moiety and H318 and W317 respectively, and the α -amino moiety and the carboxylate moiety of E190, the backbone of E292 and one water molecule provide hydrogen bond donators as well acceptors.

As mentioned above, clear differences in the binding mode of the glutamate substrate is the five-coordinated Co(II) ion and the missing polar contact between the N-terminal glutamate side chain (due to the absence of γ -amido nitrogen) and D228.

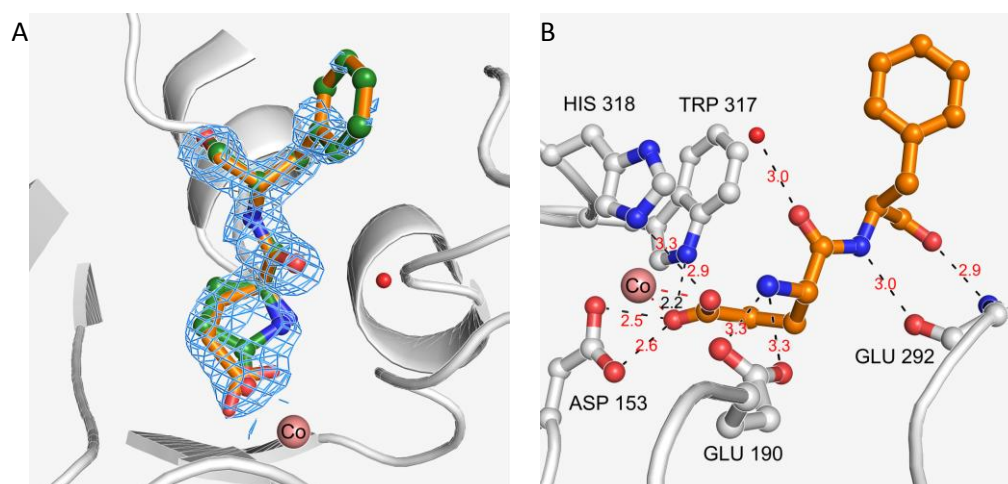


Figure 3.12 Crystal structure of Co(II)-isoDromeQC wild type co-crystallized with the N-terminal glutamate substrate EFRH The resolved structure of a crystal co-crystallized with EFRH (orange rods) resolution: 1.42, R-work = 0.154, R-free = 0.1940) provides an observed electron density of the substrate and accumulated reaction product pEFRH (green rods) (A). The γ -carboxylate oxygens of the N-terminal substrate glutamate indicate bidentate coordination of Co(II)(dark salmon sphere) (B) Both ligands are surrounded by a $2F_o - F_c$ electron density map with a sigma contour level of 1.0 σ .

3.5.5 X-ray structure of the enzyme product complex

The observed electron density of the product pEFRH in the enzyme demonstrates the conformation of the N-terminal glutamate residue (figure 3.13 A). Besides the three Co(II) ion coordinating residues (D153, E191 and H318), the keto-oxygen of the N-terminal pyroglutamic acid is the fourth ligand of the Co(II) ion. The product-enzyme complex possesses a tetrahedral coordinated Co(II). The coordinative bond length between the keto-oxygen of the pyroglutamate residue and the Co(II) ion is with 2.1 Å and thus 0.1 Å shorter compared to the bond length between both the γ -carboxylate oxygen atoms of the substrate and the Co(II) ion (*cf.* Figure 3.12 B). Additional polar contacts are comparable to the glutamate substrate EFRH, as described in Section 3.5.4 (*cf.* Figure 3.12 C) with the exception that the hydrogen bond interaction between the side chain of E190 and the nitrogen of the pyroglutamic acid is missing.

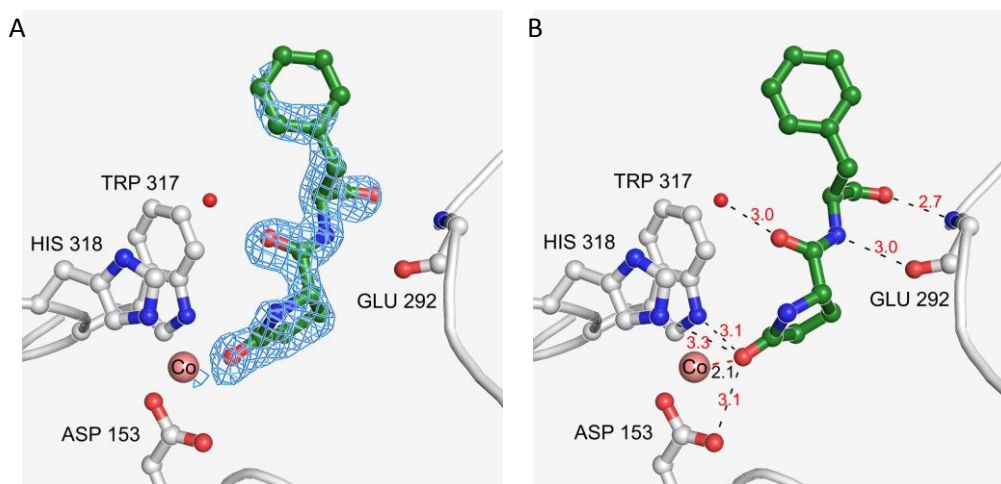


Figure 3.13 Crystal structure of Co(II) *isoDromeQC* wild type in complex with the reaction product of pEFRH after the conversion of EFRH The structure of the enzyme-product complex (resolution: 1.42, R-work = 0.154, R-free = 0.1940) reveals the first two N-terminal positions of the product pEFRH (green). The monodentate keto-oxygen of the N-terminal pyroglutamic acid represents the fourth coordination partner of the tetrahedral Co(II) ion. In addition, polar contacts between the product residues and the active center side chains function as potential binding motifs. The product is surrounded by a $2F_o - F_c$ electron density map with a sigma contour level of 1.0 σ .

3.5.6 Crystal structure of Co(II)-*isoDromeQC* wild type co-crystallized with the tripeptide AFA reveals an enzyme inhibitor complex

Kinetic analysis of incubations of the tripeptide AFA with Zn(II)-*isoDromeQC* (performed by Dr. Franziska Seifert), indicated that this compound functions as a competitive inhibitor. AFA was thus used for co-crystallization experiments to obtain structural explanations for the inhibiting effect. When these crystals were analyzed, electron density for the first two amino acids could be observed.

The AFA tripeptide bound in the active center of Co(II)-*isoDromeQC* wild type exists in two distinct conformations. In the first conformation (*cf.* Figure 3.14 A), the distance between the α -amino nitrogen of the N-terminal alanine and the Co(II) ion is 2.3 Å and displays a stretched tetrahedral coordinative bond. Besides polar contacts to unbound water, this structure does not show any further direct interactions between AFA and the enzyme.

The second conformation of AFA bound to Co(II)-*isoDromeQC* is shown in Figure 3.14 B. Here, the α -nitrogen (peptide bond) of the phenylalanine in the second position of AFA interacts with the oxygen of the main chain of E292. A second interaction between AFA and the enzyme exists between the α -nitrogen (peptide bond) of the main chain of E292 and the carbonyl oxygen of phenylalanine. Further, in this conformation, polar contact exists between three free water molecules. The localization of the N-terminal alanine disables Co(II) interactions.

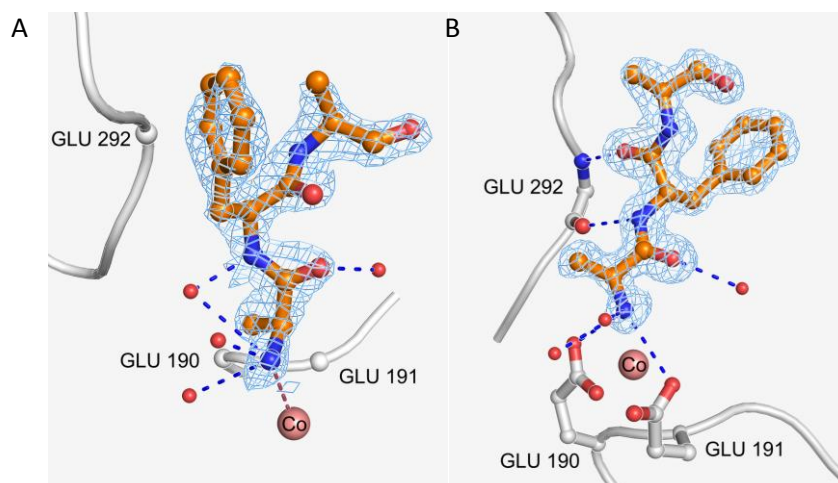


Figure 3.14 Crystal structure of two distinct conformations of the inhibitor AFA in complex with active center of Co(II)-isoDromeQC wild type This structure (resolution: 1.31 Å, R-work = 0.162, R-free = 0.196) represents the first two N-terminal residues from the competitive inhibiting tripeptide AFA surrounded by a $2F_o - F_c$ difference electron density map (1.0 σ) (orange rods) in two distinct conformations. The α -amino nitrogen of the N-terminal alanine coordinates the Co(II) ion in the fourth position (A) as the only direct interaction with active center (grey rods). Alternatively, the peptide is bound to the backbone of the active center residue E292 while the contact to Co(II) is punctuated (B).

3.6 Electron paramagnetic resonance spectroscopy (EPR)

The investigation of the electronic environment of a catalytically active metal ion in the active center of an enzyme during the catalysis can provide information about the reaction trajectory. In order to observe changes in the coordination number or coordination geometry of the metal ion, the EPR technique was employed. Due to the fact that the Zn(II) ion in the native *isoDromeQC* raises no EPR signals, the insertion of a catalytically active Co(II) ion into the active center is a necessary pre-requisite. Here the observation of the EPR-active transition metal ion is the central issue of interest. In order to gather insights about binding states of substrates, transient intermediate reaction states or the liberation of the product, the following EPR experiments were performed.

Further, to explore the functions of the active center amino acids E190, D228 and D293, variants of Co(II)-*isoDromeQC* were analyzed in which one of these amino acids was substituted.

The EPR experiments were carried out under the supervision of Prof. Dr. Brian Bennett at the Department of Biophysics at the Medical College of Wisconsin in Milwaukee (Wisconsin, USA). The enzyme and used compounds (e.g. substrates, product and inhibitors) were dissolved in buffer containing 50 mM sodium phosphate, 100 mM sodium chloride at pH 6.8. The frozen protein samples (*cf.* Section 2.12.5 sample preparation/freeze techniques) were measured with the EleXsys E600 (Bruker BioSpin Corporation, Billerica, USA). The spectrometer was applied at 4 K, 10 K and 25 K to examine the high spin $S = 3/2$ EPR signal as well as the $S = 1/2$ signal. In the following sections only the EPR spectra of the high spin $S = 3/2$ EPR signals measured at 4 K are in the focus of interest.

For the experiments in the recent work three characteristics of the EPR signals are of particular importance. The number of appearing signals, the signal position (resonance position or signal maximum) and the band width. The signal position and the number of appearing signals provide information regarding the Co(II) coordination number. A four-coordinate Co(II) in the active center presents one prominent resonance position in the range of 1000 Gauss– 1100 Gauss. Whereas, a five-coordinate Co(II) ion presents one signal in a range of 1100 and 1200 Gauss and at least one second signal at over 1200 Gauss. EPR spectra of samples containing both four- and five-coordinated Co(II) species present a signal between 1000 G and 1100 G (four-coordinated Co(II)) and a mostly less pronounced second signal between 1100 G and 1200 G, indicating five-coordinated Co(II) species. The second signal that is typical for five-coordinated Co(II) is in these cases often not clearly observable.

3 Results

Changes in the resonance position are indicative for distorted (stretched or compressed) coordination geometry. Such changes are observable when ligands effectuate a delocalization of electron(s) along the Z-axis.

The band width can be altered depending on the flexibility of the coordination geometry. A narrow band width correlates to a rigid Co(II) coordination sphere. In contrast, broad signals imply that the coordination sphere is flexible due to a weakly bound or small ligand *e.g.* water.

3.6.1 EPR-analysis of Co(II)-isoDromeQC wild type and variants in the resting state

The EPR measurement of the Co(II)-isoDromeQC wild type and the variants Co(II)-isoDromeQC_E190Q, Co(II)-isoDromeQ_D228N and Co(II)-isoDromeQC_D293N in the resting state is the basis for the following experiments with substrates and inhibitors.

For this purpose the protein samples with a molar concentration of approx. 680 μ M were frozen in liquid nitrogen and measured as described above.

The obtained EPR spectrum of Co(II) ion in the resting Co(II)-isoDromeQC wild type (*cf.* Figure 3.15 A/B) shows a maximum at 1038 G ($g = 6.443$).

This type of EPR spectrum is characteristic for a predominantly four-coordinate Co(II) ion. A small percentage of about ten percent of the cobalt bears a five-coordinate signal (internal discussion with Prof. Dr. Brian Bennett). This is also true for the EPR spectrum of Co(II)-isoDromeQC_E190Q that shows a shifted maximum of the resonance signal 1056 G, ($g = 6.333$) into the high field. The signal of this variant in the resting state is broadened compared to the resting state of Co(II)isoDromeQC wild type.

The variant Co(II)-isoDromeQC_D228N gives a signal, that corresponds to a spectrum of tetrahedrally bound Co(II) and does not show any clear difference to that of Co(II)-isoDromeQC wild type. The maximum of this resonance signal is encountered at 1036 G with resonance condition at ($g = 6.455$). The substitution of this side chain obviously does not bring about any significant change in the coordination sphere of the Co(II) ion.

The maximum of the resonance position of the signal of Co(II)-isoDromeQC_D293N is found at 1058 G ($g = 6.321$) and presents a similar shift as the Co(II)-isoDromeQC_E190Q of 16 G compared to the Co(II)-isoDromeQC wild type. The measured spectrum corresponds to a tetrahedrally coordinated Co(II) ion.

The crystal structure of Co(II)-isoDromeQC wild type, Co(II)-isoDromeQC_E190Q and Co(II)-isoDromeQC_D228N (*cf.* Figure 3.10 A/B) disclose that in the resting state, a water molecule is

the fourth coordination partner of the metal ion. Such a solvent molecule frequently represents a flexible ligand that often leads to broadened band width of a signal. The distortions of the bond angles of Co(II) and its coordinating ligands (*cf.* Table 3.4), are shown in the crystal structure of Co(II)-*isoDromeQC*_E190Q (*cf.* Figure 3.10 A). These alterations in the active center may cause measurable changes in the resonance condition.

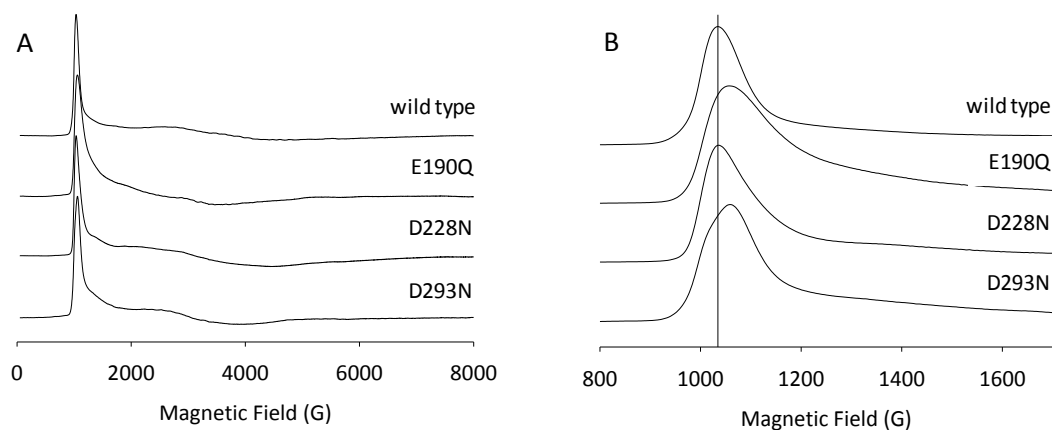


Figure 3.15 Co(II) EPR spectra of the Co(II)*isoDromeQC* wild type and variants in the resting state

Figure A depicts the entire EPR-spectra of Co(II)-*isoDromeQC* wild type and variants in the resting state. Figure B presents a zoomed diagram to illustrate the details of the spectra in the magnetic field of interest. The shown spectra are characteristic for predominantly tetrahedrally coordinated Co(II) ions. The perpendicular black line defines the resonance position of Co(II)-*isoDromeQC* wild type. Measured at 4.0 K, 20 mW at X-band wavelength (9.36 GHz) in 50 mM sodium phosphate buffer, 100 mM sodium chloride, pH 6.8 with a molar enzyme concentration wt/variants 0.68 mM.

3.6.2 Freeze quench EPR analysis of Co(II)-isoDromeQC wild type and variants after defined incubation times with the substrate QQ

Potential intermediates of the reaction might lead to differences in the coordination geometry of the catalytically active Co(II). In order to investigate these discrete steps of the catalysis, incubations of Co(II)-isoDromeQC wild type and mentioned variants with QQ as substrate were quenched at defined points in time. The quench of the reaction after 20 ms was executed by rapid freeze quenching in cryogenic isopentane. The incubation was quenched after 2 s by manual freeze quenching in cryogenic isopentane. After 2 min, 30 min and 6 h, the incubations were stopped by freezing in liquid nitrogen. By this means, the reaction should be halted at different states of the catalysis. The used concentration of the substrate QQ was 10 mM or 15 mM for rapid freeze quench and for manual freeze quench EPR spectroscopy, respectively. The enzyme concentration was set to 0.40 mM for rapid freeze quench EPR and 0.3 mM for manual freeze quench EPR experiments. The incubations were carried out at 20°C.

The experiments with Co(II)-isoDromeQC wild type incubated with QQ were performed by Dr. Franziska Seifert. As shown in Figure 3.17 A, a significant shift of the signal maximum from 1077 G ($g = 6.209$) (resting state with defined experimental setup of 4.8 K, 9.36 GHz and 200 mW) to 1046 G ($g = 6.393$) to the lower magnetic field was observed after 10 ms reaction time. The maximum shift of the band position can be observed after 160 ms. Here, the signal maximum appears at 1030 G ($g = 6.493$). After 160 ms the resonance signal appears with its narrowest width.

After 2 s incubation time with the substrate, the resonance signal becomes broader and the signal maximum at 1056 G ($g = 6.333$) returns to the higher magnetic field. The spectra after 2 min and 16 h are comparable, revealing signal maxima at 1060 G ($g = 6.309$) and the band width becomes narrower. Even after 16 hours, the signal does not return completely to the resting state situation. The coordination of the enzyme bound Co(II) ion can be assigned as predominantly four-coordinate. A small population ($\sim 10\%$) of the cobalt is five-coordinate (internal discussion with Prof. Dr. Brian Bennett and Dr. Franziska Seifert).

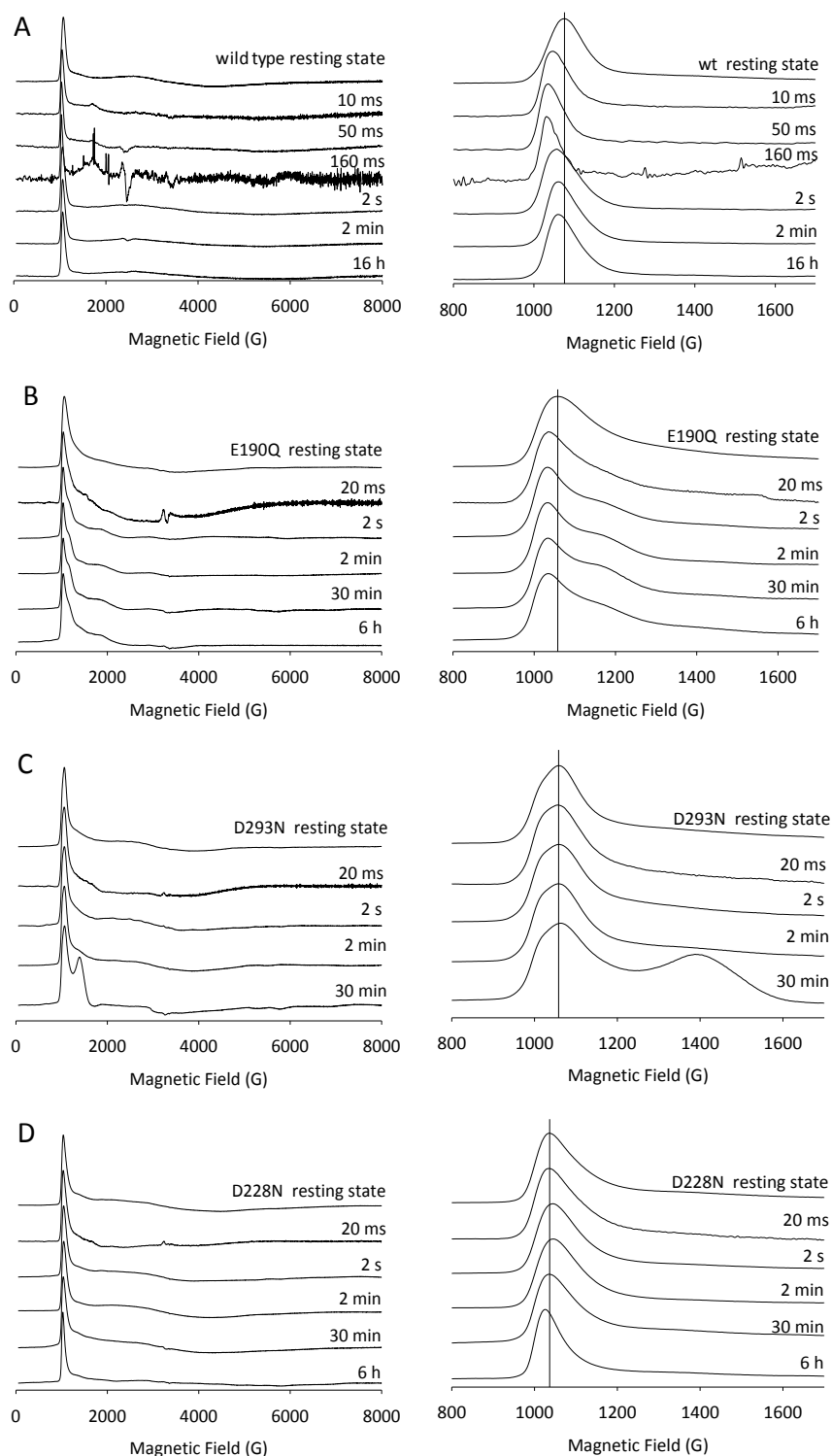


Figure 3.17 EPR spectra of Co(II)isoDromeQC wild type and variants freeze quenched after defined incubation times with the substrate QQ Entire (left) and zoomed EPR spectra (right) from the Co(II)-isoDromeQC wild type (A) and the variants (Co(II)-isoDromeQC_E190Q –B, Co(II)-isoDromeQC_D293N –C, Co(II)-isoDromeQC_D228N –D). The reaction was (rapid) freeze quenched after different reaction times to monitor the coordination sphere of the catalytically Co(II) ion at varying steps of catalysis. The perpendicular black line defines the resonance position of Co(II)-isoDromeQC wild type in the resting state. Measured at 4.0 K, 20 mW at X-band wavelength (9.36 GHz) in 50 mM sodium phosphate buffer, 100 mM sodium chloride, pH 6.8 with a molar enzyme concentration wild type/variants 0.30 mM (manual freeze quenche) and 0.40 mM RFQ and QQ 15 mM or 10 mM (RFQ) after mixing.

3 Results

Analogous experiments were performed with the different Co(II)-isoDromeQC variants. The results from these analyses showed a certain EPR-profile for each variant (*cf.* Figure 3.17 B).

In case of Co(II)-isoDromeQC_E190Q the maximum of the signal in its resting state was observed at 1056 G ($g = 6.333$). The signal for resonance conditions shifts to lower magnetic field after 20 ms to 1033 G ($g = 6.474$) and its shape becomes narrower. The signal maximum and the band width stays constant at all times at which the reaction was freeze quenched. The signal, corresponding to the Co(II) coordination is indicative for four-coordinated Co(II) but a distinct signal of Co(II) with a higher coordination number appears after 20 ms at approx. 1150 G ($g = 5.815$). After 2 s this signal arises with a maximum distinction after 30 min. After 6 h this signal decreases slightly. This signal can be assigned to five or six-coordinated Co(II).

The signal maxima of the Co(II) ion in the Co(II)-isoDromeQC_D293N variant (*cf.* Figure 3.17 C) remains constant at 1058 G ($g = 3.321$) after the reaction was quenched at specific incubation times. After 30 min a new signal at 1390 G ($g = 4.811$) appears. These spectra indicate four and five-coordinated Co(II) ions.

The EPR spectra of the variant Co(II)-isoDromeQC_D228N exhibit only marginal changes compared to the resting state (*cf.* Figure 3.17 D). After 2 s the signal maximum is shifted from 1036 G ($g = 6.455$) to 1044 G ($g = 6.406$) to the higher magnetic field. When the incubation with QQ was stopped after 2 min, the maximum signal returned to 1036 G ($g = 6.455$). After 6 h incubation time the signal maximum shifted slightly to the lower magnetic field to 1024 G ($g = 6.531$). These spectra indicate a tetrahedrally coordinated Co(II) ion with a residual probability that the Co(II) ion is five-coordinated (internal discussion with Prof. Dr. Brian Bennett). The spectrum monitored after 6 h incubation time indicates a pure four-coordinated Co(II).

3.6.3 EPR spectroscopic analysis of the coordination sphere of the catalytically active Co(II) ion in Co(II)-isoDromeQC wild type and variants after incubation with N-terminal glutamine and N-terminal glutamate substrates

These substrates mimic pathophysiological QC substrates. In this context, the EFRH hold a prior position because this substrate has the same initial amino acid sequence as the truncated A β peptide named A β (3E-40/42). With their propensity to form insoluble fibrils and soluble

neurotoxic oligomers these peptides play a key role in the development of toxic plaque deposition in the brain of AD patients [7, 23].

In order to analyze differences in the Co(II) coordination sphere induced by glutamate-substrates (e.g. EFRH, EW), the following experiment was performed. The N-terminal glutamate substrates were incubated at 20° C with the Co(II)-*isoDromeQC* wild type, Co(II)-*isoDromeQC_E190Q*, Co(II)-*isoDromeQC_D228N* and Co(II)-*isoDromeQC_D293N* for 5 min before the reaction was stopped by freezing in liquid nitrogen. In contrast to the attempts with N-terminal glutamine substrates, the incubation time was increased due to the low rate constant of N-terminal glutamate substrates as determined for *hQC* (Dr. Franziska Seifert, internal discussion).

The reaction of Co(II)-*isoDromeQC* wild type with the N-terminal glutamine substrate QFRH was stopped after 20 ms using the RFQ technique (*cf.* Section 2.12). The determined rate constants of the Zn(II) containing variants (*cf.* section 3.2) are 10,000-fold slower compared to the Zn(II)-*isoDromeQC* wild type. For this reason the incubation time for these measurements was increased to 5 s. The used concentrations of the substrate QFRH were 15 mM or 10 mM for rapid freeze quench and for manual freeze quench technique, respectively. The enzyme concentrations were set to 0.40 mM for rapid freeze quench EPR (only Co(II)-*isoDromeQC* wild type plus QFRH) and 0.34 mM Co(II)-*isoDromeQC_E190Q*, 0.32 mM Co(II)-*isoDromeQC_D228N* and 0.30 mM Co(II)-*isoDromeQC_D293N* (for manual freeze quench EPR experiments).

After 20 ms of QFRH incubation time, the measured EPR spectra of Co(II)-*isoDromeQC* wild type exhibits a shift to the lower magnetic field from 1038 G ($g = 6.443$) (resting state) to 1024 G ($g = 6.531$) (*cf.* Figure 3.18 A). The band width of the resonance signal is narrowed. This type of EPR spectrum indicates a four-coordinated Co(II) ion.

A more significant shift into the lower magnetic field could be observed with the Co(II)-*isoDromeQC_E190Q* (*cf.* Figure 3.18 A). The signal maximum was displaced from 1056 G ($g = 6.333$) (resting state) to 1026 G ($g = 6.518$). The band width of this signal is also narrowed significantly. The EPR spectra mirrors a predominantly four-coordinated Co(II) ion with indications that also five-coordinated Co(II) ions exist in the sample.

The signal maximum of the variant Co(II)-*isoDromeQC_D228N* after 5 s incubation time shows also deviation into the lower magnetic field from 1036 G ($g = 6.455$) (resting state) to 1022 G ($g = 6.544$). This resonance signal shows a narrower band width compared to the resting state. Interestingly, this EPR spectrum contains a second signal at 1140 G ($g = 5.866$), implying that besides the predominantly four-coordinate Co(II) ions also five and six-coordinated Co(II) ions are present in the sample (*cf.* Figure 3.18 A). The variant Co(II)-*isoDromeQC_D293N* shows a shifted maximum of the resonance signal from 1058 G ($g = 6.321$) (resting state) to 1042 G

3 Results

($g = 6.418$) into the lower magnetic field combined with a narrower band width. This EPR spectrum is typical for four-coordinated Co(II) ions (*cf.* Figure 3.18 A).

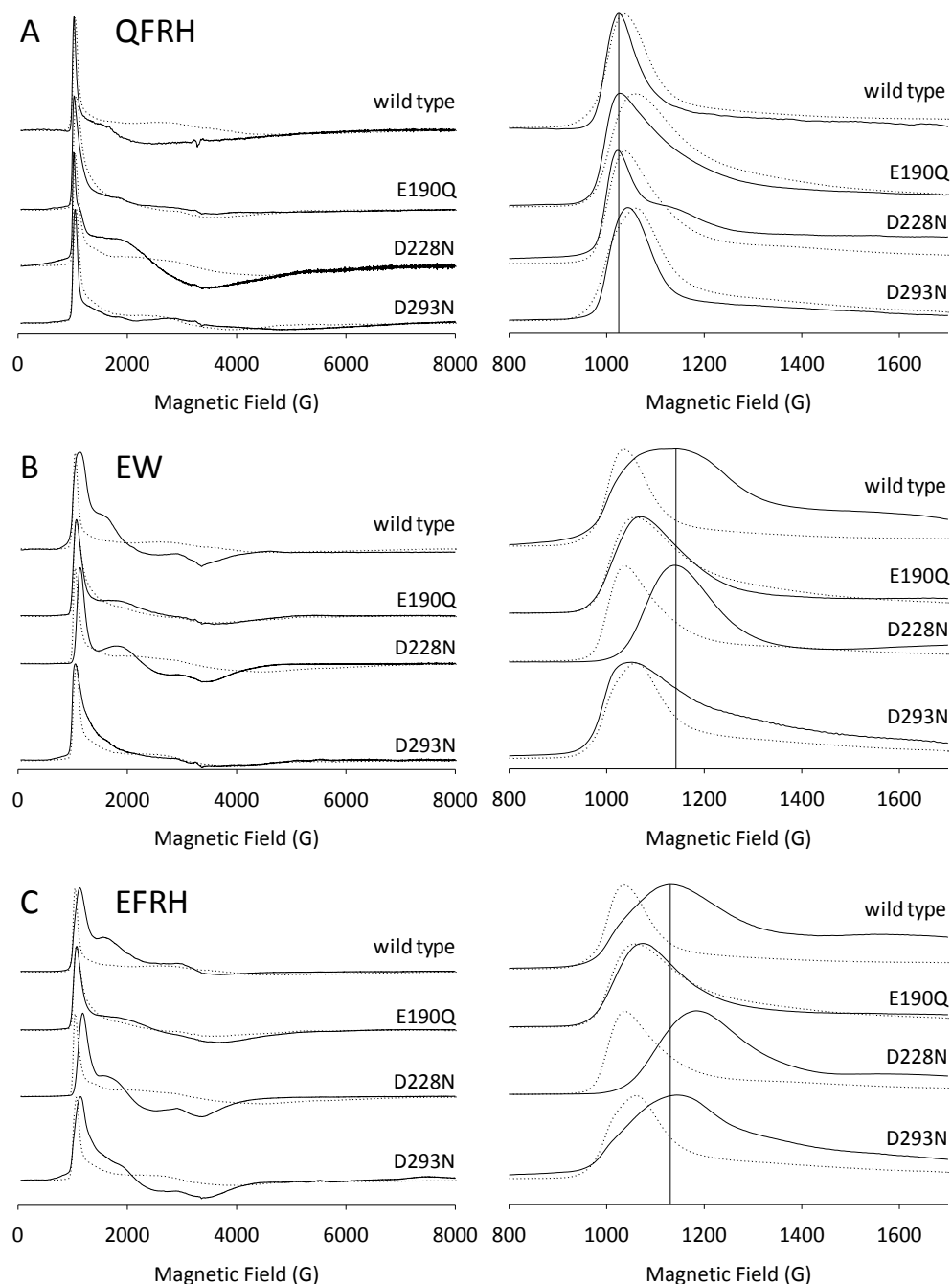


Figure 3.18 EPR spectra of Co(II)-isoDromeQC wild type and variants after incubation with N-terminal glutamine substrate and two N-terminal glutamate substrates The EPR spectra of Co(II)-isoDromeQC wild type and QFRH were measured after 20 ms. The variants and QFRH were incubated for 5 s (A). The incubation time for the reaction between Co(II)isoDromeQC wild type and the variants with the substrates EW (B) and EFRH (C) were set to 5 min. The EPR spectra illustrate different binding modes between substrate with N-terminal glutamine (A) displaying a tetrahedrally coordinated Co(II) and N-terminal glutamate (B, C) which evokes a five-coordinate Co(II) ion. The dotted line marks the resting state spectrum and the perpendicular black line defines the signal maximum of Co(II)-isoDromeQC wild type. Measured at 4.0 K, 20 mW at X-band wavelength (9.36 GHz) in 50 mM sodium phosphate buffer, 10 mM sodium chloride, pH 6.8 with a molar enzyme concentration wt/variants 0.23 μ M B, C and 0.34 μ M A rapid freeze quenche), QFRH 5 mM, EW, EFRH 15 mM after mixing.

The EPR spectra of Co(II)-iso*Drome*QC wild type incubated with the dipeptide EW (15 mM) points out a significantly broadened EPR signal. The maximum of the signals is shifted compared to the resting state from 1038 G ($g = 6.443$) to 1142 G ($g = 5.856$) (*cf.* Figure 3.18 B). Besides this signal a further less pronounced signal appears at approx. 1560 G ($g = 4.29$). This spectrum indicates a five-coordinated Co(II) ion.

The EPR measurement of Co(II)-iso*Drome*QC_E190Q yields a spectrum that is not significantly changed from that of the resting state of this variant. The maximum of the resonance signal is shifted into the higher magnetic field from 1056 G ($g = 6.333$)(resting state) to 1069 G ($g = 6.256$). The bandwidth of this signal is comparable to the resting state and indicates a four-coordinate Co(II) ion.

In contrast to Co(II)-iso*Drome*QC_E190Q, the EPR spectrum Co(II)-iso*Drome*QC_D228N incubated with EW presents a significant deviation of the signal maximum from 1036 G ($g = 6.455$) (resting state) to 1142 G ($g = 5.856$) into the higher magnetic field combined with a broadened band width. A second, smaller signal occurs at aprox. 1800 (G) ($g = 3.75$). This signal can be assigned to a five-coordinated Co(II) ion (*cf.* Figure 3.18 B).

The spectrum of Co(II)-iso*Drome*QC_D293N measured after the incubation with EW depicts that the maximum of the EPR signal is marginally shifted from 1058 G ($g = 6.321$) to 1052 G ($g = 6.357$) (*cf.* Figure 3.18 B). The difference of this spectrum to the resting state is that the descending branch of the signal is transferred into the higher magnetic field. This spectrum correlates to a predominantly four-coordinated Co(II) ion with indications that also five-coordinated Co(II) exists in the sample.

Nearly the same results were obtained when Co(II)-iso*Drome*QC wild type and the mentioned variants were measured after incubation with the substrate EFRH (15 mM).

The measurement of Co(II)-iso*Drome*QC_D293N after incubation with EFRH reveals an EPR signal that shows a significant shift of the signal maximum from 1058 G ($g = 6.321$) to 1144 G ($g = 5.846$) (*cf.* Figure 3.18 C). Additionally, a second signal appears in the range of 1800 to 1900 G. The bandwidth is extended significantly. In contrast to the attempt with EW, this spectrum implies that the Co(II) ion is five-coordinated.

3.6.4 EPR spectroscopic analysis of the coordination sphere of the catalytically active Co(II) ion in Co(II)-isoDromeQC wild type and variants after incubation with competitive inhibitors

The recent strategy in AD treatment is the inhibition of QC in order to avoid harmful accumulation of highly amyloidogenic species in the brain. The issue of interest in this regard is to analyze the type of influence of the inhibitor on the electronic environment of the catalytically active Co(II) ion.

Former investigations by Dr. Franziska Seifert reveal that also the reaction product acts as a competitive inhibitor (*cf. Supplemental 8.10*). Thus, a product analog compound pEFA (pyroglutamic acid-phenylalanine-alanine) was analyzed to investigate the effect of the reaction product on the Co(II) ion.

In these experiments the inhibitors were incubated at 20° C with Co(II)-isoDromeQC wild type, Co(II)-isoDromeQC_E190Q, Co(II)-isoDromeQC_D228N and Co(II)-isoDromeQC_D293N for two minutes. To freeze the samples, liquid nitrogen was used. Analogously to the former EPR experiments, these attempts were carried out using continuous wave (X-band) EPR at 4 K and 20 mW.

3.6.4.1 EPR analysis of Co(II)-isoDromeQC wild type and variants incubated with the tripeptide AFA

The EPR data of Co(II)-isoDromeQC wild type incubated with AFA and pEFA (described in the following section) were measured by Dr. Franziska Seifert. Here a qualitative comparison of the Co(II)-isoDromeQC wild type in resting state and incubated with these inhibitors is presented.

The used concentration of AFA was 7.5 mM ($K_i = 0.62$ mM). The concentration of Co(II)-isoDromeQC_D228N and Co(II)-isoDromeQC_D293N was 0.30 mM. The concentration of Co(II)-isoDromeQC_E190Q was 0.34 mM.

The EPR spectrum of Co(II)-isoDromeQC wild type incubated with AFA shows two signals. The first signal displays a maximum around 1050 G ($g \sim 6.37$) and the second around 1250 G ($g \sim 5.35$). This spectrum implies a clear five-coordinate Co(II) ion in the active center.

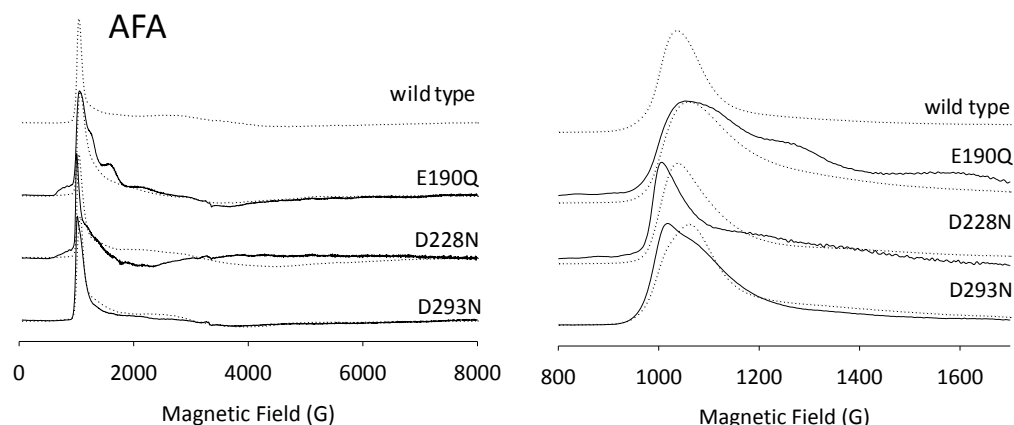


Figure 3.19-1 Manual freeze quench EPR experiments with the inhibiting tripeptide AFA The EPR spectra of Co(II)-iso*DromeQC* wild type (resting state), Co(II)-iso*DromeQC*_E190Q and Co(II)-iso*DromeQC*_D228N reveal a signal that indicates a Co(II)-hyperfine pattern in the magnetic field range between 620 G and 940 G. The left diagram shows entire spectra and the right depicts the zoomed spectra. While the bandwidth of Co(II)-iso*DromeQC*_D228N and Co(II)-iso*DromeQC*_D293N is narrowed with a shift of the signal maximum to lower magnetic field, the variant Co(II)-iso*DromeQC*_E190Q depicts a broadened resonance signal without any noticeable shift of the signal maximum. The dotted lines hallmark the EPR spectra of the resting state. Measured at 4.0 K, 20 mW at X-band wavelength (9.36 GHz) in 50 mM sodium phosphate buffer, 100 mM sodium chloride, pH6.8 with a molar enzyme concentration variants 0.30 mM (0.34 mM Co(II)-iso*DromeQC*_E190Q) and AFA concentration 7.5 mM.

The EPR spectrum of the variant Co(II)iso*DromeQC*_E190Q (*cf.* 3.19-1) displays a marginal shift of the maximum resonance signal from 1056 G ($g = 6.333$) to 1054 G ($g = 6.345$), in connection with a broadened band width. The spectrum shows a second signal at approx. 1250 G ($g = 5.350$) and a small but broad third signal occurs around 1560 G ($g = 4.287$). This spectrum implies that the Co(II) is predominantly four-coordinate but includes indications for five-coordinated Co(II). Interestingly, this spectrum indicates a Co(II)-hyperfine pattern in the low magnetic field from approx. 620 G to 940 G (*cf.* Figure 3.19-2)).

A clearly pronounced shift of the signal maximum into the lower magnetic field can be observed in the case of Co(II)iso*DromeQC*_D228N from 1036 G ($g = 6.455$) to 1005 G ($g = 6.654$) and exhibits a significantly smaller band width. This spectrum correlates to a four-coordinated Co(II) geometry. This EPR spectrum reveals an Co(II)-hyperfine signal occurring in the same magnetic field range as described for Co(II)-iso*DromeQC*_E190Q but with decreased amplitudes (*cf.* Figure 3.19-2) .

In the case of Co(II)iso*DromeQC*_D293N incubated with AFA, the signal maximum is transferred from 1058 G ($g = 6.321$) to 1017 G ($g = 6.576$) to the lower magnetic field. This EPR spectrum indicates four-coordinate Co(II). An additional five-coordinate signal, as observed in the resting state, has completely disappeared.

3 Results

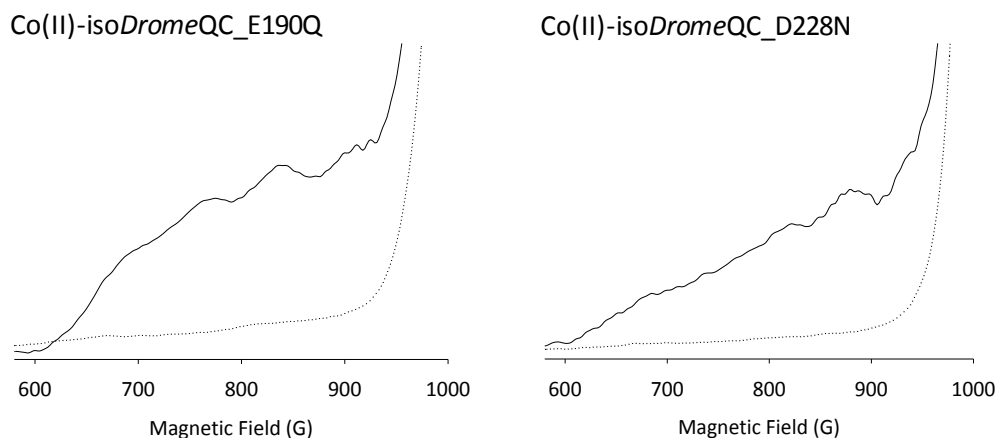


Figure 3.20 Co(II) hyperfine structure measured in Co(II)-isoDromeQC E190Q and Co(II)-isoDromeQC_D228N incubate with AFA The zoomed EPR spectra of Co(II)-isoDromeQC_E190Q and Co(II)-isoDromeQC_D228N reveal a signal that indicates a Co(II)-hyperfine pattern in the magnetic field range between 620 G and 940 G. The dotted lines hallmark the EPR spectra of the resting state.

3.6.4.2 EPR analysis of Co(II)-isoDromeQC wild type and variants incubated with the reaction product pEFA

The tripeptide pEFA possessing an N-terminal pyroglutamic acid corresponds to the reaction product of the QC reaction. As described above, QC reaction products act as competitive inhibitors. This experiment was performed to reveal potential interactions between the reaction product and the catalytically active Co(II) ion. For the EPR analysis, 10 mM pEFA ($K_i = 3.12$ mM) and 0.4 mM QC were used.

The EPR spectrum of Co(II)-substituted wild type enzyme incubated with pEFA presents a signal that indicates a four-coordinated Co(II) ion. Further, the signal maximum is slightly shifted into the lower magnetic field corresponding to a changed electronic Co(II) sphere along the Z-axis. This in turn corresponds to binding interaction between the product and the metal ion.

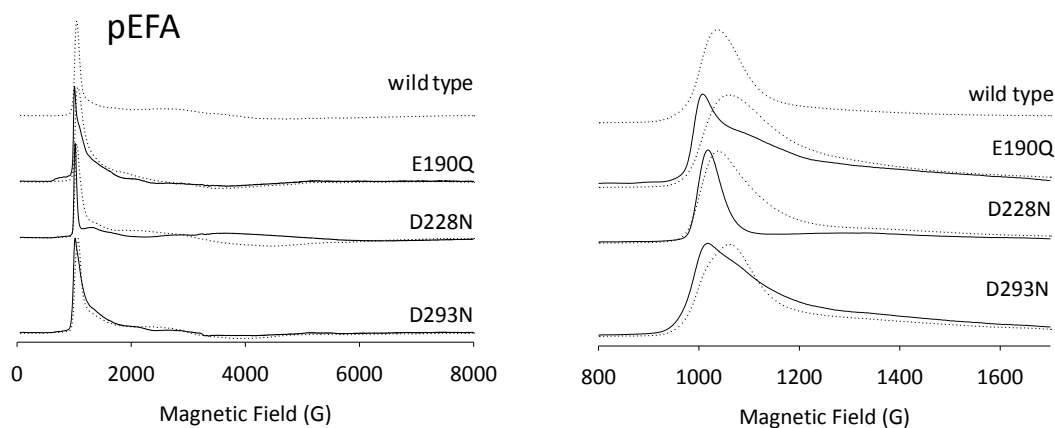


Figure 3.21 Manual freeze quench EPR experiments of Co(II)(II)-isoDromeQC wild type and variants after incubation with the product analog pEFA The influence of pEFA to the catalytically active Co(II) ion is reflected clearly in the EPR spectra of the variants which exhibit significant deviations of the signal maximum into the lower magnetic field. A second hallmark of the spectra is the narrowed bandwidth of the resonance signals compared to their resting states. The left diagram shows entire spectra and the right depicts the zoomed spectra. The dotted line represents the EPR spectra of Co(II)-isoDromeQC wild type and variants in the resting state while the solid line represents the EPR spectrum of Co(II)-isoDromeQC incubated with pEFA. The spectrum with wild type is described in the Supplemental due to missing ASCII files. The analysis was performed at 4.0 K, 20 mW at X-band frequency (9.36 GHz) in 50 mM sodium phosphate buffer, 100 mM sodium chloride, pH 6.8 with a molar enzyme concentration of 0.40 mM and a pEFA concentration of 15 mM.

The EPR spectrum of the variant Co(II)isoDromeQC_E190Q (*cf.* Figure 3.23) exhibits a significant low-field shift of the maximum resonance signal from 1056 G ($g = 6.333$) to 1007 G ($g = 6.641$), in conjunction with a clearly narrowed band width. In addition, the spectrum shows a second but not very pronounced signal at approx. 1100 G ($g = 6.08$). This spectrum implies that the Co(II) is predominantly four-coordinate but includes indications for higher coordination numbers (5 and 6).

A shift of the maximum of the EPR resonance signal into the lower magnetic field was observed in the case of Co(II)isoDromeQC_D228N. The signal maximum moves from 1036 G ($g = 6.455$) to 1017 G ($g = 6.576$) and displays a significantly smaller band width. This spectrum correlates to Co(II) which is four-coordinated.

In the case of Co(II)isoDromeQC_D293N, the signal maximum is displaced from 1058 G ($g = 6.321$) to 1017 G ($g = 6.576$). This EPR spectrum, too, is typical for four-coordinate Co(II).

4 Discussion

4.1 Characterization of the active center and the binding mode of N-terminal glutamine substrate binding

4.1.1 The lock-and-key principle – Basic correlations between active center and the substrate

The architecture of an enzyme, in particular of the binding pocket and the active center, plays the key role in substrate recognition and selectivity. The exploration of a binding pocket's structural design often explains the acceptance and preferences for substrates. Along with the identification of distinct amino acids constituting the substrate binding motif, information about the lock (enzyme) -and-key (substrate) principle can be gathered. Thus the knowledge about the structure-function relationship of specific amino acids in the binding pocket contributes to understanding different details about the catalytic mechanism. Furthermore, these findings might help to design potential inhibitors, which can be useful for drug development in the treatment of dementia.

The following section discusses the meaning of the results described above with regard to the interplay between the structure of the substrate and that of the binding pocket. In this context, the function of different amino acids in the active center is discussed.

4.1.1.1 *The electronic surface charge around and in the binding pocket is crucial for substrate selectivity*

Figure 4.1 demonstrates the electrostatic surface potential of Zn(II)-isoDromeQC wild type. As indicated, the surface in and around the active center is highly negatively charged. This can be explained by the presence of several carboxylic amino acid side chains that are localized within the substrate channel (*e.g.* E292, D293, D228, E190). Consequently, QC substrates possessing positively charged residues (*e.g.* arginine in QFRH) can be considered as preferred substrate due to electrostatic attractant forces between enzyme and substrate (*cf.* Section 3.2, Table 3.2). In line with this idea are former investigations indicating that substrates containing a negatively charged amino acid have high (worse) K_M values and a low rate constant [73].

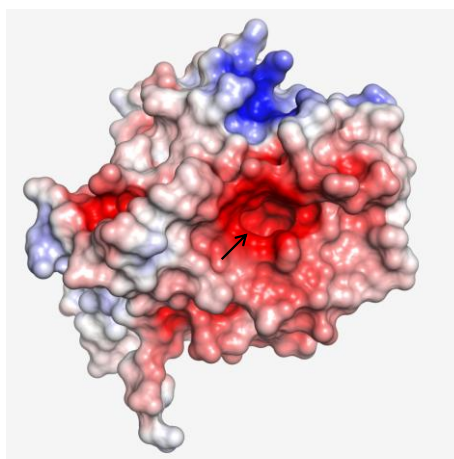


Figure 4.1 Electrostatic surface potential Displayed is the electrostatic potential level of the *isoDromeQC* surface from -7 (red surface is negatively charged) to 7 (blue surface is positively charged) in arbitrary units. The arrow marks the substrate binding pocket.

4.1.1.2 *The length of the substrate sequence is decisive for substrate affinity and catalytic efficiency*

The length of the substrates improves the kinetic constants as described in Section 3.2. The Zn(II)-*isoDromeQC* wild type measured with QFRH depicts a strong decrease of the K_M value that indicates a higher affinity between substrate and enzyme. Further the catalytic efficiency (k_{cat}/K_M) is increased by the factor of 6 to 19 compared to QQ or QGP representing a di- and tripeptide, respectively. Interestingly, the turnover number (k_{cat}) of QFRH is comparable to that observed with QGP and only two-fold higher than that found with QQ. This shows that the strongly increased k_{cat}/K_M is only due to the very low K_M value. Thus it can be concluded that compared to shorter substrates the equilibrium between substrate association and dissociation is extensively shifted to the enzyme substrate complex. The variants Zn(II)-*isoDromeQC*_D293A, Zn(II)-*isoDromeQC*_D293N and Zn(II)-*isoDromeQC*_D228N show in general higher K_M values and approx. 10,000-fold decreased k_{cat}/K_M . Nevertheless incubated with QFRH, these variants present the lowest K_M value and the highest k_{cat}/K_M . In line with these results are the data acquired by the Probiobdrug Company revealing that longer physiological oligopeptides as for example the decapeptide Gonadotropin releasing hormone (Q¹-GnRH) or Q¹-Gastrin (consisting of 17 residues) are highly preferred by *hQC* [57]. With *hQC* this tendency can also be observed with truncated A β peptides containing an N-terminal glutamine residue [90].

The crystal structure of the Co(II)-*isoDromeQC* in complex with the substrate QFRH (*cf.* Figure 3.11 A, D and E) implies that only the first two N-terminal amino acid residues of the substrate

are directly bound to the binding pocket. It can be assumed that an increasing peptide length provokes a rising number of hydrogen bonds on the surface of the QC supporting the substrate binding for QFRH.

4.1.1.3 Hydrophobic effects between aromatic amino acids in the second N-terminal position of the substrate and the active center may improve kinetic constants

As described in Section 3.2, substrates containing voluminous and aromatic amino acid side chains in the second N-terminal position (*e.g.* phenylalanine) are preferably converted by Zn(II)-isoDromeQC. This was indicated by low K_M values. It was speculated that this effect is due to π -stacking interactions between the enzyme and this particular amino acid. Interestingly, no interaction partner could be found in the structure of the substrate binding pocket. Since no π -stacking interaction partner is available, another reason for the preference could be the hydrophobicity of these amino acids. Possibly due to the high flexibility of the amino acid in the second position, the crystal structures reveal no specific hydrophobic interactions. The presence of several non-polar amino acids in and around the substrate binding pocket *e.g.* I291, F313, W196 (not depicted) increase the likelihood that such interactions support the substrate binding.

4.1.1.4 Active-center residues correlate with thermal stability

An additional aspect regarding the structure of the active center of isoDromeQC is the conformational stability. As described in Section 3.1, the conformational stability was studied by thermal unfolding utilizing the circular dichroism spectroscopy. The determined midpoints (or melting points) of the thermal unfolding transition curves can be used as measures for thermal stability. Enzymes with high thermal stability present the midpoint at higher temperatures.

The midpoint of the transition curve of the wild type is approx. 55°C (*cf.* Table 3.1). The side chain substitution of D293 either by alanine or asparagine yields midpoints at lower temperatures corresponding to less conformational stability. The crystal structure of Zn(II)-isoDromeQC wild type (*cf.* Figure 3.10 A and B) shows a network of possible hydrogen bonds between the amino acids E190, D293 and D228. The substitution of D293 as the central

amino acid in this network by alanine or asparagine would interrupt these connections. These interrupted hydrogen bond interactions may be causal for the loss of stability. This finding might thus indicate that amino acid side chains of the active center have a strong influence on the overall structural stability of *isoDromeQC*.

4.1.2 The function of the native Zn(II) ion in the catalysis of animal QCs

4.1.2.1 The metal in the active center

A multitude of metalloenzymes requires Zn(II) ions for enzymatic activity. Zn(II) can easily switch the coordination geometry between four-, five- or six-fold coordination numbers. In enzymes Zn(II) is often coordinated by four or five ligands [91]. Therefore, in the coordination geometry at least one binding site is free that can be occupied by different ligands. For example substrates can bind to the free binding site by raising the coordination number [91]. Ligand binding or dissociation events provoke changes in the electronic environment of the bioactive metal. Furthermore, the chemical reaction that the ligand undergoes during the catalysis is mostly combined with delocalization of electronic charges. Delocalized electronic charges influence the coordination sphere for example by stretching or compressing bond lengths or by distorting bond angles. Thus the investigation of the metal coordination geometry during the catalysis can help to understand discrete mechanistic steps of the catalysis.

The divalent and diamagnetic Zn(II) ion with the electron configuration $[\text{Ar}] 3d^{10} 4s^2$ ion exhibits neither optical electronic absorption signals nor paramagnetic resonances. For this reason the Zn(II) ion was exchanged for a divalent and paramagnetic Co(II) ion. Co(II) has the electron configuration $[\text{Ar}] 3d^7 4s^2$ and possesses three orbitals with one unpaired electron and is suitable for probing the coordination sphere by photospectroscopic methods as well as by the EPR method.

Despite the propensity to adopt higher coordination geometries [92], in *isoDromeQC* the Co(II) ion adopts the original tetrahedral coordination of the Zn(II) ion and thus helps to mimic the catalytically active form of the Zn(II) enzyme. Compared to native Zn(II)-QC, the Co(II)-substituted *isoDromeQC* exhibited a catalytic activity of approx. 85 % – 95 % (in rare cases higher) measured by Dr. Franziska Seifert (Supplemental 8.7). The loss of approximately 5 % - 15 % catalytic activity of the Co(II)-substituted *isoDromeQC* wild type is possibly due to the

formation of catalytically inactive five-coordinated Co(II) besides the four-coordinated Co(II). This hypothesis was strengthened by the finding that EPR signals of the wild type in its resting state displays four and five-coordinate Co(II) in a ratio of 90 % to 10 % (internal discussion with Prof. Dr. Brian Bennett)(*cf.* Section 3.6.1, Figure 3.15 A and B). Nevertheless, the reasons for good commutability of the metals are especially the almost equal ionic radii and the Alfred-Rochow electronegativities. Octahedral Zn(II) has an ionic radius of 0.88 Å and high-spin octahedral Co(II) 0.89 Å. Electronegativities (Zn, 1.66 and Co, 1.70) are also comparable. [87].

4.1.2.2 The characterization of the metal site in Zn(II)-isoDromeQC

That isoDromeQC requires the zinc ion was proven by adding the chelating agent 1,10-phenanthroline. The molecules of that compound are small and fit into the binding channel, where it coordinates the Zn(II) ion in a very tight manner. It leaves the apo-enzyme, which does not exhibit any catalytic activity [56]. The question of how many Zn(II) ions are required was unresolved for a long time. The bacterial aminopeptidase of *Aeromonas proteolytica* (ApAP), which is the potential evolutionary ancestor of animal QCs [56, 60] (*cf.* Section 1.4.1) requires two Zn(II) ions. Structural alignment of the active centers of isoDromeQC, hQC and ApAP (*cf.* Figure 1.6) demonstrated that both Zn(II) binding motifs are conserved isoDromeQC as well as hQC. However, the crystal structure of hQC and isoDromeQC showed an unoccupied second Zn(II) binding motif, which is in close proximity (3.5 Å) to the occupied Zn(II) binding motif on the bottom surface of the active center. Furthermore, increasing concentration of Zn(II) *in vitro* leads to a loss of catalytic activity [56]. For these reasons it is established that for catalysis only one Zn(II) ion is required.

The binding site of the catalytically active Zn(II) ion is located at the bottom of the substrate channel. Inorganic Zn(II) ions have a high affinity towards nitrogen and oxygen donor atoms [91]. Hence, it is not very remarkable that in QC the metal binding site is characterized by two carboxylic amino acid site chains (D153, E191) and one imidazole moiety (H318). As described above, the fourth coordination ligand is a water molecule in the resting state. The Zn(II) and the Co(II) ion, respectively, hold a slightly distorted tetrahedral coordination sphere. For an ideal tetrahedral geometry all bond angles between the substituents would be $\cos^{-1}(-1/3) \approx 109.5^\circ$. Table 4.1 depicts selected angles including one amino acid, the metal ion and the water molecule. Even in the wild type, the bond angles deviate from 109.5°. This is in line with

obtained EPR data. A perfect four-coordinate central atom would be EPR silent (internal discussion with Prof. Dr. Brian Bennett).

Table 4.1 Bond angles between Zn(II) coordinating residues, Zn(II) and water molecule in the active center of Zn(II) isoDromeQC. The bond angles were determined by analyzing x-ray crystal structure in the “pymol” program version 1.3.

Bond angles	D153/OD2-Zn(II)-H ₂ O	E191/OE1-Zn(II)-H ₂ O	H318/NE2-Zn(II)-H ₂ O
Wild type	108.0°	115.1°	112.5°
E190Q	124.8°	98.4°	112.7°
D228N	129.5°	113.6°	110.8°

The bond angles in the active center of the variants are partially significantly distorted. Data from EPR (*cf.* Section 3.6.1 and Figure 3.15) and stopped flow UV/Vis spectroscopy (section 3.4.1 and Figure 3.4) visualize clear distinctions in the coordination geometry Co(II) between Co(II)-isoDromeQC wild type and variants. Changes in the bond angles due to side chain substitution in the variants affect the geometry of the metal ion.

4.1.2.3 The Zn(II) as Lewis acid activates the γ -carbonyl moiety of the N-terminal glutamine

The role of the Zn(II) ion for catalysis of QCs is currently becoming clearer. The crystal structure of isoDromeQC in complex with QFRH (*cf.* 3.11 A and B) showed that the γ -amido oxygen atom of the substrates' N-terminal glutamine residue binds to the fourth position of the Co(II) ion. This finding might indicate that the Co(II) ion is used to activate the substrate carbonyl for nucleophilic attack. The formation of a coordinative bond between Co(II) and the γ -amido oxygen induce a delocalization of electronically negative charge from the γ -amido carbon atom towards the γ -amido oxygen-Co(II) bond. Subsequently the positively polarized γ -amido carbon can be attacked nucleophilically by the α -amino nitrogen [60].

4.2 The catalytic cycle of the cyclization reaction of substrates with N-terminal glutamine

4.2.1 Substrate binding

The formation of the enzyme substrate complex is the initial event in the trajectory of a catalytic cycle. Enzyme kinetic studies, EPR experiments and x-ray crystallography were employed to analyze this catalytic step in terms of binding velocity, involved binding motifs and structural features.

UV/Vis and EPR spectroscopic trials visualize the binding between substrate and Co(II)-substituted enzyme when the electronic environment of the Co(II) is affected. In the UV/Vis experiments the absorbance spectra change due to altered extinction coefficients of the Co(II) ion when a substrate ligand is bound. The EPR spectra of the Co(II)-enzyme substrate complex tended to show shifted band positions due to stretched or compressed bond length along the Z-axes.

The stopped-flow UV/Vis absorption spectra of Co(II)-*isoDromeQC* wild type after rapid mixing with the substrates QQ (*cf.* Figure 3.5-1 A; 3.5-2 A) and QFRH (*cf.* Figure 3.5-3 A and B) present an increase in the absorption at several wavelengths within the dead time of the stopped-flow detector device. Considering the EPR results, the binding of QQ (*cf.* Figure 3.17 A) and QFRH (*cf.* Figure 3.18 A) affect the coordination sphere of Co(II) after 10 ms in case of QQ and 20 ms in case of QFRH. Thus we can conclude that the replacement of the water molecule by the substrate in the fourth coordination position occurs immediately after the mixing. Hence the substrate binding can be assigned as a very rapid step in that reaction trajectory.

The EPR spectra of Co(II)-*isoDromeQC* wild type incubated with both QQ and QFRH also indicate a tetrahedrally coordinated Co(II) ion. The N-terminal glutamine of the substrate thus binds in a monodentate manner. This result tallies with the crystal structure (*cf.* Figure 3.11 A and B) showing a coordinating interaction between the γ -amido oxygen of the N-terminal glutamine and the Co(II) ion with a bond length of approx. 2.0 Å. The crystal structure further discloses polar contacts between the substrate and side chains of active-center amino acids D228 and E190 (*cf.* Section 3.5.3) as well as the main chain of D292. As described in the introduction, also the active-center amino acids D293 may act as substrate binding motifs. Further evidence for the hypothesis that these side chains are involved in substrate binding were accumulated by side-chain substitution of E190, D228 and D293. The kinetic constants of the variants were determined by UV/Vis and fluorescent spectroscopic assays (*cf.* Section 2.6 and 3.2). In particular

the variants Zn(II)-isoDromeQC_D293N, _D393A and Zn(II)-isoDromeQC_D228N showed six to eight-fold higher K_M values reflecting an impaired substrate binding. EPR and stopped-flow experiments performed analogously to those of the Co(II)-isoDromeQC wild type yield results implying a tremendously reduced substrate metal interaction (*cf.* stopped flow: Section 3.4.2 Figure 3.5-1,2; Section 3.4.3 Figure 3.5-3; EPR: Section 3.6.2 Figure 3.17). This means that the substrate binding is strongly impaired in these variants.

Contrarily, the K_M value determined with the variant Zn(II)-isoDromeQC_E190Q is decreased (*cf.* Section 3.2, Table 3.2). EPR (*cf.* Section 3.6.2 Figure 3.17) and stopped-flow (*cf.* Section 3.4.2 Figure 3.5-1,2) analysis of the Co(II)-substituted variant showed a rapid change (after 20 ms) in the Co(II) coordination sphere after the mixing. At least the postulated interaction between the γ -carbonyl oxygen of the N-terminal substrate glutamine and the Co(II) ion may occur (*cf.* Section 1.4.3). The EPR spectra obtained after longer incubation times are nearly identical to those obtained after 20 ms. This indicates that after the substrate binding no further changes in the Co(II) sphere occur. This is in line with the low K_M value and the strongly decreased k_{cat} and k_{cat}/K_M . Due to a missing crystal structure, the reason for substrate binding cannot be clarified. It is likely that the formation of a hydrogen bond between γ -amido oxygen in position 190 and α -amino nitrogen of the N-terminal substrate glutamine mediates the substrate affinity as depicted in Figure 4.2.

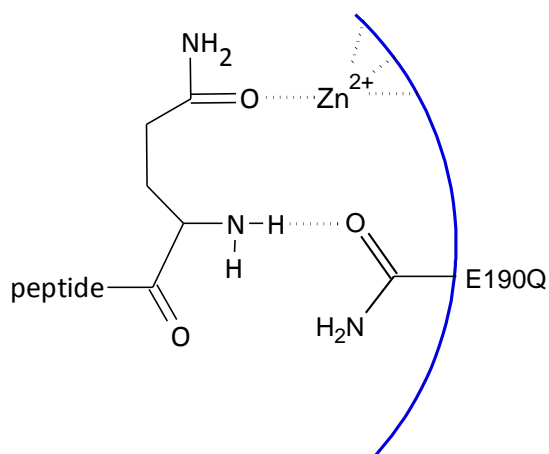


Figure 4.2 Postulated substrate enzyme interaction in Zn(II)-isoDromeQC_E190Q Kinetic studies and EPR data indicate a fast substrate binding. Hypothetically this could be mediated by the non-covalent interactions between the Zn(II) and the γ -carbonyl oxygen and in particular between substituted asparagine and the α -amino group of the substrate.

4.2.1.1 Mild alkaline pH supports the substrate affinity by deprotonation of the α -amino group of the substrate's N-terminal glutamine

A further aspect relevant to the formation of a substrate enzyme complex is the protonation degree of the α -amino group of the N-terminal glutamine. The pH dependence measurement allows the calculation of pK_a values (inflection points in pH-catalytic efficiency curve) of amino acids which act as acid/base catalysts. The pK_{a2} values calculated from the measurements with Zn(II)-isoDromeQC wild type as well as all variants indicate a value of approx. 9.13 (*cf.* 3.3, Table 3.3-2). This is in accordance with the literature pK_a value for α -amino groups of glutamine [93]. This identifies this α -amino group as the acid/base catalyst in the QC reaction. In this and former work, a pH optimum [57] for activity of (isoDrome) QC at the alkaline pH range around pH 7.9 has been reported. At this pH the α -amino group is predominantly deprotonated. Additionally, the conclusion that a deprotonated α -amino group is required for substrate binding (and catalysis) is strengthened by the fact that the K_M values decrease at alkaline pH and increase at acidic pH (*cf.* 3.3, Table 3.3-1). This means that the substrate affinity increases with the rising concentration of deprotonated α -amino groups.

4.2.2 Characterization of discrete mechanistic steps in the trajectory of QCs

The chemical reaction from glutamine to pyroglutamic acid is assigned to the addition-elimination mechanism S_N2_t [60]. This bimolecular reaction is characterized by the concerted addition of a nucleophile to a polarized molecule and the release of a leaving group (elimination). During the reaction a short-lived tetrahedral transition state occurs. Considering the cyclization reaction of glutamine, the nucleophile and the polarized group belong to the same molecule. The QC enhances this intra-molecular ring closure reaction by the activation of both reacting moieties. In the following section the discrete steps of the QC catalysis are discussed.

4.2.2.1 Chemical activation of substrate moieties support the nucleophilic attack

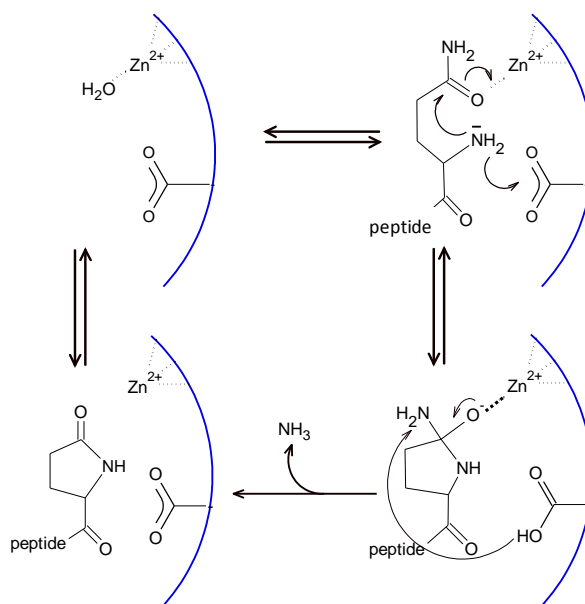


Figure 4.3 Postulated reaction cycle of Zn(II)-dependent QC The postulated catalytic cycle of glutaminyl cyclase depicts the formation of a tetrahedral reaction intermediate after the α -amino group has attacked the γ -carbonyl nucleophilically. This intermediate breaks down into ammonia and pyroglutamic acid.

Once the substrate is bound to the enzyme, it is suggested that it becomes activated from two sides (*cf.* Figure 4.3). As shown in Section 3.6.2 and Figure 3.17, the EPR data obtained with the Co(II)-isoDromeQC wild type after several incubation periods depict a strong shift of the signal maximum after 10 ms. This shift is at its maximum after 160 ms. As described above, the substrate binding can already be observed after 10 ms. Almost simultaneously with the detected deformation of the coordination geometry of Co(II) induced by substrate binding, a further increase of the deformation occurs. This indicates that electron(s) from Co(II) become strongly delocalized along the Z-axis of the Co(II) coordination sphere. According to the postulated mechanism, this electron delocalization would occur along the axis of the γ -carbonyl carbon - γ -carbonyl oxygen and the Co(II) ion. This non-covalent metal-oxanion interaction effectuates a polarization of the γ -carbonyl carbon and increases its electrophilic force. Simultaneously, as indicated in the crystal structure (*cf.* Figure 3.11), it is most likely that the γ -carboxylic group of E190 abstracts a proton from the α -amino group of the N-terminal glutamine. This deprotonation step enhances the already high nucleophilicity of the α -amino nitrogen. [73, 90]. Presumably, the consequence is that the α -amino nitrogen attacks the γ -carbonyl and forms a

highly excited and short-lived tetrahedral intermediate. In this state the bond formation between the nucleophile and the polarized carbon atom is still incomplete. The bond between the leaving group and the carbon atom is prolonged but still existent. The tetrahedral intermediate is possibly stabilized by the catalytically active metal ion. Currently the existence of this intermediate state is likely but remains for now hypothetical.

The question of whether the formation or decomposition of the tetrahedral intermediate is rate-limiting was investigated by Dr. Franziska Seifert employing beta-secondary isotope effect experiments (results see Supplemental Section 8.8). For this trial the deuterated Q-AMC (*cf.* Figure 4.4 A) was used as substrate for the fluorescence spectroscopic assay (*cf.* Section 2.6.2). Characteristic for β -secondary isotope effects is that the moiety harboring the isotope, in this case deuterated methylene groups, are in the proximity of these moieties which are involved in bond formation. This experiment can unveil differences in the activation energies that are required for the formation or stabilization of the tetrahedral intermediate when this step is rate limiting. The stabilization of this tetrahedral intermediate is most likely due to hyperconjugation. In this case an electron from the orbital of the σ -bond between the δ -carbon atom and the hydrogen or deuterium stabilizes the polarized γ -carbon by mesomeric effect (*cf.* Figure 4.4. B). Hyperconjugation and the related stabilizing effects to transition states are a source of β -secondary isotope effects [98]. In case of a deuterated δ -methylene group the stabilization of the transition state requires higher activation energy. This in turn leads to lower reaction velocity. The quotient of the determined kinetic constants of the reaction with deuterated and undeuterated substrate corresponds to the equilibrium isotopic effect (K_M) and the kinetic isotopic effect (k_{cat}). The isotopic effects become significant in a range between 1.5 and 7. The determined isotopic effects were below 1.5 and consequently not significant. Hence, we can conclude that the formation or the decomposition of the suggested tetrahedral intermediate is most likely not the rate-limiting step.

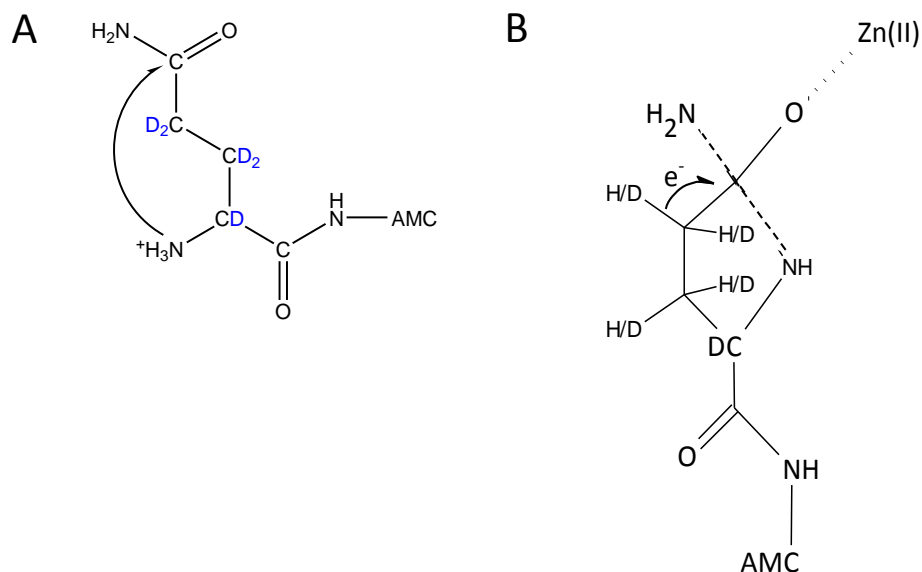


Figure 4.4 Deuterated fluorogenic substrate Q-AMC and the postulated tetrahedral intermediate (A) The fluorogenic substrate was utilized to examine a beta-secondary isotope effect employing fluorescence spectroscopy. (B) The postulated tetrahedral intermediate is possibly stabilized by hyperconjugation. In case of deuterated methylene groups, the hyperconjugation requires higher activation energy compared to hydrogen-containing groups. When the formation of this intermediate is rate-limiting, this effect causes lower rate constants.

4.2.2.2 The release of ammonia (deamination) is accompanied by the decomposition of the reaction intermediate

The EPR data of Co(II)-isoDromeQC wild type incubated with QQ after several incubation times show that the shift of the signal maximum after 2 s becomes smaller compared to the signal after 160 ms. This indicates that the strong distortion in the coordination sphere of Co(II) is reconstituted. This relaxation can be induced by the decomposition of the putative tetrahedral intermediate. This step includes the cleavage of the γ -amino moiety and the removal of the delocalized electron (*cf.* Figure 4.3). Crystal structures of Co(II)-isoDromeQC wild type (*cf.* Figure 3.11 B and C) depict that the γ -carboxylic moiety of D228 and γ -amino nitrogen are in hydrogen bond distance. It is suggested that this amino acid provides a proton to the leaving γ -amino group. This proton transfer possibly enhances the elimination of ammonia. The release of ammonia makes the cyclization reaction quasi-irreversible. Schilling *et al.* showed that ammonia concentration up to 50 mM does not inhibit the reaction [80]. The missing product inhibition indicates that the deamination step is most likely not rate-limiting.

4.2.2.3 Proton transfer pathways are crucial for the release of ammonia

As described above, in this reaction mechanism at least two different proton transferring steps are included. First, E190 abstracts a proton from the α -amino group of the substrate. Second D228 transfers a proton to the leaving group. Furthermore, for a complete regeneration of the enzyme, E190 has to be deprotonated.

Crystal structures of this work and of other investigators imply that the transport of protons in *isoDromeQC* as well in *hQC* [94] is presumably organized by at least three conserved carboxylate moieties in the active center residues (*cf.* Figure 4.5). In *isoDromeQC* the supposed residues are E190 (proton abstraction from α -amino group of the N-terminal glutamine), D293 (proton transfer) and D228 (protonation of the leaving γ -amino group). Kinetic studies with variants Zn(II)-*isoDromeQC*_E190Q, Zn(II)-*isoDromeQC*_D293N and Zn(II)-*isoDromeQC*_D228N (*cf.* Section 3.2) present vastly diminished rate constants. Along with the crystal structure and the results from the kinetic investigations, it seems that these three amino acids are involved in this postulated proton transfer.

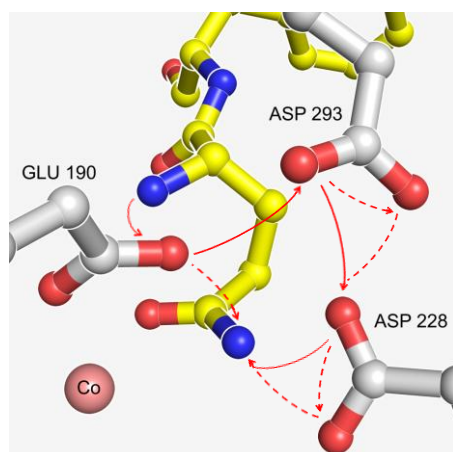


Figure 4.5 Suggested proton transfer pathways in *isoDromeQC* during the catalysis The crystal structure image of Co(II)-*isoDromeQC* wild type depicts the supposed proton transfer pathways (red arrows) and possible (in hydrogen bond range) alternatives (dashed arrows). This supposed pathway explains the proton abstraction from the α -amino moiety of the N-terminal glutamine (yellow rods) and the protonation of the leaving γ -ammonia group.

Experiments investigating solvent isotope effects (performed by Dr. Franziska Seifert, results see Supplemental 8.6) were carried out to investigate whether the proton transfer is the rate-limiting step of catalysis. In these experiments, deuterated water was used for buffer preparation to replace protons in the relevant acid/base catalysts *e.g.* the α -amino group of the N-terminal glutamine by deuterons. Due to the doubled mass of this ion, the transfer requires higher activation energy. This effect can be reflected in lower rate constants of the enzymatic reaction when this transfer is rate-limiting for the catalysis. Kinetic constants of Zn(II)-*isoDromeQC* were determined in water and deuterium oxide-based buffers, respectively. The quotient of the kinetic constants (k_{cat}) of both measurements corresponds to the solvent isotope effects. Solvent isotopic effect in a range from 1.5 and 7 seems to indicate that proton transfers

are involved in rate-limiting mechanistic events. The measurements showed no significant solvent isotopic effect. Thus we can conclude that the proton transfer can be excluded as rate-limiting step in the QC reaction.

4.2.2.4 Release of pyroglutamic acid as final step of the catalytic cycle

Product release is the final step of catalysis. The substrate-derived compounds used here i.e. pEFA and pEFRH, were determined to be competitive inhibitors with inhibition constants in the low millimolar range. The structure of the product possesses the same binding motif as the substrate (*cf.* Figure 3.13 and 3.12). The aromatic amino acid phenylalanine mediates the moderate affinity (*cf.* 4.1.1; 3.2) to the active center. Furthermore, the keto-oxygen still interacts with the catalytic metal ion. The EPR-measurements with the compound pEFA (*cf.* Figure 3.20) and QQ (*cf.* figure 3.17) presumes that the product enzyme complex is stable even 16 hours after the reaction. The band position of the EPR signal after two min (and even after six hours) reaction time is not completely identical with the EPR signal obtained from the enzyme in the resting state (*cf.* Figure 3.17 A) The interactions between product and enzyme (*cf.* Figure 3.13) mediate a certain stability of the enzyme product complex which is a condition for a successful co-crystallization attempt. The stability of this complex is most likely the reason for the product inhibition. This indicates that the product release is rate-limiting in the QC reaction. Further, the former catalytic steps can be excluded as rate-limiting factors. Nevertheless, the product release cannot be determined with reliability as the rate-limiting step in the catalytic cycle. In all experiments the concentration of the product was in the millimolar range (7.5 mM – 15 mM) and thus higher than *in vivo*. Hence, the equilibrium between product association and dissociation is shifted to the associated complex due to the experimental conditions.

4.3 QCs provide unfavorable conditions for conversion N-terminal glutamate substrates

A multitude of investigations concerning toxic depositions in the brain revealed that truncated A β peptides *e.g.* A β (E3-40/42) and A β (E11-40/42) possessing an N-terminal glutamate residue play a major role in development of neurodegenerative disorders [23, 31, 95, 96]. For this reason, the examination of discrete catalytic steps during N-terminal glutamate cyclization reaction is very important but poorly investigated so far with animal QC. The first crystallographic, UV/Vis- and EPR spectroscopic experiments concerning N-terminal glutamate cyclization led to new insights, which are discussed in the following section.

4.3.1 N-terminal glutamate conversion lacks efficiency due to protonation conflict between crucial functional groups

In this work, EPR and UV/Vis spectroscopic approaches were performed with Co(II)-*isoDromeQC* wild type and variants using two N-terminal glutamate substrate derivatives. These substrates were EFRH or A β (3-6) a shortened form of A β (3-40/42) and EW. The UV/Vis stoppedflow analysis (*cf.* Section 3.4.3) measured at pH 8.0 depicts no significant change of the Co(II) absorbance spectra after incubation with both EFRH and EW. The change of the Co(II)'s coordination number from four to five accompanied by spectral changes was unfortunately not detectable via UV/Vis spectroscopy. Interestingly the crystal structure obtained from co-crystallization attempts of Co(II)-*isoDromeQC* wild type with EFRH (*cf.* Section 3.5.4) reveals a bidentate coordination between both γ -carboxylate oxygen atoms from the substrate and the catalytically active Co(II) ion. However, EPR spectroscopic analysis of Co(II)-*isoDromeQC* wild type and the variants Co(II)-*isoDromeQC*_D228N and Co(II)-*isoDromeQC*_D293N at pH 6.8 (*cf.* 3.6.3) points to a clear change of the absorption spectra. The obtained spectra indicate a five-coordinated Co(II) ion, which is in line with crystallographic results. The EPR spectra of the variant Co(II)-*isoDromeQC*_E190Q is nearly superimposable with the resting state spectrum, indicating hampered substrate binding. Those results solely demonstrate that N-terminal glutamate substrates bind to the active center of the Co(II)-*isoDromeQC*. Using these approaches, a catalytic conversion could not be determined in a quantitative manner. One unique indication of substrate conversion is given by the co-crystallization experiment with EFRH leading to observable electron density of pyroglutamic acid in the active center of

Co(II)*isoDromeQC* after an incubation time of approx. one week at 20° C. The fact that electron density for EFRH was still detectable in the same crystal indicates that the turnover velocity is very slow. In former studies with *hQC*, the conversion velocity of N-terminal glutamate was found to be approx. 10,000-fold slower than the glutamine conversion [52]. The animal QCs show an explicit preference for N-terminal glutamine substrates. Seifert *et al.* demonstrated that spontaneous cyclization of N-terminal glutamine residues occur with a rate constant of approx. 10^{-6} s^{-1} and can be accelerated by a factor of 10^7 by *hQC*. On the other hand, the rate constant of spontaneous N-terminal glutamate cyclization is approx. 10^{-9} s^{-1} and can be enzymatically enhanced by a factor of 10^5 [52]. There are two cogent reasons for the low efficiency of the glutamate conversion. The first reason is that the N-terminal glutamate is bivalently charged around neutral pH. The determined pK_a values for N-terminal glutamate were 4.2 for γ -carboxylic group and 7.5 for the α -amino group in papaya QC which most likely converts the N-terminal glutamate in a similar mechanistic manner[90]. Around neutral pH the N-terminal glutamate bears a protonated positively charged α -amino group and an unprotonated, negatively charged γ -carboxylic group. In this state neither the electrophilicity of the γ -carbonyl nor the nucleophilicity of the α -amino nitrogen is adequate for an intra-molecular nucleophilic attack (*cf.* Figure 4.3.). Glutamate conversion by animal QCs in dependence of pH has not been reported so far. Schilling *et al.* reported that Zn(II)-independent *papaya QC* showed maximum activity at pH 6.0 in terms of glutamate conversion [90]. Considering the pK_a values of the N-terminal glutamate, these findings are coherent. At pH 6 the population of protonated γ -carboxylic moieties increases. The generated γ -hydroxyl group leads to an increasing electrophilicity of the γ -carbonyl group. Further, the concentration of unprotonated nucleophilic α -amino nitrogen is still sufficient. In accordance with the glutaminy cyclization reaction, these circumstances are required for the nucleophilic attack of the α -amino nitrogen. To summarize, the mildly acidic milieu reflects a “compromise” pH at which low concentrations of both activated groups are still present [90].

A further reason for slow glutamate conversion is possibly due to the bidentate coordination of the catalytically active metal ion of the γ -carboxylic group.

As mentioned above, EPR studies and x-ray crystallography experiments of Co(II)-substituted *isoDromeQC* wild type indicate a different binding mode of the N-terminal γ moiety. In contrast to four-fold coordinated Co(II) during glutaminy cyclization, substrates with an N-terminal glutamate residue generate EPR signals which are indicative of five-coordinate Co(II). The structure shows a five-coordinated Co(II) in which the γ -carboxylic group is bound in a bidentate

manner. In this context it is important to note that the EPR as well the x-ray crystallography experiments were carried out at pH 6.8 and pH 8.0, respectively. At this pH-range the γ -carboxylate group is most likely partially (pH 6.8) or nearly completely deprotonated (pH 8.0). Considering the bidentate coordination of Co(II) in the Co(II)-*isoDromeQC* structure (*cf.* Figure 3.12 B), it can be assumed that Co(II) functions as a Lewis acid and receives electrons from both γ -carbonyl oxygen atoms of the substrate. This makes a ring closure reaction unlikely since no hydroxyl leaving group is available. Thus one can speculate that the five-coordinate Co(II) mirrors an almost catalytically inactive state of *isoDromeQC* (wild type).

4.3.2 N-terminal glutamine substrates assist the delineation of postulated amino acids as substrate binding motifs

In order to further analyze the substrate binding mode of Co(II)-*isoDromeQC*, additional EPR measurements with different enzyme variants were performed. In particular, EPR analysis of incubations of Co(II)-*isoDromeQC_D228N* with substrates harboring an N-terminal glutamate residue (*i.e.* EW and EFRH) should demonstrate if this D228 residue is an important substrate binding motif as described for N-terminal glutamine substrates depicted in Figure 3.11 B and C. This experiment was also used to investigate the role of D228 in the postulated proton transfer pathway (*cf.* Section 4.2.2.3, and Figure 4.5). The EPR spectrum of *isoDromeQC_D228N* incubated with QQ (*cf.* Figure 3.17 D) showed that signal maxima after several incubation times do not show significant shifts. This implies that the substrate has no influence on the electronic environment of the Co(II) ion. This leads to the conclusion that (hardly) any substrate binding occurs with this substrate. However, when incubated with EW as substrate, this variant shows a prominent EPR signal that is indicative for five-coordinated Co(II). This suggests that an interaction between substrate and metal occurs (*cf.* Figure 3.18 B). Thus, this observation underlines the function of D228 as a glutamine substrate binding mediator.

As shown in Figure 4.6 A, N-terminal glutamine substrates may interact via hydrogen bond between γ -amino nitrogen of the N-terminal substrate glutamine and the the γ -carboxylic oxygen of D228 in the wild type. Conversely, in *isoDromeQC_D228N* (*cf.* Figure 4.6. C) the γ -amino nitrogen of asparagine in position 228 can mediate hydrogen-bond contact with the γ -carboxylic oxygen of the N-terminal glutamate substrate.

Considering the results of the substrate specificity study (*cf.* Section 3.2 and Figure 3.2) Zn(II)-*isoDromeQC_D293N* or -D293A depict worse K_M values compared to the wild type, and this

suggests that D293 is also involved in substrate binding. In line with this result, the EPR spectra of the variant Co(II)-*isoDromeQC_D293N* incubated with QQ or QFRH (*cf.* Section 3.6.2, Figure 3.17 and Section 3.6.2, Figure 3.18) show also no significant change in the coordinative geometry of Co(II). This finding is indicative for a frustrated substrate binding. EFRH induces strongly altered EPR signal when incubated with Co(II)-*isoDromeQC_D293N*; this implies a substrate-induced distortion of the Co(II) geometry. Hypothetically, this could be the result of an inverse hydrogen bond donor/acceptor situation as previously described for Co(II)-*isoDromeQC_D228N* incubated with EW or EFRH. The nitrogen of the substituted γ -amido residue in position 293 may form a hydrogen bond to the γ -carboxylic oxygens of the N-terminal glutamate in EFRH and possibly enables an early substrate binding step.

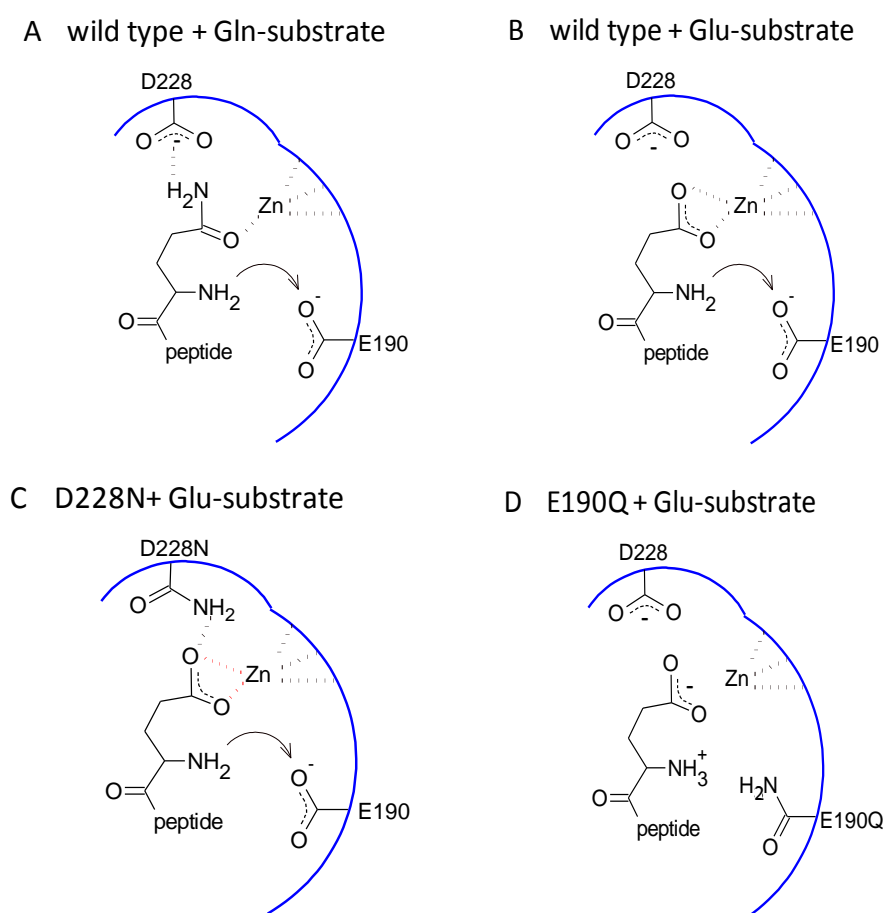


Figure 4.6 Suggested interactions between substrates and *isoDromeQC* wild type, *isoDromeQC_D228N* and *isoDromeQC_E190Q* in the active center The scheme illustrates the active center in Zn(II)-*isoDromeQC* wild type with N-terminal glutamine substrates and tetrahedrally coordinated Zn(II) (A). In contrast, the N-terminal glutamate substrates are bidentately bound to the catalytically active metal ion (B). In *isoDromeQC_D228N* (C) the N-terminal glutamate is also bidentately bound to Zn(II). A hypothetically inverse hydrogen bond donor/acceptor situation between the γ -carboxylic group of the N-terminal glutamate and γ -amido group of the substituted residue 228 may occur. Around pH 7 in *isoDromeQC_E190Q* (D) it is likely that the substrate α -amino group and the γ -amino group are protonated (according to their pK_a values). This postulated situation would lead to repulsion forces between enzyme and substrate.

4.3.3 The glutamyl cyclization requires protonation of the leaving group - a proposed proton transferring pathway

Analogously to the postulated reaction cycle of substrates with N-terminal glutamine, the glutamate cyclization depends on proton transfer as depicted in Figure 4.7 for two reasons. First, the α -amino group has to be deprotonated to enhance the nucleophilicity of the nitrogen (*cf.* Figure 4.7). Second, the leaving group (hydroxyl ion) has to be protonated. The crystal structure of N-terminal glutamate substrate in complex with the wild type (*cf.* 4.8 A) shows many possible polar contacts, which can be employed as proton transfer pathway. In Figure 4.8 B, possible pathways for proton transfers are depicted. The proposed network uses the same active center residues as described in the cyclization reaction of N-terminal glutamine (*cf.* Section 4.2.2, Figure 4.5). It is most likely that E190 acts as proton abstracting group which transfers the proton to D293. D228 receives this proton and protonates the leaving hydroxyl ion with the result that water will be released. In case that the γ -carboxylic group is deprotonated *e.g.* at pH 8, one proton has to be received from the solvent.

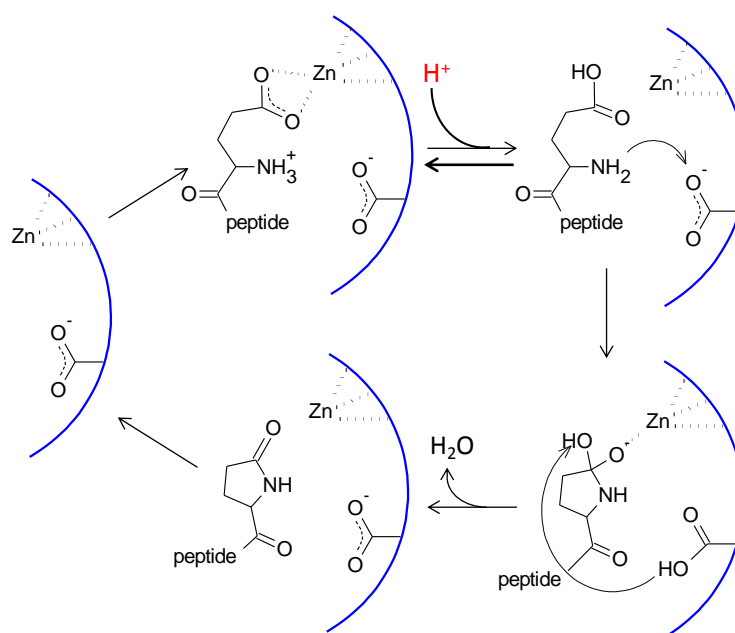


Figure 4.7 Postulated reaction cycle of N-terminal glutamate substrates Under mild acidic conditions the major part of N-terminal glutamates are bivalently charged and the γ -carboxylic group of N-terminal glutamate is bidentately bound to Zn(II). A minor population of glutamates bears an unprotonated α -amino group and a protonated γ -carboxylate moiety. In those molecules, the α -amino group can attack the electrophilic γ -carbonyl.

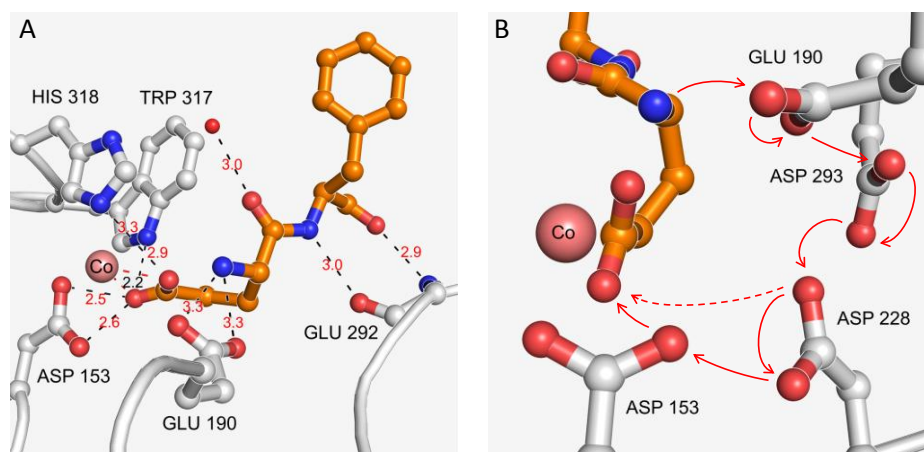


Figure 4.8 N-terminal glutamyl substrate in complex with Co(II) isoDromeQC wild type The γ -carboxylic group (A) of the N-terminal glutamate substrate EFRH (orange rods) coordinates the catalytically active Co(II) (firebrick-red sphere) in a bidentate manner. All distances (red arrows in B) between the Co(II) isoDromeQC wild type residues (grey rods) and the substrate are in hydrogen bond ranges and describe the supposed proton transfer pathway.

4.4 Investigation of the binding mode of enzyme inhibiting tripeptide AFA

Considering the fact that *h*QCs support the release of toxic A β peptides in a pathophysiological side reaction as described in the introduction, this enzyme represents a suitable target enzyme in the treatment of dementia diseases like AD. The inhibitors which were investigated so far interact with the catalytically active Zn(II) ion. To avoid severe or toxic side effects by the interference of these inhibitors with other Zn(II)-dependent enzymes, it is the long-term goal to explore enzyme-specific and mechanism-based inhibitors.

As a prerequisite the Zn(II)-*isoDromeQC* and Co(II)-*isoDromeQC* were used to study two inhibiting components with respect to their binding mode and their interaction with the catalytically active metal ion. Furthermore, the investigation of inhibitor binding can provide information about putative substrate binding motifs.

For that purpose, Co(II)-*isoDromeQC* wild type and the variants Co(II)-*isoDromeQC*_D228N, Co(II)-*isoDromeQC*_E190Q and Co(II)-*isoDromeQC*_D293N were incubated with the peptide-based competitive inhibitor AFA. Crystallographic attempts, EPR experiments and UV/Vis spectroscopic trials were used to investigate this enzyme inhibitor complex.

The results of the crystallographic experiments with Co(II)-*isoDromeQC* and AFA (*cf.* Figure 3.14) showed that the α -nitrogen of the N-terminal alanine residue acts as coordination partner of the Co(II) ion. This is in contrast to the result from the EPR experiments. The obtained EPR signal of Co(II)-*isoDromeQC* wild type and AFA at pH 6.8 indicates a five-coordinated Co(II) ion (*cf.* Section 3.6.4, Supplemental 8.13). This indicates that the AFA influence the electronic sphere of Co(II). One reason for this conflicting result could be that the electron density of a water molecule is not observable due to high flexibility. This water molecule may act as a fifth coordination partner. Nevertheless, considering all results we can conclude that the α -amino nitrogen interacts with the Co(II) ion. In contrast to the substrate or product compounds, in this case the Co(II) ion interacts with a nitrogen atom instead of an oxygen atom. The precise delineation of the binding mode in terms of the coordination partner currently remains hypothetical.

In case of the variant Co(II)-*isoDromeQC*_E190Q, the EPR data indicate four- and five coordinate Co(II) ions and Co(II) hyperfine structure. The latter fact is typical for Co(II) ions when their coordination geometry is very rigid resulting from a tightly bound ligand. It is most likely that the insertion of a glutamine provides an additional binding motif for AFA. It was previously discussed in Section 4.2.1 that this variant produces an additional hydrogen bond between γ -amido oxygen

in position 190 and α -amino nitrogen of the N-terminal glutamine that enhances the substrate affinity. The tight AFA binding might be mediated by an analog hydrogen bond.

Interestingly, EPR spectra of the variants Co(II)-isoDromeQC_D228N and D293N incubated with AFA are indicative for four-coordinated Co(II) ions. Significantly shifted band positions and altered band width revealed evidence for a ligand-metal interaction. The Co(II) hyperfine pattern in case of Co(II)-isoDromeQC_D228N as described above is indicative for a tight ligand binding. The substitution of active center amino acids, which were discussed as putative binding motives for N-terminal glutamine substrates (*cf.* Sections 4.2.1 and 4.3.2) does not impair the binding of AFA. The above-mentioned crystal structure (*cf.* Figure 3.14 A and B) shows two distinct conformations of the AFA in the active center. Figure 3.14 A depicts the Co(II)-bound conformation with additional hydrogen bonds to several water molecules. The alternative conformation in Figure 3.14 B shows no Co(II) interaction but a direct hydrogen bond contact between the main chain of amino acid E292 and the phenylalanine in the second position of the substrate. A further hydrogen bond can be established between α -amino nitrogen of the substrate and the γ -carbonyl oxygen of amino acid E190. These binding motifs are similar to the substrate binding motifs and most likely mediate the inhibitor binding. The γ -carboxylate group of residue 228 would interact with the γ -amino nitrogen of the N-terminal glutamine of the substrate (*cf.* Section 4.2.1 and Figure 3.11 B and C). The substitution of the γ -carboxylate group in Co(II)-isoDromeQC_D228N leads to impaired substrate binding (*cf.* Section 3.2; 3.4.2, 3.6.2 and 4.2.1). In case of AFA binding this γ -amino nitrogen is missing. Thus the substitution of this moiety in Co(II)-isoDromeQC_D228N has no influence on AFA binding. This observation strengthens the hypothesis that D228 is involved in substrate binding indirectly.

5 Summary

Zn(II)-dependent QC converts N-terminal glutamine or glutamate residues of peptides and proteins [25, 30, 90]. The reaction product is in both cases pyroglutamic acid. In animals the glutaminylation is involved in posttranslational modification and activation of peptide-based hormone and chemokine precursors [30]. Recently it was established that the driving force in neurodegenerative processes is the pyroGlu modification at the N-terminus of A β peptides processed by QC. In humans one isoform is localized in Golgi-vesicles, the other isoform is present in the regulated secretory pathway. In the brain, the secretory isoform is predominantly expressed. This unveils the inhibition of secretory QC as a strategy in AD treatment without side effects. The enzyme-specific inhibition is required in order to avoid noxious side effects. The elucidation of the reaction mechanism might make the development of mechanism-based QC inhibitors (*e.g.* transition-state analog compounds) possible.

Mechanistic and structural investigations were accomplished using the mitochondrial isoform of QC from *Drosophila melanogaster*. Regarding enzyme kinetic and structural properties, this enzyme is highly similar to the secretory hQC. Zn(II)-isoDromeQC wild type and variants harboring mechanism-relevant amino acids substitutes were heterologously expressed in *E. coli*. The His₆-tagged enzyme was purified using Ni-chelating chromatography, whereas the untagged protein was purified employing hydrophobic interaction chromatography, anion exchange chromatography and size exclusion chromatography. With the purified Zn(II) enzymes kinetic investigations were carried out including substrate specificity and pH-dependence studies. The substitution of the catalytically active Zn(II) ion into Co(II) yields an UV/Vis and EPR-active enzyme with almost the same enzymatic activity compared to the Zn(II) enzyme. The mentioned spectroscopic methods were used to obtain information about reaction trajectory, the binding modes of substrates and products. In addition the structure-function relationship of the enzyme was investigated in terms of the active center residues E190, D228 and D293. In particular the functions of these activecenter amino acids could be elucidated by successful crystallization trials.

The analysis of the results reveal that the active-center amino acids D288, D293, E190 (side chains) and D293 (main chains) as well the metal ion are required for sufficient substrate binding. The function of D293 remains hypothetical due to the absence of a direct substrate-amino acid interaction. Substrate binding can also be mediated by hydrogen bonds between N-terminal substrate amino acids in the active center and between C-terminal substrate amino acids and the protein surface around the binding pocket. Highly preferred substrates possess an

5 Summary

aromatic amino acid in the second N-terminal position, a positive charge and at least two or more amino acids. A special role for substrate binding could be assigned for residue E190 and the catalytically active metal. Preferentially at mild alkaline pH, E190 accepts one proton from the α -amino group of the N-terminal substrate glutamine and increases nucleophilicity of the appropriate α -nitrogen. In a synchronized manner the metal and the γ -carboxamide oxygen form a non-covalent interaction and leave a polarized γ -carbon lacking a negative charge. In particular the EPR data indicate a highly distorted Co(II) coordination geometry as a very early (within 160 ms) event in the course of catalysis. The reaction mechanism postulated by Schilling *et al.* proposes a tetrahedral reaction intermediate that is typical for an addition-elimination mechanism or second order nucleophilic substitution with a tetrahedral reaction intermediate (S_N2_t), respectively [60]. This hypothetical intermediate state could be stabilized by the metal-oxanion interaction. This might be the reason for the observed strong and short-lived delocalization in the electronic sphere of the metal. The relaxation of this excited state, observed by EPR spectroscopy, might be caused by the decomposition of the mentioned intermediate state accompanied by the release of ammonia. The liberation of the gaseous ammonia was indicated by crystal structures. Putatively a proton is transferred by the amino acid D228 to the leaving amino group. Former investigations [94] suggested a proton transfer pathway using amino acids E190, D293 and D228. The substitution of one of these residues leaves an almost enzymatic inactive variant. Controversially discussed was the liberation of the product as rate-limiting step. A stable product-enzyme complex, product inhibition and the exclusion of preceding catalytic steps as rate-limiting would confirm this idea. Nevertheless, the high concentration of product compounds or substrates used in the applied assays might disarrange the dissociation equilibrium.

New information about the binding mode of N-terminal glutamate substrates were obtained by crystallization and EPR measurements. In contrast to four-coordinate Co(II) during the conversion of glutamine substrates, the binding of N-terminal glutamate provokes a five-coordination sphere of the metal ion. Both γ -carbonyl oxygens are non-covalently bound to the metal ion. Assuming that this conformation is catalytically inactive due to lack of a leaving hydroxyl group, it was proposed that the glutamyl cyclization takes up a proton from the solvent. Statements concerning the mechanism remain hypothetical for now.

Information with regard to the mentioned substrate-binding motifs was obtained by co-crystallization of QC with AFA and confirmed by EPR experiments. Further, a nitrogen-metal interaction could be observed by the application of this competitive inhibitor.

6 Outlook

The question of the existence and the structure of the tetrahedral intermediate could not clearly be answered in this work. First trials to inhibit the QC activity using phenylphosphorodiamidate that mimics a tetrahedral transition state did not yield any results. Possibly a randomized attempt with further tetrahedral intermediate analogs will provide information about the appearance and the structure of such an intermediate. The question of whether further active-center residues are involved in substrate binding could be answered by further site-directed mutagenesis. Especially the function of W317 that may form hydrophobic interactions to the N-terminal substrate amino acid could be helpful. Substitutions of the mentioned non-polar amino acids in the substrate binding pocket (I291, F313, W196) by polar amino acids (*cf.* Section 4.1.1) could shed light on whether the preference for substrates with aromatic amino acids in the second position is caused by hydrophobic interactions.

A further aspect will be the specific inhibition of secretory *hQC* which is mainly responsible for pyroGlu modification in the brain.

Kinetic measurements and EPR studies regarding the reaction trajectory of the glutamyl cyclase mechanism need to be performed. The detected substrate binding in Co(II)-*isoDromeQC_D228N* and *D293N* raise the question whether these variants are catalytically active when incubated with N-terminal glutamate substrates. Open questions in terms of the cyclization mechanism, in particular of the protonation of the leaving water, can possibly be answered by measuring glutamyl cyclization activity in dependence of pH. If the leaving water molecule receives protons from the solvent during the reaction, an increase of the pH value in the applied reaction tube should be detectable during the reaction. This would provide important insights into the mechanism of this reaction and would unveil a significant difference to the glutaminylation mechanism. Additionally it is worth investigating whether bidentate substrates and the resulting five-coordinate Co(II) is catalytically active.

Hypothetically, should the entire elucidation of the glutamyl cyclization mechanism unveil stark differences to that of glutaminylation, it could be possible to diminish the pathophysiological pyroGlu modification of A β peptides without impairment of the physiological glutaminylation reaction.

Bibliography

Bibliography

1. **Prince MP, Prina M, Gurchet M**, Journey of Caring, An analysis of long-term care for dementia *World Alzheimer Report 2013*: p. 1 - 92
2. **Wimo AP, Prince, M.**, The global economic impact of Dementia, *World Alzheimer Report 2010*, 2010: p. 1-56
3. **Selkoe DJ**, Alzheimer's disease: genes, proteins, and therapy. *Physiol. Rev.*, 2001. **81** (2): p. 741-66
4. **Prince M**, *World Alzheimer Report 2009*. 2009. **96**: p. 1-96
5. **Mikulca JA, Nguyen V, Gajdosik DA, Teklu SG, Giunta E A, Lessa EA, Tran CH, Terak EC, Raffa R B**, Potential novel targets for Alzheimer pharmacotherapy: II. Update on secretase inhibitors and related approaches. *J. Clin. Pharm. Ther.*, 2013. **39** (1): p. 25-37
6. **Walsh DM, Klyubin I, Fadeeva JV, Cullen WK, Anwyl R, Wolfe MS**, Naturally secreted oligomers of amyloid beta protein potently inhibit hippocampal long-term potentiation in vivo. *Nature*, 2002. **416** (6880): p. 535-9
7. **Lue LF, Kuo YM, Roher AE, Brachova L, Shen Y, Sue L, Beach T, Kurth JH, Rydel RE, Rogers J**, Soluble amyloid beta peptide concentration as a predictor of synaptic change in Alzheimer's disease. *Am. J. Pathol.*, 1999. **155** (3): p. 853-62.
8. **Dahlgren, K.N., Manelli, A.M.; Stine W.B. Jr., Lorinda K. Baker, L.K., Grant A. Krafft, G.A., LaDu, M.J.** Oligomeric and fibrillar species of amyloid-beta peptides differentially affect neuronal viability. *J. Biol. Chem.*, 2002. **277** (35): p. 32046-53.
9. **Lambert MP, Barlow AK, Chromy BA, Edwards C, Freed R, Liosatos M, Morgan TE, Rozovsky I, Trommer B, Viola KL, Wals P, Zhang C, Finch CE, Krafft GA, Klein WL**, Diffusible, nonfibrillar ligands derived from Abeta1-42 are potent central nervous system neurotoxins. *Proc. Natl. Acad. Sci. USA*, 1998. **95** (11): p. 6448-53.
10. **Goedert M, Crowther RA, Garner CC**, Molecular characterization of microtubule-associated proteins tau and MAP2. *Trends Neurosci.*, 1991. **14** (5): p. 193-9.
11. **Mawal-Dewan M, Henley J, Van de Voorde A, Trojanowski JQ, Lee VM**, The phosphorylation state of tau in the developing rat brain is regulated by phosphoprotein phosphatases. *J. Biol. Chem.*, 1994. **269**(49): p. 30981-7

7 Bibliography

12. **Wang JZ , Xia YY, Grundke-Iqbal I, Iqbal K**, Abnormal hyperphosphorylation of tau: sites, regulation, and molecular mechanism of neurofibrillary degeneration. *J. Alzheimers Dis.*, 2012. **33 Suppl 1**: p. S123-39
13. **Goedert M, Jakes R, Crowther RA, Six J, Lübke U, Vandermeeren M, Cras P, Trojanowski JQ, Lee VM**, The abnormal phosphorylation of tau protein at Ser-202 in Alzheimer disease recapitulates phosphorylation during development. *Proc. Natl. Acad. Sci. USA*, 1993. **90**(11): p. 5066-70
14. **Hung, AY, Selkoe DJ**, Selective ectodomain phosphorylation and regulated cleavage of beta-amyloid precursor protein. *EMBO J.*, 1994. **13**(3): p. 534-42
15. **Oltersdorf T, Ward, PJ, Henriksson T, Beattie EC, Neve R, Lieberburg I, Fritz LC**, The Alzheimer amyloid precursor protein. Identification of a stable intermediate in the biosynthetic/degradative pathway. *J. Biol. Chem.*, 1990. **265**(8): p. 4492-7
16. **Walter J, Capell A, Hung AY, Langen H, Schnölzer M, Thinakaran G, Sisodia SS, Selkoe DJ, Haass C**, Ectodomain phosphorylation of beta-amyloid precursor protein at two distinct cellular locations. *J. Biol. Chem.*, 1997. **272**(3): p. 1896-903
17. **Weidemann A, König G, Bunke D, Fischer P, Salbaum JM, Masters CL, Beyreuther K**, Identification, biogenesis, and localization of precursors of Alzheimer's disease A4 amyloid protein. *Cell*, 1989. **57**(1): p. 115-26
18. **Saitoh T, Sundsmo M, Roch JM, Kimura N, Cole G, Schubert D, Oltersdorf T, Schenk DB**, Secreted form of amyloid beta protein precursor is involved in the growth regulation of fibroblasts. *Cell*, 1989. **58**(4): p. 615-22
19. **Mattson MP, Cheng B, Culwell R, Esch FS, Lieberburg I, Rydel RE**, Evidence for excitoprotective and intraneuronal calcium-regulating roles for secreted forms of the beta-amyloid precursor protein. *Neuron*, 1993. **10**(2): p. 243-54
20. **Soscia SJ, Kirby JE, Washicosky KJ, Tucker SM, Ingelsson M, Hyman B, Burton MA, Goldstein LE, Duong S, Tanzi RE, Moir RD**, The Alzheimer's disease-associated amyloid beta-protein is an antimicrobial peptide. *PLoS One*, 2010. **5**(3): p. e9505
21. **Lichtenthaler SF**, alpha-secretase in Alzheimer's disease: molecular identity, regulation and therapeutic potential. *J. Neurochem.* **116**(1): p. 10-21
22. **Vassar R, Kandalepas PC**, The beta-secretase enzyme BACE1 as a therapeutic target for Alzheimer's disease. *Alzheimers Res. Ther.*, 2011. **3**(3): p. 20
23. **Schlenzig D, Rönicke R, Cynis H, Ludwig HH, Scheel E, Reymann K, Saido T, Hause G, Schilling S, Demuth HU**, N-Terminal pyroglutamate formation of Abeta38 and Abeta40 enforces oligomer formation and potency to disrupt hippocampal long-term potentiation. *J. Neurochem.*, 2012. **121**(5): p. 774-84

24. **Mori H, Takio K, Ogawara M, Selkoe DJ**, Mass spectrometry of purified amyloid beta protein in Alzheimer's disease. *J Biol Chem*, 1992. **267**(24): p. 17082-6
25. **Saido TC, Iwatsubo T, Mann DM, Shimada H, Ihara Y, Kawashima S**, Dominant and differential deposition of distinct beta-amyloid peptide species, A beta N3(pE), in senile plaques. *Neuron*, 1995. **14**(2): p. 457-66
26. **Liu K, Doms RW, Lee VM**, Glu11 site cleavage and N-terminally truncated A beta production upon BACE overexpression. *Biochemistry*, 2002. **41**(9): p. 3128-36
27. **Messer M**, Enzymatic cyclization of L-glutamine and L-glutaminy peptides. *Nature*, 1963. **197**: p. 1299
28. **Busby WH Jr., Quackenbush GE, Humm J, Youngblood WW, Kizer JS**, An enzyme(s) that converts glutaminy-peptides into pyroglutamyl-peptides. Presence in pituitary, brain, adrenal medulla, and lymphocytes. *J. Biol. Chem.*, 1987. **262**(18): p. 8532-6
29. **Dahl SW, Slaughter C, Lauritzen C, Bateman RC Jr, Connerton I, Pedersen J**, Carica papaya glutamine cyclotransferase belongs to a novel plant enzyme subfamily: cloning and characterization of the recombinant enzyme. *Protein Expr Purif*, 2000. **20**(1): p. 27-36
30. **Fischer WH, Spiess J**, Identification of a mammalian glutaminy cyclase converting glutaminy into pyroglutamyl peptides. *Proc. Natl. Acad. Sci. USA*, 1987. **84**(11): p. 3628-32
31. **Schlenzig D, Manhart S, Cinar Y, Kleinschmidt M, Hause G, Willbold D, Funke SA, Schilling S, Demuth HU**, Pyroglutamate formation influences solubility and amyloidogenicity of amyloid peptides. *Biochemistry*, 2009. **48**(29): p. 7072-8
32. **He W, Barrow CJ**, The A beta 3-pyroglutamyl and 11-pyroglutamyl peptides found in senile plaque have greater beta-sheet forming and aggregation propensities in vitro than full-length A beta. *Biochemistry*, 1999. **38**(33): p. 10871-7
33. **Kuo YM, Webster S, Emmerling MR, De Lima N, Roher AE**, Irreversible dimerization/tetramerization and post-translational modifications inhibit proteolytic degradation of A beta peptides of Alzheimer's disease. *Biochem. Biophys. Acta*, 1998. **1406**(3): p. 291-8
34. **Schilling S, Lauber T, Schaupp M, Manhart S, Scheel E, Böhm G, Demuth HU**, On the seeding and oligomerization of pGlu-amyloid peptides (in vitro). *Biochemistry*, 2006. **45**(41): p. 12393-9
35. **Piccini A, Russo C, Gliozzi A, Relini A, Vitali A, Borghi R, Giliberto L, Armirotti A, D'Arrigo C, Bachi A, Cattaneo A, Canale C, Torrassa S, Saido TC, Markesbery W, Gambetti P, Tabaton M**, Beta-amyloid is different in normal aging and in Alzheimer disease. *J. Biol. Chem.*, 2005. **280**(40): p. 34186-92

36. **Van Coillie E, Proost P, Van Aelst I, Struyf S, Polfliet M, De Meester I, Harvey DJ, Van Damme J, Opdenakker G**, Functional comparison of two human monocyte chemotactic protein-2 isoforms, role of the amino-terminal pyroglutamic acid and processing by CD26/dipeptidyl peptidase IV. *Biochemistry*, 1998. **37**(36): p. 12672-80
37. **Stefani M, Dobson CM**, Protein aggregation and aggregate toxicity: new insights into protein folding, misfolding diseases and biological evolution. *J. Mol. Med. (Berl)*, 2003. **81**(11): p. 678-99
38. **Scarpini E, Scheltens P, Feldman H**, Treatment of Alzheimer's disease: current status and new perspectives. *Lancet Neurol.*, 2003. **2**(9): p. 539-47
39. **Bowen DM, Francis PT, Pangalos MN, Stephens PH, Procter AW**, Treatment strategies for Alzheimer's disease. *Lancet*, 1992. **339**(8785): p. 132-3
40. **Rogers SL, Farlow MR, Doody RS, Mohs R, Friedhoff LT**, A 24-week, double-blind, placebo-controlled trial of donepezil in patients with Alzheimer's disease. Donepezil Study Group. *Neurology*, 1998. **50**(1): p. 136-45
41. **Corey-Bloom J, Veach J**, A randomized trial evaluating the efficacy and safety of ENA713 (rivastigmine tartrate), a new acetylcholinesterase inhibitor in patients with mild to moderately severe Alzheimers disease. *Int. J Geriatr Psychopharmacol.* 1998. **1**
42. **Tariot PN, Solomon PR, Morris JC, Kershaw P, Lilienfeld S, Ding C**, A 5-month, randomized, placebo-controlled trial of galantamine in AD. The Galantamine USA-10 Study Group. *Neurology*, 2000. **54**(12): p. 2269-76
43. **Doody RS, Stevens JC, Beck C, Dubinsky RM, Kaye JA, Gwyther L, Mohs RC, Thal LJ, Whitehouse PJ, DeKosky ST, Cummings JL**, Practice parameter: management of dementia (an evidence-based review). Report of the Quality Standards Subcommittee of the American Academy of Neurology. *Neurology*, 2001. **56**(9): p. 1154-66
44. **Barten DM, Meredith JE Jr, Zaczek R, Houston JG, Albright CF**, Gamma-secretase inhibitors for Alzheimer's disease: balancing efficacy and toxicity. *Drugs. R. D.*, 2006. **7**(2): p. 87-97
45. **Basi GS, Hemphill S, Brigham EF, Liao A, Aubele DL, Baker J, Barbour R, Bova M, Chen XH, Dappen MS, Eichenbaum T, Goldbach E, Hawkinson J, Lawler-Herbold R, Hu K, Hui T, Jagodzinski JJ, Keim PS, Kholodenko D, Latimer LH, Lee M, Marugg J, Mattson MN, McCauley S, Miller JL, Motter R, Mutter L, Neitzel ML, Ni H, Nguyen L, Quinn K, Ruslim L, Semko CM, Shapiro P, Smith J, Soriano F, Szoke B, Tanaka K, Tang P, Tucker JA, Ye XM, Yu M, Wu J, Xu YZ, Garofalo AW, Sauer JM, Konradi AW, Ness D, Shopp G, Pleiss MA, Freedman SB, Schenk D**, Amyloid precursor protein selective gamma-secretase inhibitors for treatment of Alzheimer's disease. *Alzheimers Res. Ther.*, 2010. **2**(6): p. 36
46. **Bandyopadhyay S, Goldstein LE, Lahiri DK, Rogers JT**, Role of the APP non-amyloidogenic signaling pathway and targeting alpha-secretase as an alternative drug target for treatment of Alzheimer's disease. *Curr. Med. Chem.*, 2007. **14**(27): p. 2848-64

47. **Skovronsky DM, Moore DB, Milla ME, Doms RW, Lee VM**, Protein kinase C-dependent alpha-secretase competes with beta-secretase for cleavage of amyloid-beta precursor protein in the trans-golgi network. *J. Biol. Chem.*, 2000. **275**(4): p. 2568-75
48. **Lemere CA, Maron R, Spooner ET, Grenfell TJ, Mori C, Desai R, Hancock WW, Weiner HL, Selkoe DJ**, Nasal A beta treatment induces anti-A beta antibody production and decreases cerebral amyloid burden in PD-APP mice. *Ann. N. Y. Acad. Sci.* 2000. **920**: p. 328-31
49. **Schenk D, Barbour R, Dunn W, Gordon G, Grajeda H, Guido T, Hu K, Huang J, Johnson-Wood K, Khan K, Kholodenko D, Lee M, Liao Z, Lieberburg I, Motter R, Mutter L, Soriano F, Shopp G, Vasquez N, Vandever C, Walker S, Wogulis M, Yednock T, Games D, Seubert P**, Immunization with amyloid-beta attenuates Alzheimer-disease-like pathology in the PDAPP mouse. *Nature*, 1999. **400**(6740): p. 173-7
50. **Bard F, Cannon C, Barbour R, Burke RL, Games D, Grajeda H, Guido T, Hu K, Huang J, Johnson-Wood K, Khan K, Kholodenko D, Lee M, Lieberburg I, Motter R, Nguyen M, Soriano F, Vasquez N, Weiss K, Welch B, Seubert P, Schenk D, Yednock T**, Peripherally administered antibodies against amyloid beta-peptide enter the central nervous system and reduce pathology in a mouse model of Alzheimer disease. *Nat. Med.*, 2000. **6**(8): p. 916-9
51. **DeMattos RB, Bales KR, Cummins DJ, Dodart JC, Paul SM, Holtzman DM**, Peripheral anti-A beta antibody alters CNS and plasma A beta clearance and decreases brain A beta burden in a mouse model of Alzheimer's disease. *Proc. Natl. Acad. Sci. USA*, 2001. **98**(15): p. 8850-5
52. **Seifert F, Schulz K, Koch B, Manhart S, Demuth HU, Schilling S**, Glutaminyl cyclases display significant catalytic proficiency for glutamyl substrates. *Biochemistry*, 2009. **48**(50): p. 11831-3
53. **Cynis H, Schilling S, Bodnár M, Hoffmann T, Heiser U, Saido TC, Demuth HU**, Inhibition of glutaminyl cyclase alters pyroglutamate formation in mammalian cells. *Biochim. Biophys Acta*, 2006. **1764**(10): p. 1618-25
54. **Schilling S, Zeitschel U, Hoffmann T, Heiser U, Francke M, Kehlen A, Holzer M, Hutter-Paier B, Prokesch M, Windisch M, Jagla W, Schlenzig D, Lindner C, Rudolph T, Reuter G, Cynis H, Montag D, Demuth HU, Rossner S**, Glutaminyl cyclase inhibition attenuates pyroglutamate Aβ and Alzheimer's disease-like pathology. *Nat. Med.*, 2008. **14**(10): p. 1106-11
55. **Schilling S, Kohlmann S, Bäuscher C, Sedlmeier R, Koch B, Eichentopf R, Becker A, Cynis H, Hoffmann T, Berg S, Freyse EJ, von Hörsten S, Rossner S, Graubner S, Demuth HU**, Glutaminyl cyclase knock-out mice exhibit slight hypothyroidism but no hypogonadism: implications for enzyme function and drug development. *J. Biol. Chem.*, 2011. **286**(16): p. 14199-208
56. **Schilling S, Niestroj AJ, Rahfeld JU, Hoffmann T, Wermann M, Zunkel K, Wasternack C, Demuth HU**, Identification of human glutaminyl cyclase as a metalloenzyme. Potent

7 Bibliography

- inhibition by imidazole derivatives and heterocyclic chelators. *J. Biol. Chem.*, 2003. **278**(50): p. 49773-9
57. **Schilling S, Manhart S, Hoffmann T, Ludwig HH, Wasternack C, Demuth HU**, Substrate specificity of glutaminyl cyclases from plants and animals. *Biol. Chem.*, 2003. **384**(12): p. 1583-92
58. **Carr PD, Ollis DL**, Alpha/beta hydrolase fold: an update. *Protein Pept. Lett.*, 2009. **16**(10): p. 1137-48
59. **Wintjens R, Belrhali H, Clantin B, Azarkan M, Bompard C, Baeyens-Volant D, Looze Y, Villeret V**, Crystal structure of papaya glutaminyl cyclase, an archetype for plant and bacterial glutaminyl cyclases. *J. Mol. Biol.*, 2006. **357**(2): p. 457-70
60. **Schilling S**, Charakterisierung der humanen Glutaminyl-Cyclase im Vergleich mit dem analogen Enzym aus *Carica papaya*. Dissertation 2004
61. **Schilling S, Cynis H, von Bohlen A, Hoffmann T, Wermann M, Heiser U, Buchholz M, Zunkel K, Demuth HU**, Isolation, catalytic properties, and competitive inhibitors of the zinc-dependent murine glutaminyl cyclase. *Biochemistry*, 2005. **44**(40): p. 13415-24
62. **Huang KF, Liu YL, Cheng WJ, Ko TP, Wang AH**, Crystal structures of human glutaminyl cyclase, an enzyme responsible for protein N-terminal pyroglutamate formation. *Proc. Natl. Acad. Sci. USA*, 2005. **102**(37): p. 13117-22
63. **Bennett B, Holz RC**, Spectroscopically distinct cobalt(II) sites in heterodimetallic forms of the aminopeptidase from *Aeromonas proteolytica*: characterization of substrate binding. *Biochemistry*, 1997. **36**(32): p. 9837-46
64. **Carrillo DR, Parthier C, Jänckel N, Grandke J, Stelter M, Schilling S, Boehme M, Neumann P, Wolf R, Demuth HU, Stubbs MT, Rahfeld JU**, Kinetic and structural characterization of bacterial glutaminyl cyclases from *Zymomonas mobilis* and *Myxococcus xanthus*. *Biol. Chem.*, 2010. **391**(12): p. 1419-28
65. **Hartley M, Yong W, Bennett B**, Heterologous expression and purification of *Vibrio proteolyticus* (*Aeromonas proteolytica*) aminopeptidase: a rapid protocol. *Protein Expr Purif.* 2009 Jul;66(1):91-101. /j.pep.2009.02.011. Epub 2009 Feb 20., 2009: p. 91–101
66. **Noe BD, Debo G, Spiess J**, Comparison of prohormone-processing activities in islet microsomes and secretory granules: evidence for distinct converting enzymes for separate islet prosomatostatins. *J. Cell. Biol.*, 1984. **99**(2): p. 578-87
67. **Pohl T, Zimmer M, Mugele K, Spiess J**, Primary structure and functional expression of a glutaminyl cyclase. *Proc. Natl. Acad. Sci. USA*, 1991. **88**(22): p. 10059-63
68. **Böckers TM, Kreutz MR, Pohl T**, Glutaminyl-cyclase expression in the bovine/porcine hypothalamus and pituitary. *J. Neuroendocrinol.*, 1995. **7**(6): p. 445-53

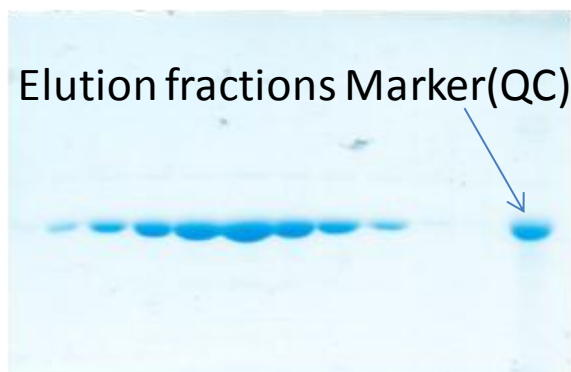
69. **Awadé AC, Cleuziat P, Gonzalès T, Robert-Baudouy J**, Pyrrolidone carboxyl peptidase (Pcp): an enzyme that removes pyroglutamic acid (pGlu) from pGlu-peptides and pGlu-proteins. *Proteins*, 1994. **20**(1): p. 34-51
70. **Morty RE, Bulau P, Pellé R, Wilk S, Abe K**, Pyroglutamyl peptidase type I from *Trypanosoma brucei*: a new virulence factor from African trypanosomes that de-blocks regulatory peptides in the plasma of infected hosts. *Biochem J.*, 2006. **394**(Pt 3): p. 635-45
71. **Abraham GN, Podell DN**, Pyroglutamic acid. Non-metabolic formation, function in proteins and peptides, and characteristics of the enzymes effecting its removal. *Mol. Cell. Biochem.*, 1981. **38 Spec No**(Pt 1): p. 181-90
72. **Cynis H, Hoffmann T, Friedrich D, Kehlen A, Gans K, Kleinschmidt M, Rahfeld JU, Wolf R, Wermann M, Stephan A, Haegele M, Sedlmeier R, Graubner S, Jagla W, Müller A, Eichertopf R, Heiser U, Seifert F, Quax PH, de Vries MR, Hesse I, Trautwein D, Wollert U, Berg S, Freyse EJ, Schilling S, Demuth HU**, The isoenzyme of glutaminyl cyclase is an important regulator of monocyte infiltration under inflammatory conditions. *EMBO Mol. Med.*, 2011. **3**(9): p. 545-58
73. **Schilling S, Lindner C, Koch B, Wermann M, Rahfeld JU, von Bohlen A, Rudolph T, Reuter G, Demuth HU**, Isolation and characterization of glutaminyl cyclases from *Drosophila*: evidence for enzyme forms with different subcellular localization. *Biochemistry*, 2007. **46**(38): p. 10921-30
74. **Koch B, Kolenko P, Buchholz M, Carrillo DR, Parthier C, Wermann M, Rahfeld JU, Reuter G, Schilling S, Stubbs MT, Demuth HU**, Crystal structures of glutaminyl cyclases (QCs) from *Drosophila melanogaster* reveal active site conservation between insect and mammalian QCs. *Biochemistry*, 2012. **51**(37): p. 7383-92
75. **Ruiz-Carrillo D, Koch B, Parthier C, Wermann M, Dambe T, Buchholz M, Ludwig HH, Heiser U, Rahfeld JU, Stubbs MT, Schilling S, Demuth HU**, Structures of glycosylated mammalian glutaminyl cyclases reveal conformational variability near the active center. *Biochemistry*, 2011. **50**(28): p. 6280-8
76. **Huang KF, Liaw SS, Huang WL, Chia CY, Lo YC, Chen YL, Wang AH**, Structures of human Golgi-resident glutaminyl cyclase and its complexes with inhibitors reveal a large loop movement upon inhibitor binding. *J. Biol. Chem.*, 2011. **286**(14): p. 12439-49
77. **Cynis H, Rahfeld JU, Stephan A, Kehlen A, Koch B, Wermann M, Demuth HU, Schilling S**, Isolation of an isoenzyme of human glutaminyl cyclase: retention in the Golgi complex suggests involvement in the protein maturation machinery. *J. Mol. Biol.*, 2008. **379**(5): p. 966-80
78. **Stephan A, Wermann M, von Bohlen A, Koch B, Cynis H, Demuth HU, Schilling S**, Mammalian glutaminyl cyclases and their isoenzymes have identical enzymatic characteristics. *FEBS J.*, 2009. **276**(22): p. 6522-36

79. **Buchholz M, Heiser U, Schilling S, Niestroj AJ, Zunkel K, Demuth HU**, The first potent inhibitors for human glutaminyl cyclase: synthesis and structure-activity relationship. *J. Med. Chem.*, 2006. **49**(2): p. 664-77
80. **Schilling S, Hoffmann T, Wermann M, Heiser U, Wasternack C, Demuth HU**, Continuous spectrometric assays for glutaminyl cyclase activity. *Anal. Biochem.*, 2002. **303**(1): p. 49-56
81. **Tsuru D, Fujiwara K, Kado K**, Purification and characterization of L-pyrrolidonecarboxylate peptidase from *Bacillus amyloliquefaciens*. *J. Biochem.*, 1978. **84**(2): p. 467-76
82. **Adams PD, Afonine PV, Bunkóczi G, Chen VB, Davis IW, Echols N, Headd JJ, Hung LW, Kapral GJ, Grosse-Kunstleve RW, McCoy AJ, Moriarty NW, Oeffner R, Read RJ, Richardson DC, Richardson JS, Terwilliger TC, Zwart**, PHENIX: a comprehensive Python-based system for macromolecular structure solution. *Acta Crystallogr. D. Biol. Crystallogr.*, 2010. **66**(Pt 2): p. 213-21
83. **Emsley P, Lohkamp B, Scott WG, Cowtan K**, Features and development of Coot. *Acta Crystallogr. D. Biol. Crystallogr.*, 2010. **66**(Pt 4): p. 486-501
84. **Pace CN, Hebert EJ, Shaw KL, Schell D, Both V, Krajcikova D, Sevcik J, Wilson KS, Dauter Z, Hartley RW, Grimsley GR**, Conformational stability and thermodynamics of folding of ribonucleases Sa, Sa2 and Sa3. *J. Mol. Biol.*, 1998. **279**(1): p. 271-86
85. **Berg JM, Tymoczko JL, Stryer L**, Stryer Biochemie. *Spektrum Akademischer Verlag*; Auflage: 6. Aufl. 2007, korr. Nachdruck 2010 (14. Oktober 2009), 2009, p. 243-248
86. **Ellis KJ, Morrison JF**, Buffers of constant ionic strength for studying pH-dependent processes. *Methods Enzymol.*, 1982. **87**: p. 405-26
87. **Bennett, B., (Hanson G, Berliner L (eds.))**, Biological Magnetic Resonance, Metals in Biology- Applications of High-Resolution EPR. 2010: chapter 10, Volume **29**, p. 345-370
88. **Garrity JD, Bennett B, Crowder MW**, Direct evidence that the reaction intermediate of metallo-beta-lactamase L1 is metal bound. *Biochemistry*, 2005. **44**(3): p. 1078-87
89. **Kleifeld O, Rulisek, L, Bogin O, Frenkel A, Havlas Z, Burstein Y, Sagi I**, Higher metal-ligand coordination in the catalytic site of cobalt-substituted *Thermoanaerobacter brockii* alcohol dehydrogenase lowers the barrier for enzyme catalysis. *Biochemistry*, 2004. **43**(22): p. 7151-61
90. **Schilling S, Hoffmann T, Manhart S, Hoffmann M, Demuth HU**, Glutaminyl cyclases unfold glutamyl cyclase activity under mild acid conditions. *FEBS Lett*, 2004. **563**(1-3): p. 191-6
91. **Bertini IG, Lippard HB, Valentine SJ**, Bioinorganic Chemistry University Science Book) 1994, Chapter 2: The reaction pathway of Zinc Enzymes and Related Biological Catalysts), p. 37-107

92. **Kremer-Aach A, Kläui W, Bell R, Strerath A, Wunderlich H, Mootz D**, Cobalt as a Probe for Zinc in Metalloenzyme Model Compounds? A Comparison of Spectroscopic Features and Coordination Geometry of Four- and Five-Coordinate Complexes. Crystal and Molecular Structures of [Co(η^3 -Tp(Ph))(η^2 -Tp(Ph))], [(η^3 -Tp(Ph))Zn(anthranilate)], and [(η^3 -Tp(Ph))M(η^2 -acac)] (Tp(Ph) = Hydrotris(3-phenylpyrazol-1-yl)borate, acac = Pentane-2,4-dionate, and M = Zn, Co). *Inorg. Chem.*, 1997. **36**(8): p. 1552-1563
93. **Voet D, Voet JG, CW Pratt**, Lehrbuch der Biochemie. 2002 *Wiley-VCH Verlag, GmbH*, p. 86-87
94. **Huang KF, Wang YR, Chang EC, Chou TL, Wang AH**, A conserved hydrogen-bond network in the catalytic centre of animal glutaminyl cyclases is critical for catalysis. *Biochem. J.*, 2008. **411**(1): p. 181-90
95. **Becker A, Kohlmann S, Alexandru A, Jagla W, Canneva F, Bäuscher C, Cynis H, Sedlmeier R, Graubner S, Schilling S, Demuth HU, von Hörsten S**, Glutaminyl cyclase-mediated toxicity of pyroglutamate-beta amyloid induces striatal neurodegeneration. *BMC Neurosci.*, 2013. **14**: p. 108
96. **Jawhar S, Wirths O, Schilling S, Graubner S, Demuth HU, Bayer TA**, Overexpression of glutaminyl cyclase, the enzyme responsible for pyroglutamate A{beta} formation, induces behavioral deficits, and glutaminyl cyclase knock-out rescues the behavioral phenotype in 5XFAD mice. *J. Biol. Chem.*, 2011. **286**(6): p. 4454-60

8 Supplemental

8.1 Purification: final 15% Acrylamide SDS-Gel



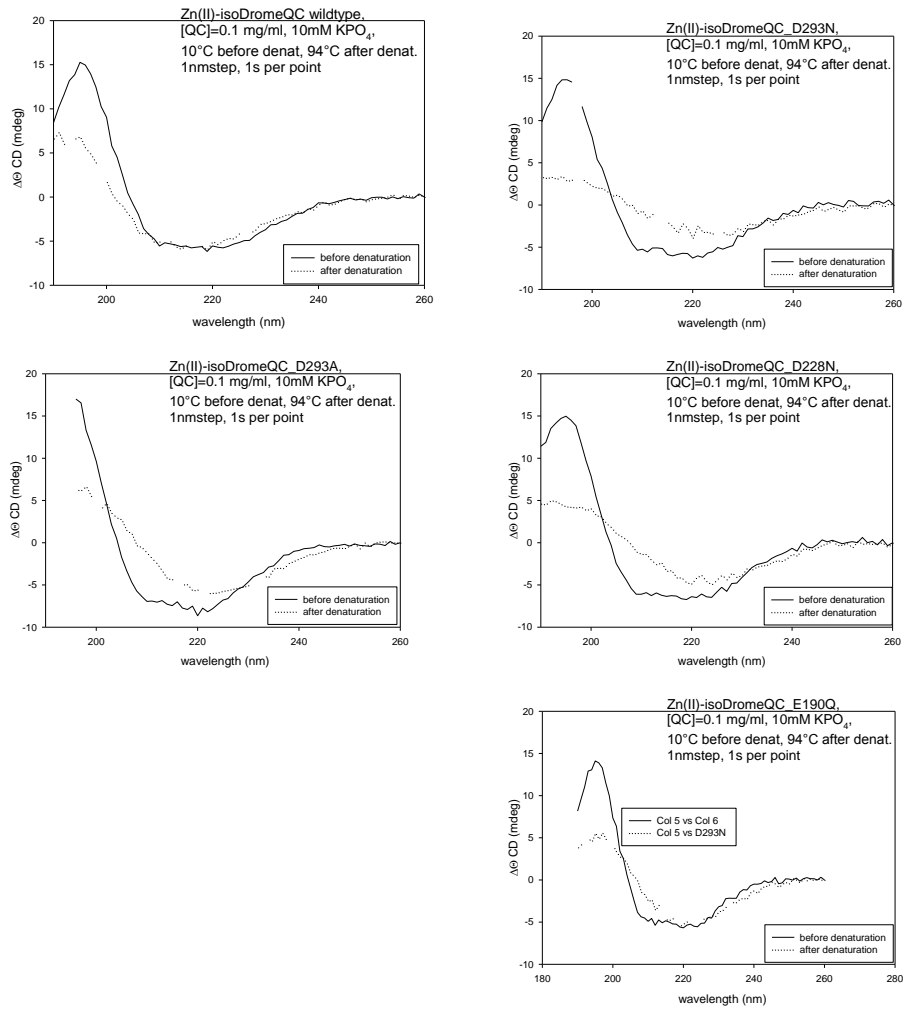
8.2 Thermal stability study of the iDQC wild type and the variants

Table 4.1 Single measurements of the thermal denaturation

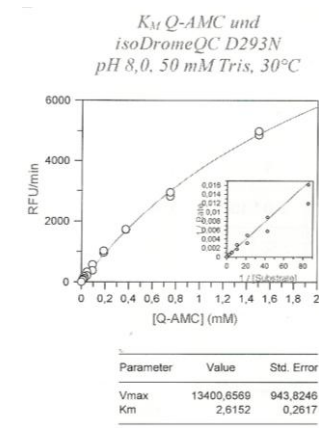
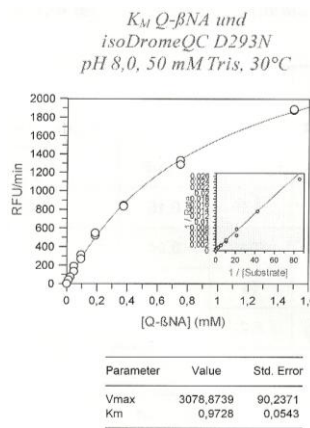
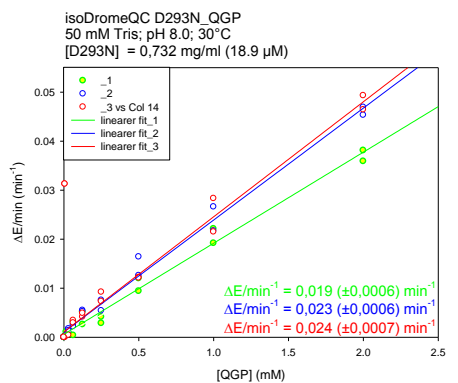
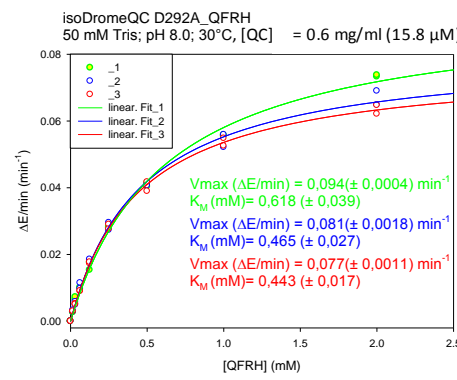
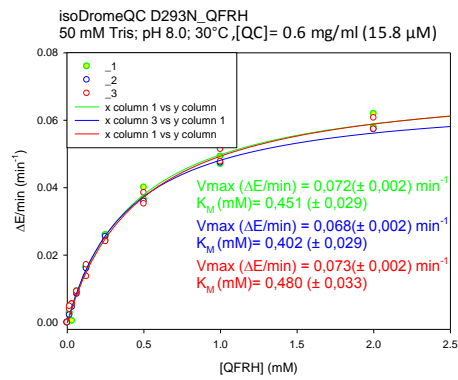
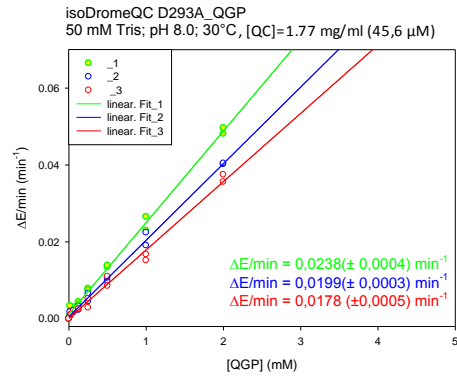
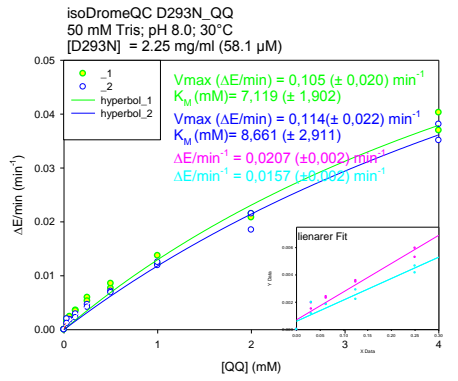
enzyme	melting points ^A	mean value ^B
	328 (\pm 0.05)	
wild typ (His ₆)	330 (\pm 0.07)	330 (\pm 2.00)
	332 (\pm 0.08)	
	334 (\pm 0.28)	
E190Q (native)	334 (\pm 0.24)	334 (\pm 0.00)
	--	
	318 (\pm 0.06)	
D293N (His ₆)	321 (\pm 0.05)	320 (\pm 1.73)
	321 (\pm 0.05)	
	323 (\pm 0.06)	
D293A (His ₆)	322 (\pm 0.06)	322 (\pm 1.00)
	321 (\pm 0.07)	
	334 (\pm 0.12)	
D228N (His ₆)	332 (\pm 0.09)	332 (\pm 1.53)
	331 (\pm 0.14)	

^A) Single measurements in the absolute temperature (K) with standard error

^B) Mean values in the absolute temperature (K) (with standard deviation, not in case of E190Q)

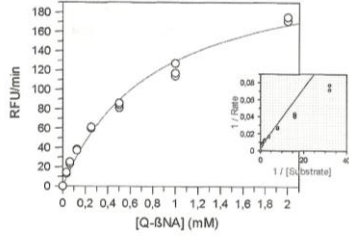
8.3 CD spectroscopic spectra of the his₆-tagged Zn(II)isoDromeQC before and after the temperature treatment

8.4 Single measurements of the substrate specificity study



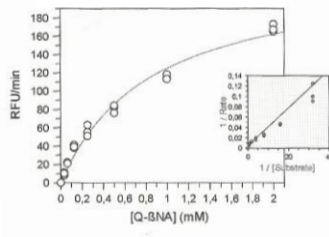
8 Supplemental

K_M Q-βNA und isoDromeQC D228N_1
pH 8,0, 50mM Tris, 30°C
[QC]= 1.05 mg/ml (27,7 μM)



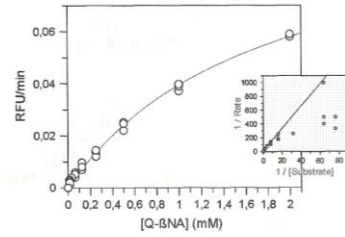
Parameter	Value	Std. Error
Vmax	234,6458	10,9213
Km	0,8132	0,0831

K_M Q-βNA und isoDromeQC D228N_2
pH 8.0, 50mM Tris, 30°C
[QC]= 1.05 mg/ml (27,7 μM)



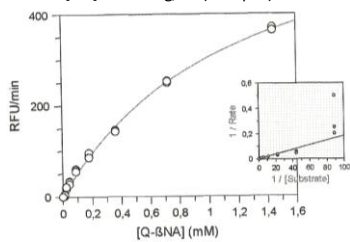
Parameter	Value	Std. Error
Vmax	230,7051	11,4650
Km	0,8492	0,0918

K_M QFRH und isoDromeQC D228N_1
pH 8.0, 50mM Tris, 30°C
[QC]= 0.6 mg/ml (15.8 μM)



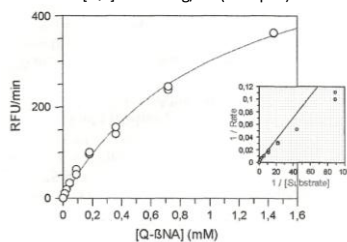
Parameter	Value	Std. Error
Vmax	0,1095	0,0049
Km	1,7753	0,1362

K_M Q-AMC und isoDromeQC D228N_1
pH 8.0, 50mM Tris, 30°C
[QC]= 1.05 mg/ml (27.7 μM)



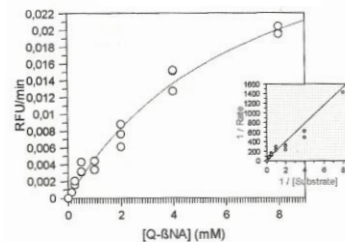
Parameter	Value	Std. Error
Vmax	675,0256	23,9746
Km	1,2154	0,0755

K_M Q-AMC und isoDromeQC D228N_2
pH 8.0, 50mM Tris, 30°C
[QC]= 1.05 mg/ml (27.7 μM)

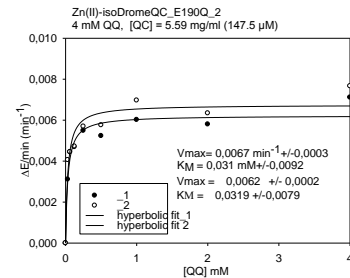
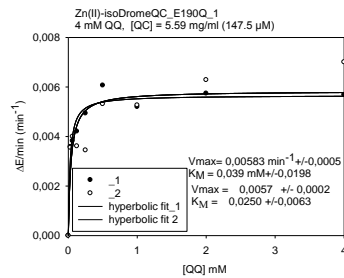
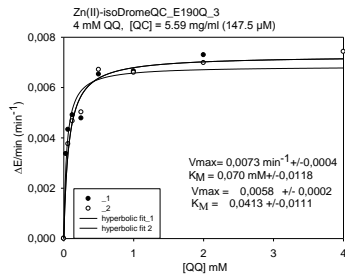


Parameter	Value	Std. Error
Vmax	626,2807	30,1968
Km	1,0824	0,0843

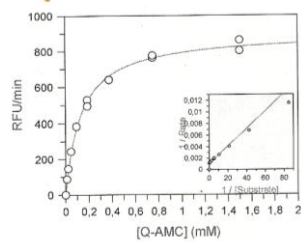
K_M QQ und isoDromeQC D228N_1
pH 8,0, 50mM Tris, 30°C
[QC]= 2.12 mg/ml (54.55 μM)



Parameter	Value	Std. Error
Vmax	0,0377	0,0039
Km	7,0621	1,2715

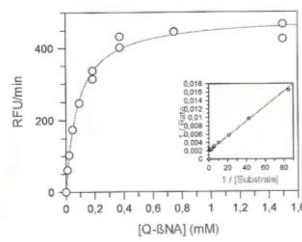


K_M Q-AMC und isoDromeQC E190Q
pH 8,0, 50 mM Tris, 30°C



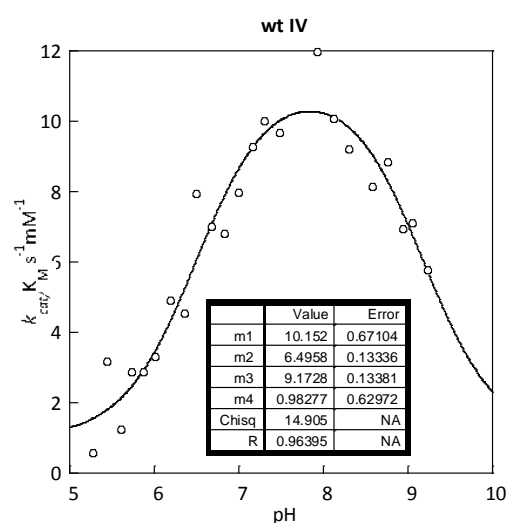
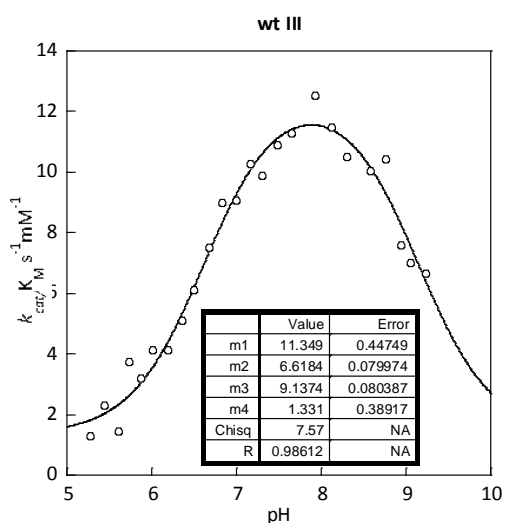
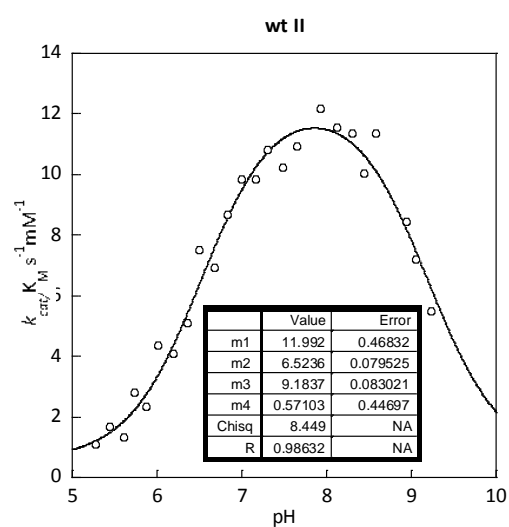
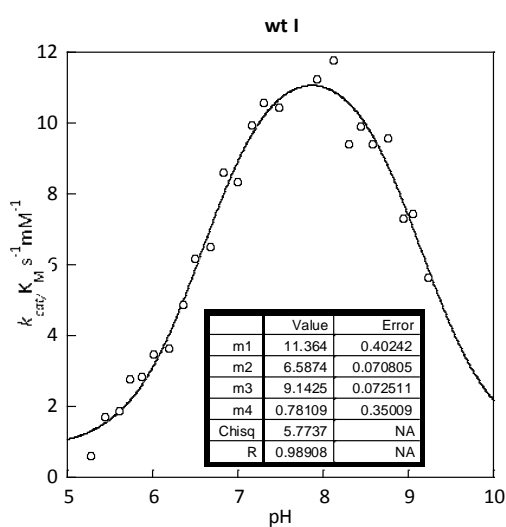
Parameter	Value	Std. Error
Vmax	898,3060	14,5755
Km	0,1353	0,0083

K_M Q-βNA und isoDromeQC E190Q
pH 8,0, 50 mM Tris, 30°C



Parameter	Value	Std. Error
Vmax	487,0897	10,4556
Km	0,0855	0,0081

8.5 Catalytic efficiency in dependence of pH

pH dependence: mitochondrial isoform of *Drosophila melanogaster* QC-wild type (*his₆-tag*)-Single determination of k_{cat}/K_M ($s^{-1}mM^{-1}$):[QC] = 0.005 mg/ml (0.132 μM); substrate: 11.85 μM Q- β NA ($K_M = 0.15 mM \pm 0.01$)100 mM Tris, 50 mM Mes, 50 mM Na⁺-acetate, T = 303 K

Mean values

	mean	standard deviation	standard error
$k_{cat}/K_M(\max)$ ($s^{-1}mM^{-1}$)	11.2	0.78	0.39
pK_{a1}	6.56	0.06	0.03
pK_{a2}	9.1	0.02	0.01
y_0	0.92	0.32	0.16
R	0.98	0.01	0.01

Kinetic constants

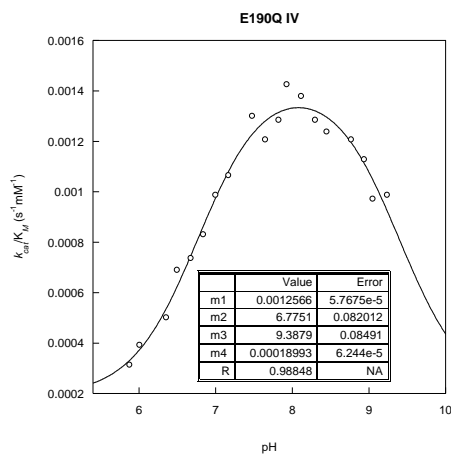
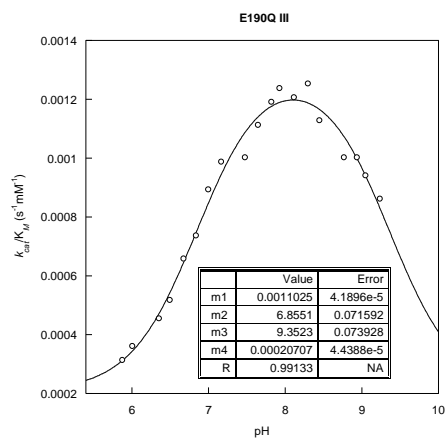
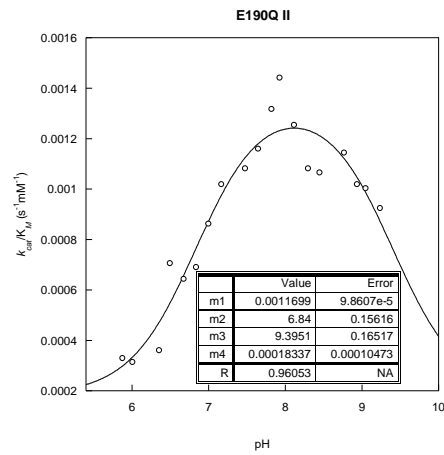
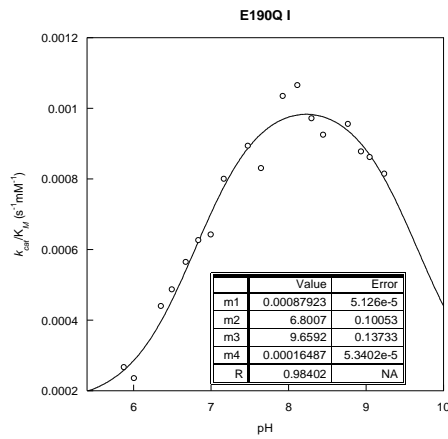
pH	K_M (mM)	k_{cat} (s^{-1})	k_{cat}/K_M ($s^{-1}mM^{-1}$)
5.24	2.59 (± 0.40)	2.17 (± 0.24)	0.84
7.00	0.73 (± 0.03)	2.955 (± 10)	4.02
8.39	0.60 (± 0.05)	3.22 (± 0.11)	5.40

8 Supplemental

pH-dependence: IsoDromeQC E190Q (his₆-tag), determination of k_{cat}/K_M

[QC] = 4.85 mg/ml (125.13 μ M); Substrat: 19.57 μ M Q- β NA ($K_M = 0.15 \text{ mM} \pm 0.01$)

100 mM Tris, 50 mM Mes, 50 mM Na⁺-Acetat, T = 30 $^{\circ}$ C



Mean values

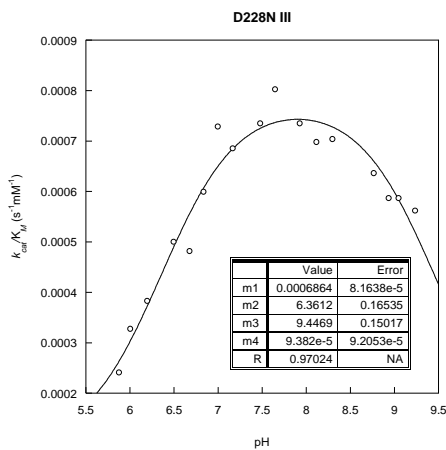
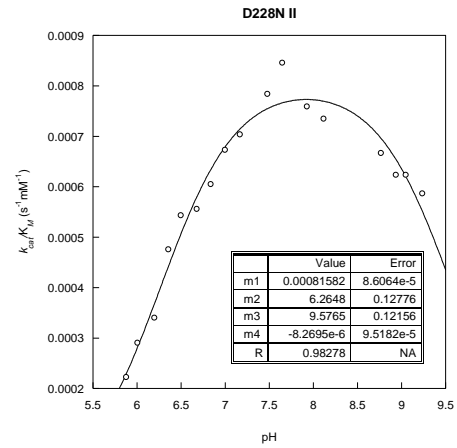
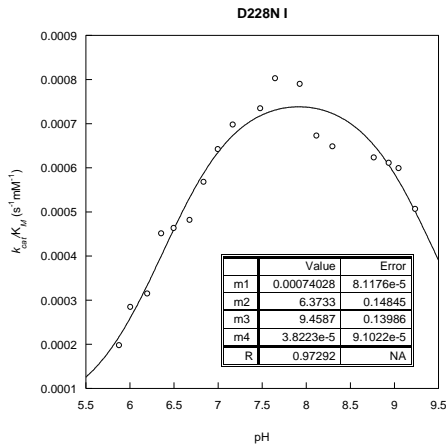
	Mittel	Standard-abweichung	Standard-fehler
$k_{cat}/K_M(\text{max})$ ($\text{s}^{-1}\text{mM}^{-1}$)	1.10e-3	1.61e-4	8.07e-5
pK_{a1}	6.82	0.04	0.02
pK_{a2}	9.45	0.14	0.07
γ_0	0.98	0.01	0.01
R	1.10e-3	1.61e-4	8.07e-5

Kinetic constants

pH	K_M (mM)	k_{cat} (s^{-1})	k_{cat}/K_M ($\text{s}^{-1}\text{mM}^{-1}$)
5.24	<i>n.d.</i>	(\pm)	
7.00	0.43 \pm 0.011	(\pm)	
8.39	0.31 \pm 0.025	(\pm)	

pH-dependence: IsoDromeQC D228N- (his₆-tag), determination of k_{cat}/K_M

[QC] = 5.51 mg/ml (142.40 μ M); Substrat: 43.50 μ M Q- β -NA (K_M = 0.435 mM, in 3KP,
pH 7.0, T = 30 °C) 100 mM Tris, 50 mM Mes, 50 mM Na⁺-Acetat, T = 30 °C

**Mean values**

	Mittel	Standard- abweichung	Standard- fehler
$k_{cat}/K_M(\max)$ ($s^{-1}mM^{-1}$)	$7.47 \cdot 10^{-4}$	$\pm 6.50 \cdot 10^{-5}$	$\pm 3.75 \cdot 10^{-5}$
pK_{a1}	6.33	± 0.06	± 0.03
pK_{a2}	9.49	± 0.07	± 0.04
y_0	$4.13 \cdot 10^{-5}$	$\pm 5.11 \cdot 10^{-5}$	$\pm 2.95 \cdot 10^{-5}$
R	0.98	± 0.01	$\pm 3.81 \cdot 10^{-3}$

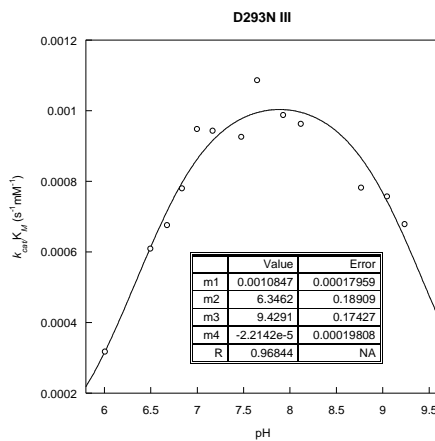
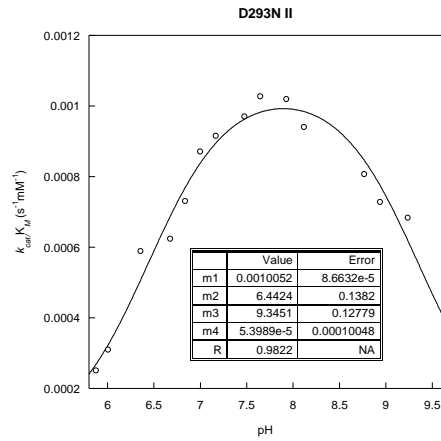
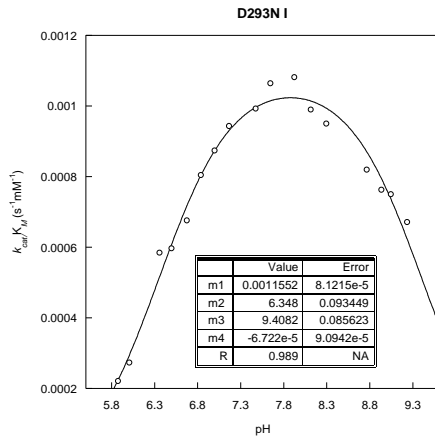
Kinetic constants (isoDromeQC nativ)

pH	K_M (mM)	k_{cat} (s^{-1})	k_{cat}/K_M ($s^{-1}mM^{-1}$)
5.88	1.20 ± 0.20	$3.02 \cdot 10^{-4}$ $\pm 2.54 \cdot 10^{-5}$	$2.52 \cdot 10^{-4}$
7.00	0.34 ± 0.02	$3.89 \cdot 10^{-4}$ $\pm 9.04 \cdot 10^{-6}$	$1.14 \cdot 10^{-3}$
8.39	0.56 ± 0.09	$5.28 \cdot 10^{-3}$ $\pm 5.27 \cdot 10^{-4}$	$5.28 \cdot 10^{-3}$

8 Supplemental

pH-dependence: IsoDromeQC D293N- (his₆-tag), determination of k_{cat}/K_M

[QC] = 6.01 mg/ml (155.3 μ M); Substrat: 99.50 μ M Q- β -NA (K_M = 0.97 mM, in 50 mM Tris, pH 8.0, T = 30 °C) 100 mM Tris, 50 mM Mes, 50 mM Na⁺-Acetat, T = 30 °C

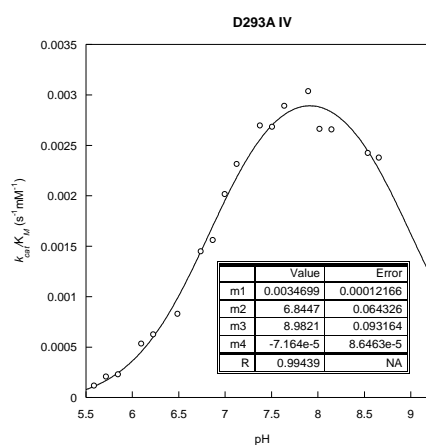
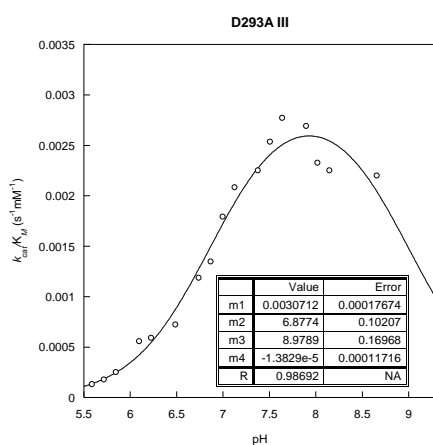
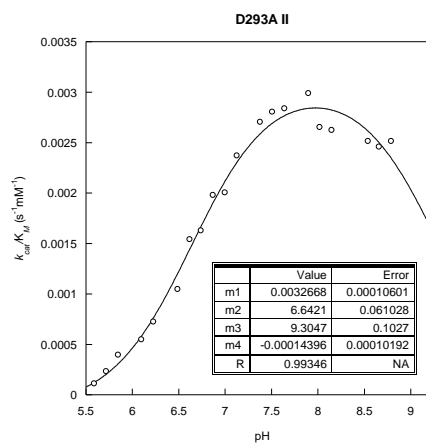
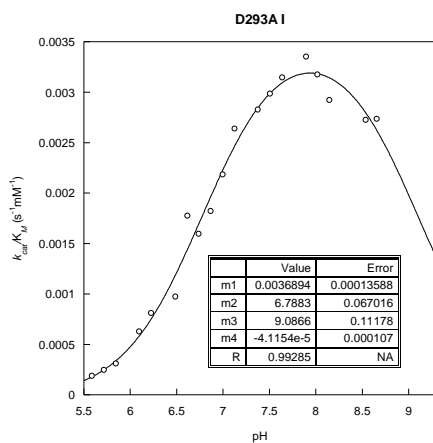


Mean values

	Mittel	Standard-abweichung	Standard-fehler
$k_{cat}/K_M(\max)$ ($s^{-1}mM^{-1}$)	$1.08 \cdot 10^{-3}$	$7.50 \cdot 10^{-5}$	$4.33 \cdot 10^{-5}$
pK_{a1}	6.38	0.06	0.03
pK_{a2}	9.39	0.04	0.03
y_0	0.98	0.01	0.01
R	$1.08 \cdot 10^{-3}$	$7.50 \cdot 10^{-5}$	$4.33 \cdot 10^{-5}$

Kinetic constants

pH	K_M (mM)	k_{cat} (s^{-1})	k_{cat}/K_M ($s^{-1}mM^{-1}$)
5.8	2.02 (± 0.66)	$9.32 \cdot 10^{-4}$ ($\pm 2.82 \cdot 10^{-4}$)	$4.62 \cdot 10^{-4}$
7.00	1.83 (± 1.25)	$3.26 \cdot 10^{-3}$ ($\pm 1.18 \cdot 10^{-3}$)	$1.35 \cdot 10^{-3}$
8.39	1.60 (± 0.18)	$4.50 \cdot 10^{-3}$ ($\pm 1.63 \cdot 10^{-3}$)	$2.81 \cdot 10^{-4}$

pH-dependence: IsoDromeQC D293A- (his₆-tag), determination of k_{cat}/K_M [QC] = 1.1 mg/ml (28.42 μ M); Substrat: 320 μ M Q- β NA (K_M = 4.35 mM, in 3 KP pH 7.0,T = 30 °C) 100 mM Tris, 50 mM Mes, 50 mM Na⁺-Acetat, T = 30 °C**Mean value**

	Mittel	Standard- abweichung	Standard- fehler
$k_{cat}/K_M(\text{max})$ ($\text{s}^{-1}\text{mM}^{-1}$)	3.37e-3	2.65e-4	1.33e-4
pk_{a1}	6.79	0.10	0.05
pk_{a2}	9.09	0.15	0.08
Y_0	--	--	--
R	0.99	3.38e-3	1.69e-3

Kinetic constants

pH	K_M (mM)	k_{cat} (s^{-1})	k_{cat}/K_M ($\text{s}^{-1}\text{mM}^{-1}$)
5.8	n.b.	n.b.	$1.86 \cdot 10^{-6}$ ($1.12 \cdot 10^{-7}$)
7.00	4.35 (± 0.70)	n.b.	$8.40 \cdot 10^{-6}$ ($\pm 1.62 \cdot 10^{-7}$)
8.39	3.42 (± 0.30)	n.b.	$1.28 \cdot 10^{-5}$ ($\pm 3.90 \cdot 10^{-7}$)
K_M -Werte from $v/[S]$ -charakteristik with hyperbolic fit, k_{cat}/K_M linear fit (1 st order conditions)			

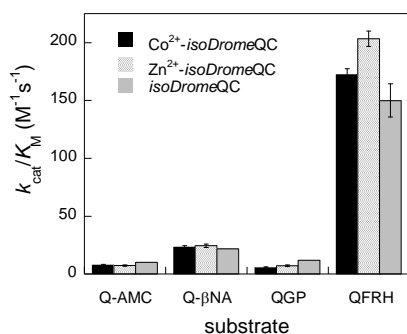
8.6 Solvent Isotopic effect

Measured by Dr. Franziska Seifert) Zn(II)-isoDromeQC wild type with Q-AMC measured using fluorescence spectroscopy assay (cf. Section 2.6.2) Assay: QC-AMC-assay (fluorescence), QC-GDH-assay (absorbance) Buffer: 25 mM sodium phosphate, 50 mM NaCl, pH/D 7.5, Temperature: 30 °C

	Specific activity (U/mg)		KIE	k_{cat} (s ⁻¹)		KIE	K_M (mM)		EIE	k_{cat}/K_M (mM ⁻¹ s ⁻¹)		KIE
	H ₂ O	D ₂ O		H ₂ O	D ₂ O		H ₂ O	D ₂ O		H ₂ O	D ₂ O	
Wild-type												
Q-AMC	0.87 ± 0.04	0.82 ± 0.11	1.06	0.55 ± 0.02	0.52 ± 0.07	1.06	0.117 ± 0.012	0.079 ± 0.006	1.49	4.72 ± 0.38	6.57 ± 0.59	0.72
QQ	4.81 ± 0.02	5.07 ± 0.35	0.95	3.04 ± 0.02	3.21 ± 0.32	0.95	1.205 ± 0.093	1.036 ± 0.040	1.16	2.53 ± 0.19	2.87 ± 0.17	0.88
QG	1.85 ± 0.19	2.07 ± 0.18	0.89	1.17 ± 0.12	1.31 ± 0.11	0.89	1.463 ± 0.242	1.292 ± 0.184	1.13	0.81 ± 0.05	1.03 ± 0.09	0.78
QHYP	7.02 ± 0.62	6.28 ± 0.24	1.12	4.43 ± 0.39	3.97 ± 0.16	1.12	0.036 ± 0.004	0.055 ± 0.002	0.65	123 ± 6.16	76.6 ± 6.19	1.60

8.7 Kinetic data Zn(II)-enzyme versus Co(II)-enzyme

Measured by Dr. Seifert Franziska. Measured using UV/Vis- and fluorescence spectroscopy (cf. Section 2.6.1 and 2.6.2) Conditions: 50 mM Tris, pH 8.0, 30°C, * from Schilling et al. 2007



	Q-AMC		Q-βNA		QGP		QFRH	
	k_{cat} (s ⁻¹)	K_M (mM)	k_{cat} (s ⁻¹)	K_M (mM)	k_{cat} (s ⁻¹)	K_M (mM)	k_{cat} (s ⁻¹)	K_M (mM)
Co ²⁺ -iDQC	1.88	0.25	4.17	0.18	6.94	1.25	11.39	0.07
Zn ²⁺ -iDQC	1.92	0.26	4.13	0.17	8.57	1.20	12.88	0.06
iDQC	*2.09	*0.21	3.13	0.15	*14.0	*1.17	13.90	0.09

Conditions: 50 mM Tris, pH 8.0, 30°C, * from Schilling et al. 2007

8.8 β-Secondary isotopic effect measured by Dr. Franziska Seifert using Q-AMC and D5-Q-AMC

Determined with fluorescence spectroscopy (cf. 2.6.2)

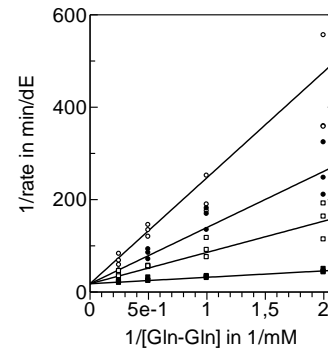
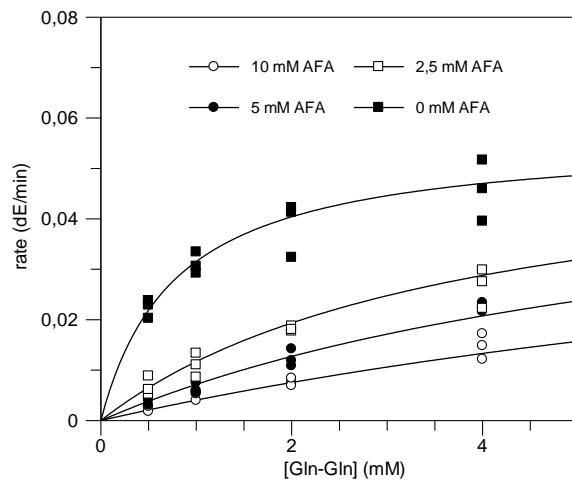
Assay: QC-AMC-assay (fluorescence) Buffer: 25 mM sodium phosphate, 50 mM NaCl, pH 7.5 Substrate: Q-AMC*, D5-Q-AMC*, Q-AMC (different synthesis) Temperature: 30 °C

	Specific activity (U/mg)	k_{cat} (s ⁻¹)	K_M (mM)	k_{cat}/K_M (mM ⁻¹ s ⁻¹)
Q-AMC*	0.71 ± 0.06	0.45 ± 0.04	0.084 ± 0.003	5.29 ± 0.57
D5-QAMC*	0.70 ± 0.06	0.44 ± 0.04	0.083 ± 0.004	5.36 ± 0.46
	KIE = 1.01	KIE = 1.02	EIE = 1.01	KIE = 0.99
Q-AMC	0.87 ± 0.04	0.55 ± 0.02	0.116 ± 0.012	4.72 ± 0.38

8.9 Determination of inhibition constant of the tripeptide AFA

Measured by Dr. Franziska Seifert using UV/Vis spectroscopic assay (cf. 6.1.1)

- Tripeptide AFA – competitive inhibitor, $K_i = 0.62 \pm 0.05$ mM

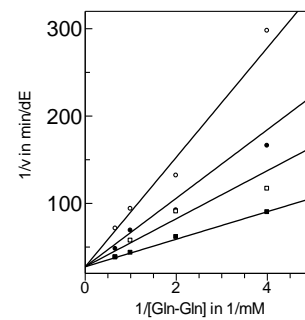
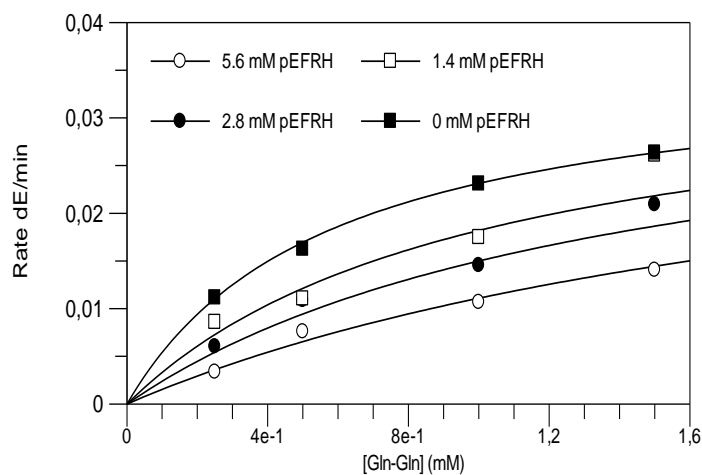


conditions: [isoDromeQC] = 0.89 µg/ml, 0.3 mM NADH, 15 mM Ketoglutarat, 30 U/ml GDH, 0.05 M Tris, pH 8.0, 30°C

8.10 Determination of product inhibition constant of pEFRH

Measured by Dr. Franziska Seifert using UV/Vis spectroscopic assay (cf. 6.1.1)

- pEFRH – competitive inhibitor, $K_i = 1.88 \pm 0.02$ mM ($K_M = 0.57$ mM)



conditions: [isoDromeQC] = 0.89 µg/ml, 0.3 mM NADH, 15 mM Ketoglutarat, 30 U/ml GDH, 0.05 M NaPP, 0.1 M NaCl, pH 6.8, 30°C

8.11 Determination of product inhibition constant of pEFA

Measured by Dr. Franziska Seifert using UV/Vis spectroscopic assay (cf. 6.1.1), conditions cf.

pEFA – competitive inhibitor, $K_i = 3.12 \pm 0.2$ mM ($K_M = 0.72$ mM)

	K _i (mM)	K _M (mM)	spez Akt (U/mg)	k _{cat} (s ⁻¹)
	3.1376	0.862	6.846	4.323
	3.3604	0.731	7.111	4.491
	2.87647	0.579	6.204	3.918
Mean	3.12482333	0.724	6.72033333	4.244
St.-Deviation	0.19777006	0.11564025	0.3807942	0.24050364

8 Supplemental

8.12 X-ray crystallography – Statistics

	Zn(II)-isoDromeQC	Zn(II)-isoDromeQC	Zn(II)-isoDromeQC
	wild type	_E190Q	_D228N
Data collection	PETRA III B14	Bessy II 14.1	Bessy14.1
Wavelength	0.826610	0.91841	0.91841
Spacegroup	P1	P1	P1
Cell dimensions			
a (Å)	46.62	46.31	45.74
b (Å)	48.13	47.98	47.82
c (Å)	74.57	74.61	74.42
α (°)	85.24	85.16	85.28
β (°)	74.61	74.64	74.16
γ (°)	73.66	73.76	73.56
Resolution range (Å)	36.321-1.119	23.980-1.703	32.878-1.930
No. of reflections	841365 (177910)	134932 (19372)	60353 (6739)
No of unique reflections	215282 (45958)	59736 (10230)	27382 (3050)
Completeness (%)	93.0 (87.8)	91.7 (86.5)	95.7 (85.9)
I/sigma (I)	15.55 (2.77)	11.75 (2.08)	12.54 (2.08)
R _{merge} (%)	4.7 (58.5)	7.4 (58.6)	8.4 (65.6)
Redundancy	3.9 (3.87)	2.26 (1.89)	2.20 (2.21)
B-factor from Wilson	16.229	24.257	37.073
Plot (Å ²)			

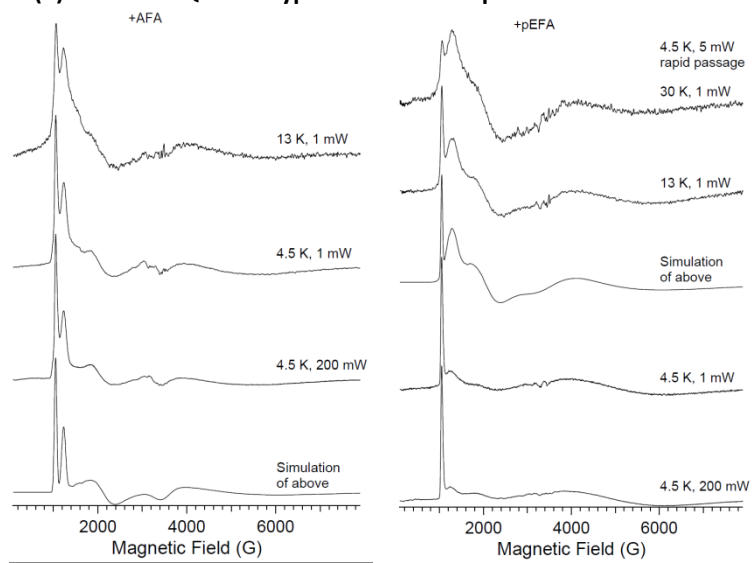
	Zn(II)-isoDromeQC	Zn(II)-isoDromeQC	Zn(II)-isoDromeQC
	wild type	_E190Q	_D228N
Refinement	PHENIX	PHENIX	PHENIX
Resolution range	36.321-1.119	23.980-1.703	32.878-2.225
Reflections(working/test)	215209	28583	27358
R _{work} /R _{free} (%)	15.58/17.94	18.25/22.75	18.26/24.26
Number of Atoms	5878	5752	5081
Protein	5008	5126	4930
Ligand			
Water	868	624	149
B-factor Protein	20.6	26.2	15.82
B-factor Ligands			
B-factor Water	35.3	39.1	15.58
Deviation from ideals (r.m.s.d.)			
Bond distances (Å)	0.014	0.005	0.008
Bond angles (°)	1.656	1.039	1.199.
Dihedrals (°)	13.378	13.231	14.557
Ramachandran Plot			
Favoured regions (%)	95.74	94.5	93.20
Allowed regions	3.44	5.14	6.30
Outlier regions	0.82	0.80	0.50

8 Supplemental

	Co(II)isoDromeQC	Co(II)isoDromeQC	Co(II)isoDromeQC
	wild type +QFRH	wild type +EFRH	wild type +AFA
Data collection	PETRA III	In-house facility	PETRA III
Wavelength	0.826610	1.541790	0.826610
Spacegroup	P1	P1	P1
Cell dimensions	-	-	-
a (Å)	46.26	46.32	46.42
b (Å)	47.83	47.81	47.92
c (Å)	74.68	74.81	74.83
α (°)	85.12	85.30	85.51
β (°)	74.71	74.65	74.25
γ (°)	73.89	74.20	74.09
Resolution range (Å)	43.023-1.312	24.044-1.419	42.138-1.308
No. of reflections	540409 (62287)	217373 (36039)	541743 (73394)
No of unique reflections	128424 (14932)	98482 (16365)	130007 (17667)
Completeness (%)	90.4 (91.3)	87.40 (78.7)	90.1 (90.7)
I/sigma (I)	15.17 (2.36)	14.01 (2.91)	20.12 (2.54)
R _{merge} (%)	5.2 (66.2)	5.4 (39.7)	65.4 (3.6)
Redundancy	4.21 (4.17)	2.20 (2.20)	2.5 (4.15)
B-factor from Wilson	20.28	20.308	22.361
Plot (Å ²)			

	Co(II)isoDromeQC	Co(II)isoDromeQC	Co(II)isoDromeQC
	wild type +QFRH	wild type +EFRH	wild type +AFA
Refinement	PHENIX	PHENIX	PHENIX
Resolution range	43.023-1.312	24.044-1.419	42.138-1.308
Reflections(working/test)			
R _{work} /R _{free} (%)	14.31/18.18	15.46/19.40	16.16/19.63
	-	-	-
Number of Atoms	5945	5951	5721
Protein	5022	5013	5013
Ligand	61	74	42
Water	860	862	664
B-factor Protein	19.39	18.99	20.78
B-factor Ligands	32.71	29.32	29.53
B-factor Water	32.97	34.31	35.59
	-	-	-
Deviation from ideals	-	-	-
(r.m.s.d.)	-	-	-
Bond distances (Å)	0.013	0.014	0.013
Bond angles (°)	1.619	1.647	1.714
Dihedrals (°)	13.869	14.234	14.459
	-	-	-
Ramachandran Plot	-	-	-
Favored regions (%)	95.77	95.11	94.94
Allowed regions	3.42	4.08	4.08
Outlier regions	0.81	0.82	0.98

8.13 EPR spectra of Co(II)-isoDromeQC wild type with AFA and pEFA



Alexander Piontek

Georg-August-Universität Göttingen
Department of Bioanalytics
Justus-von-Liebig Weg 11
Goettingen, Germany
Phone: +49 551 3914000
E-mail: apionte@gwdg.de

Date of Birth: June 14th 1982
Place of Birth: Weißenfels
Nationality: German

Education

1993-06/2002	Goethe Gymnasium Weißenfels (Abitur)
10/2002-06/2003	Military service
10/2003-9/2009	Biochemistry student, Martin-Luther Universität Halle/Wittenberg (Diploma)
11/2008-9/2009	Diploma Thesis, Martin-Luther Universität Halle/Wittenberg prepared in the Department of Bioanalytics, Georg-August Universität Göttingen: "Untersuchungen zum Katalysemechanismus und Herbizidinhibierung der Acetohydroxysäuresynthase aus <i>Arabidopsis thaliana</i> " (1.4) Supervision: Prof. Dr. Kai Tittmann, Dr. Andrea Steinmetz
11/2009-03/2014	PhD student, Georg-August Universität, Göttingen, Department of Bioanalytics: "Deciphering the catalytic mechanism of the Zn(II) enzyme glutaminyl cyclase and the deduction of transition state inhibitors" Thesis committee: Prof. Dr. Kai Tittmann, Prof. Dr. Franc Meyer

Practical experience

11/2008-9/2009 **Albrecht-v.-Haller Institute for Plant Sciences, Department of Bioanalytics, Georg-August Universität Göttingen**

Research project: Diploma Thesis

Methods: circular dichroism and UV/Vis spectroscopy, fast kinetic methods (stopped-flow), basics in NMR spectroscopy, isothermal titration calorimetry, basics in X-ray crystallography

11/2009 –present

Department of Bioanalytics, Georg-August Universität Göttingen

protein expression and purification of His-tagged and non-tagged recombinant proteins, X-ray data collection at ESRF (Grenoble), HZB (Berlin) as well as at different in-house generators, X-ray data analysis (XDS, MOSFLM), X-ray structure modeling and refinement, basics in Co(II) electron paramagnetic resonance spectroscopy, fluorescence spectroscopy, fast protein liquid chromatography,

11/2009-5/2013

Practical courses

“Electron spin resonance spectroscopy”, Supervision: Prof. Dr. Marina Bennati

“X-ray-crytallography”, Supervision: Dr. Piotr Neumann

11/2009-5/2013

Soft Skill courses

“Career planning for students: Application standards – personal strategies” performed by Dr. Simon Golin, Golin Wissenschaftsmanagement“

“Project Management”, Golin Wissenschaftsmanagement

Teaching Experience

2009 – 2012

“Principles and methods of protein purification by chromatography”

2011

“MSc/PhD Microbiology and Biochemistry”,

2012

Thermodynamic characterization of biomolecular interaction
Method course of isothermal titration calorimetry (ITC)

Conferences/ Workshops

May 26 th – 29 th 2010	“International Meeting on Proline-Specific Cleavage and Oxoprolyl Formation – Functions and Therapeutic Strategies” Halle, Germany
Feb. 2 nd – 11 th 2011	IRTG 1422 Workshop (poster presentation), Lund, Sweden
March 9 th – 13 th 2011	The 10 th International Conference on Alzheimer’s and Parkinson’s Disease, Barcelona, Spain
April 11 th – 13 th 2012	IRTG 1422 Workshop (talk), Hofgeismar, Germany
June 3 rd - 6 th 2012	“Trends in Enzymology”, Göttingen, Germany
May 23 rd – 25 th 2013	IRTG 1422 Workshop (talk), Hülse, Germany

Science related stay abroad

March 5 th – 7 th 2011	X-ray data collection ESRF, Grenoble, France
Oct. 26 th – Nov. 3 rd 2013	Co(II) EPR measurements under the supervision of Prof. Dr. Brian Bennett, Medical College of Wisconsin, Milwaukee, Wisconsin, USA

Memberships

11/2009-present	Georg-August University School of Science (GAUSS) - Biology, Graduate School
1/2010 – present	International Research Training Group (IRTG) 1422 – Metal Sites in Biomolecules: Structures, Regulations and Mechanisms

Skills and Interests

Computer Skills	Windows, Linux (basics), Crystallography software (XDS (basics), MOSFLM, CCP4, PHENIX, COOT, PYMOL, MOLEMAN (basics)) SigmaPlot, MS Office, (Origin and Kaleidagraph - both basics)
Languages	German: mother tongue English: advanced in written and spoken French: basics
Hobbies	Horse riding, sports (fitness, swimming)